CNWRA 96-011

ENGINEERED BARRIER SYSTEM PERFORMANCE ASSESSMENT CODE: EBSPAC VERSION 1.0 β

TECHNICAL DESCRIPTION AND USER'S MANUAL

Prepared for

Nuclear Regulatory Commission
Contract NRC-02-93-005

Prepared by

Center for Nuclear Waste Regulatory Analyses
San Antonio, Texas

September 1996

CNWRA 96-011

ENGINEERED BARRIER SYSTEM PERFORMANCE ASSESSMENT CODE: EBSPAC VERSION 1.0 β

TECHNICAL DESCRIPTION AND USER'S MANUAL

Prepared for

Nuclear Regulatory Commission
Contract NRC-02-93-005

Prepared by

Sitakanta Mohanty
Gustavo A. Cragnolino
Tae Ahn (NRC)
Darrell S. Dunn
Peter C. Lichtner
Randall D. Manteufel
Narasi Sridhar

Center for Nuclear Waste Regulatory Analyses
San Antonio, Texas

September 1996

PREVIOUS REPORTS IN SERIES

Number	Name	Date Issued
CNWRA 92-009	SOTEC: A Source Term Code for High-Level Nuclear Waste Geological Repositories. User's Manual: Version 1.0	July 1992
Letter Report	Selection and Evaluation of Models for Substantially Complete Containment Example Problem	September 1992
Letter Report	Preliminary Assessment of Pitting Corrosion Models	September 1992
CNWRA 93-021	Engineered Barrier System Performance Assessment Codes (EBSPAC) Progress Report—October 1, 1992, through September 25, 1993	October 1993
CNWRA 94-003	"Substantially Complete Containment"—Example Analysis of a Reference Container	January 1994
CNWRA 94-026	Engineered Barrier System Performance Assessment Codes (EBSPAC) Progress Report—October 1, 1993, through September 25, 1994	October 1994
Letter Report	SCCEX: A Computer Code for Substantially Complete Containment Example Analysis of a Reference Container. Version 1.01	January 1995
Letter Report	Planning and Status Report on the Engineered Barrier System Performance Assessment Code (EBSPAC) and Supporting Detailed Analyses	September 1995

ABSTRACT

This report contains a technical description of the various models (i.e., thermal, environmental, humid air and aqueous corrosion, gaseous and liquid radionuclide releases, among others) used or to be used in the Engineered Barrier System Performance Assessment Code (EBSPAC) to represent processes that govern the failure of waste packages (WPs) and, ultimately, the release of radionuclides from the engineered barrier system. These models are specifically adapted to the current U.S. Department of Energy (DOE) WP design for the proposed repository at Yucca Mountain, which consists of a multi-wall overpack composed of concentric containers of different metallic materials in a horizontal drift emplacement. EBSPAC is being developed to deterministically evaluate the performance of the engineered barriers and to be used in the future as the source term module incorporated in the Center for Nuclear Waste Regulatory Analyses (CNWRA)/Nuclear Regulatory Commission (NRC) Total Performance Assessment (TPA) code. Version 1.0β of EBSPAC is described in this report, in which a detailed discussion on the code structure is included. EBSPAC essentially consists of two separate codes—one dealing with WP failure calculations and the other with radionuclide release. The main output of the first code is the WP failure time, which is directly fed into the other one as an input. In addition, these two codes have the capability of being executed in a stand-alone mode. The function of different subroutines, the computer code capabilities, compilation and linking, hardware requirements, and program execution procedures are addressed in the user's manual, as well as characteristics of the input and output data files. Finally, an example problem is presented in order to provide guidance to the user through the review of data inputs and result outputs.

CONTENTS

CONTENTS (cont'd)

FIGURES

TABLES

ACKNOWLEDGMENTS

This report was prepared to document work performed by the Center for Nuclear Waste Regulatory Analyses (CNWRA) for the Nuclear Regulatory Commission (NRC) under Contract No. NRC-02-93-005. The activities reported here were performed on behalf of the NRC Office of Nuclear Material Safety and Safeguards (NMSS), Division of Waste Management (DWM). The report is an independent product of the CNWRA and does not necessarily reflect the views or regulatory position of the NRC.

The authors acknowledge the assistance provided by Ronald W. Janetzke in understanding the SOurce TErm Code (SOTEC) and Substantially Complete Containment EXample (SCCEX) code and conducting many test runs of Version 1.0β of EBSPAC. The authors also gratefully acknowledge the technical reviews of Budhi Sagar and Hersh K. Manaktala and the programmatic review of Wesley C. Patrick. Appreciation is due to Bonnie L. Garcia for her assistance in the preparation of this report.

ANALYSES AND CODES: Version 1.0β of EBSPAC is developed under the CNWRA Technical Operating Procedure (TOP)-018. This report and User's Manual satisfies one of the requirements of the Software Configuration Procedure.

QUALITY OF DATA: Sources of data are referenced in each chapter. CNWRA-generated laboratory data contained in this report meet quality assurance (QA) requirements described in the CNWRA QA Manual. Data from other sources, however, are freely used. The respective sources of non-CNWRA data should be consulted for determining their levels of quality assurance.

EXECUTIVE SUMMARY

The U.S. Department of Energy (DOE) draft strategy for radioactive waste containment and isolation for the proposed repository at the Yucca Mountain (YM) site focuses on two objectives: (i) to provide containment of the radioactive waste within emplaced waste packages (WPs) for thousands of years and (ii) to limit the dose to any member of the public. The DOE has formulated several attributes of the repository system that, if verified, would demonstrate that the waste can be isolated at the proposed YM site for long periods of time. The attributes pertaining to the performance of the engineered barriers include the following: (i) low flow of groundwater into the repository horizon, (ii) containment of waste within WPs for thousands of years, (iii) slow mobilization of radionuclides from breached WPs, and (iv) limited transport of radionuclides through the engineered barriers.

The objectives of the Engineered Barrier System Performance Assessment Code (EBSPAC) development are to provide a means and methodology to (i) evaluate these hypotheses independently and perform sensitivity analyses of WP performance, (ii) assess the adequacy of the DOE demonstration of the validity of the hypotheses, and (iii) provide input to the total system performance assessment. The EBSPAC is envisioned as a source term module to be incorporated in the Center for Nuclear Waste Regulatory Analyses (CNWRA)/Nuclear Regulatory Commission (NRC) Total Performance Assessment (TPA) code to independently assess the overall repository performance.

In the current development of EBSPAC, two factors have been contemplated:

(i) The DOE design of containers and the emplacement strategy changed significantly in recent years. Instead of a single-wall design, a multi-wall overpack composed of concentric containers of different materials was adopted. In addition, a horizontal drift emplacement was proposed instead of the vertical borehole emplacement previously considered.

(ii) Following the National Academy of Sciences (NAS) recommendations on a repository performance standard, quantitative subsystem requirements may be eliminated from a YM-specific regulation, and the performance period for the WPs may be extended considerably beyond the 300 to 1,000 yr established in Code of Federal Regulations Title 10 Part 60, Section 113 (10 CFR 60.113).

The overall strategy for EBSPAC development in the Container Life and Source Term (CLST) Key Technical Issue (KTI) consists of concurrent development of detailed analyses or models of processes affecting WP performance and abstraction of these models for incorporation into EBSPAC. Detailed analyses are used to determine the importance of a given failure process in the WP performance and identify the most suitable conceptual models for the materials and environmental conditions of interest. Although detailed conceptual models exist for many corrosion and mechanical failure processes, material-specific parameters for these models, which should be adapted to the conditions prevailing in a repository under partially saturated conditions, are scarce. These parameters are obtained through reviews of published literature and data reported by the DOE, combined with data obtained in the experimental investigations program conducted within the CLST KTI.

In this report, the processes and models incorporated or to be incorporated into EBSPAC are first described. In this initial version of EBSPAC, Version 1.0β, only the canistered fuel design for 21

pressurized water reactor (PWR) or 40 boiling water reactor (BWR) fuel assemblies, considered to be the primary choice for handling, storage, transportation, and disposal of spent fuel (SF), was taken into consideration for the development of the code. The glass waste form was not considered. As a set of external calculations to EBSPAC, the thermal model provides the temperature distribution as a function of time and position within the EBS as well as in the surrounding geosphere. The temperature and relative humidity at the WP surface as functions of time are used to predict the conditions that affect the occurrence and rate of corrosion of the WP and the subsequent release of radionuclides. The chemical composition, pH, and oxygen concentration of the fluid which is able to come in contact with the WP is determined by the environmental model, in which the evaporative effects produced by the heat released by radioactive decay are considered. Below a critical value of relative humidity, air oxidation of steel is modeled as the dominant process for the steel overpack in parallel with the evaluation of mechanical failure as a result of thermal embrittlement of the steel promoted by long-term exposure to temperatures above 150 °C. If the relative humidity is higher than the critical value, the occurrence of aqueous corrosion of the steel overpack is evaluated. No distinction is made in EBSPAC between humid air corrosion and aqueous corrosion because both processes are governed by the same principles. The corrosion models calculate the rates of uniform and localized corrosion. The corrosion process at any given time period depends on the corrosion potential and the critical potential required to initiate a particular localized corrosion process. Following penetration of the outer container, electrical contact of the inner and outer container through the presence of an electrolyte path such as that provided by modified groundwater promotes galvanic coupling. The galvanic coupling model evaluates whether penetration of the inner container by localized corrosion is possible; otherwise, mechanical fracture becomes the predominant failure mechanism.

Once penetration of the inner container occurs, the relative humidity criterion is applied to determine whether air oxidation or aqueous dissolution of the spent fuel is the subsequent process to be evaluated. Air oxidation of spent fuel leads to gaseous release of C-14 predominantly from the fuel cladding, whereas I-129, Cl-36, and C-14 are released from the fuel pellets and the pellet cladding gap. In Version 1.0β of EBSPAC, aqueous release of radionuclides from SF includes only congruent releases of the radionuclides contained in the irradiated UO_2 matrix. Only the "bathtub" model is used in Version 1.0β of EBSPAC, although dripping of modified groundwater on the SF will be implemented in future versions. Aqueous releases is treated only as solubility limited release and dissolution rate limited release. Colloidal release is discussed but not implemented in this version of EBSPAC.

EBSPAC performs calculations for a single cell, not for the overall repository, through two separate, distinctive parts. One part deals with WP failure calculations and the other, which is essentially a separate code, with release calculations, but no feedback exists from the release part into the failure part. The release code includes the incorporation of radionuclide decay, generation of daughter products in the chains, temporal variation of inventory in the waste package, and spatial variations in the properties of the surrounding material. However, the degree of the complexities incorporated varies from model to model in order to accomplish necessary simplifications while ensuring conservatism in the calculation of radionuclide release.

The report includes a detailed discussion on the structure of the code and the subroutines that are used in both the WP failure and release calculations. A complete description of input and output data are also provided. In addition, all the input parameters used in the code are compiled in tables and listed following the code line in which they appeared. The symbols of the parameters, a brief description, values used in an example, and units are included in these tables. Both the hardware and software requirements are indicated, as well as the future need of pre- and post-processors that are required to incorporate EBSPAC

as a source term model in the TPA executive code. An example problem is introduced to illustrate the use of the code, providing guidance to the user through data inputs and result outputs. A final section contains a summary of the report as well as recommendations for future developments of EBSPAC.

1 INTRODUCTION

1.1 BACKGROUND

The U.S. Department of Energy (DOE) draft strategy for radioactive waste containment and isolation for the proposed repository at the Yucca Mountain (YM) site (TRW Environmental Safety Systems, Inc., 1996) focuses on two objectives: (i) to provide containment of the radioactive waste within emplaced waste packages (WPs) for thousands of years and (ii) to limit the dose to any member of the public. The DOE has formulated several attributes of the repository system that, if verified, would demonstrate that the waste can be isolated at the proposed YM site for long periods of time. The attributes pertaining to the performance of the engineered barriers include the following: (i) low flow of groundwater into the repository horizon, (ii) containment of waste within WPs for thousands of years, (iii) slow mobilization of radionuclides from breached WPs, and (iv) limited transport of radionuclides through the engineered barriers.

The objectives of the Engineered Barrier System Performance Assessment Code (EBSPAC) development are to provide a means and methodology to (i) evaluate these hypotheses independently and perform sensitivity analyses of WP performance, (ii) assess the adequacy of the DOE demonstration of the validity of the attributes, and (iii) provide input to the total system performance assessment. For this purpose, detailed analyses on the basis of modeling and experimental investigations are conducted in the Container Life and Source Term (CLST) Key Technical Issue (KTI) and the results of these activities are abstracted for incorporation into EBSPAC (Sridhar, 1995). The EBSPAC is envisioned as a source term module to be incorporated in the Center for Nuclear Waste Regulatory Analyses (CNWRA)/Nuclear Regulatory Commission (NRC) Total Performance Assessment (TPA) code to independently assess the overall repository performance.

Previous analyses of the EBS performance (Sridhar et al., 1993; Cragnolino et al., 1994) were designed to specifically address methodologies for quantifying the subsystem performance requirement of substantially complete containment as stated in Code of Federal Regulations (CFR) Title 10, Part 60, Section 113 (10 CFR 60.113). Using the Substantially Complete Containment EXample (SCCEX) code (Cragnolino et al., 1994), both deterministic and probabilistic calculations were conducted on a WP design consisting of a single-wall container made of a corrosion-resistant alloy and emplaced vertically in a borehole. The code was designed only to evaluate the substantially complete containment requirement and did not evaluate radionuclide release (the source term). Prior to and independent of this code, a SOurce TErm Code (SOTEC) (Sagar et al., 1992) was constructed to provide input to the TPA code. While this code used the same WP design and similar conceptual model for corrosion as the SCCEX code, the functional dependencies of the corrosion models on various material and environmental parameters were significantly different.

The FY96 activities focused on developing Version 1.0β of EBSPAC, a code for evaluating the performance of the engineered barriers. In the current development of EBSPAC, two factors were contemplated.

(i) The DOE design of containers and the emplacement strategy changed significantly in FY95. Instead of a single-wall design, a multi-wall overpack design composed of concentric containers of different materials was adopted. In addition, a horizontal drift

emplacement was proposed instead of the vertical borehole emplacement previously considered.

(ii) Following the National Academy of Sciences (NAS) recommendations on a repository performance standard, quantitative subsystem requirements may be eliminated from a YM-specific regulation and the performance period may be extended considerably beyond the 300 to 1,000 yr established in 10 CFR 60.113.

The following sections outline the DOE advanced conceptual design (TRW Environmental Safety Systems, Inc., 1996) of the WP and the overall strategy of EBSPAC development.

1.2 ADVANCED CONCEPTUAL DESIGN

The major component of the EBS is the WP, which includes the waste form [irradiated UO_2 from nuclear power reactors and reprocessed high-level radioactive waste (HLW) consolidated in a borosilicate glass matrix], fuel cladding, filler, canisters [multipurpose canister (MPC) for spent fuel (SF) and pour canister for glass], and disposal overpacks. SF is generally categorized in two classes based on the type of reactor which generates the waste: boiling water reactor (BWR) and pressurized water reactor (PWR). In addition to the WP, the EBS may include backfill, concrete inverts, WP emplacement pedestals, drip shields, and other components used in the design and construction of emplacement drifts. Some of these components affect waste containment and isolation indirectly through their effects on the near-field environment (e.g., concrete inverts, steel sets, rock bolts). Other components affect containment directly (e.g., overpacks). Some components have both direct and indirect effects (e.g., backfill). In EBSPAC calculations, the indirect effects that promote the alteration of the near-field environment are used as inputs (e.g., table look-up).

Several WP designs have been proposed by DOE over the history of the YM repository program (TRW Environmental Safety Systems, Inc., 1996). In the current Advanced Conceptual Design (ACD), the canistered fuel design is considered to be the primary choice for handling, storage, transportation, and disposal of SF. The schematic cross-sectional diagram of the WP for 21 PWR or 40 BWR fuel assemblies is shown in Figure 1-1. The current list of candidate materials (TRW Environmental Safety Systems, Inc., 1996) is identified in Table 1-1, along with primary materials recommended for testing. The proposed outer length is 5.682 m, and the outer diameter is 1.802 m. The total outer surface area of such a WP is about 37 m^2 and the loaded weight is about 65,000 kg. Alternate WP designs include WPs for uncanistered fuels (no MPC), small canistered fuel (12 PWR or 24 BWR fuel assemblies), and high-level reprocessed waste.

1.3 OVERALL STRATEGY FOR EBSPAC DEVELOPMENT

The technical descriptions and the user's manual provided in this report pertain to Version 1.0β of EBSPAC. The overall strategy for EBSPAC development consists of concurrent development of detailed analyses or models of processes affecting WP performance and abstraction of models to be used in EBSPAC (Sridhar, 1995). Detailed analyses are used to determine the importance of a given failure process in the WP performance and identify the most suitable conceptual models for the materials and environmental conditions of interest. It is realized that although detailed conceptual models exist for many corrosion and mechanical failure processes, material-specific parameters for these models, which should be adapted to the conditions prevailing in a repository under partially saturated conditions, are scarce.

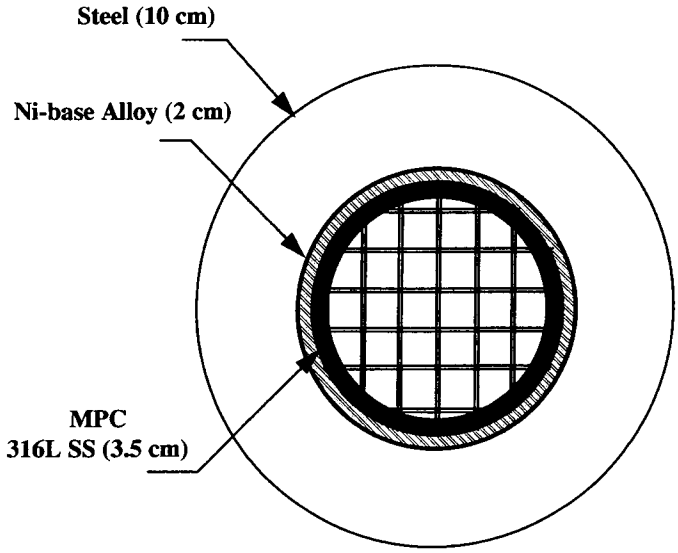

Figure 1-1. Schematic cross-sectional diagram of the waste package for 21 pressurized water reactor or 40 boiling water reactor fuel assemblies

Table 1-1. Candidate materials in the advanced conceptual design (TRW Environmental Safety Systems, Inc., 1996)

Component	Materials	
	Primary	Alternate
Inner Overpack	Alloy 825 (UNS N08825)	Ni-Base Alloys Alloy C-22 (UNS N06022) Alloy G-30 (UNS N06030) Alloy C-4 (UNS N06455) Alloy G-3 (UNS N06985) Alloy N08221 (Not in commercial production) Ti-Base Alloys Grade 12 (UNS R53400) Grade 16 (UNS R52402)
Outer Overpack	ASTM A516, Grade 55 Carbon Steel (UNS K01800)	Fe-Base Alloys ASTM A27 Grade 70-40 (UNS J02501) cast steel ASTM A387 Grade 22 (UNS K21590) alloy steel Cu-Base Alloys 90-10 CuNi (UNS C70600) 70-30 CuNi (UNS C71500) Ni-Base Alloy Alloy 400 (UNS N04400)
Outer Overpack, HLW Glass	70-30 CuNi (UNS C71500)	

These parameters are obtained through reviews of published literature and data reported by the DOE, combined with data obtained in the CNWRA experimental investigations program.

Because EBSPAC is to be used as a module in the TPA code that will execute hundreds of Monte Carlo runs, the EBSPAC code must be based on simplified models that will allow fast computation. As a rule of thumb, the design will be such that the average execution time for a single EBSPAC run will be completed in approximately 4 seconds on a CRAY-YMP with eight processors. Assuming an execution time scale factor of approximately 25, this 4 cray-seconds would be equivalent to 100 seconds on a UNIX IPX machine. Additionally, EBSPAC must be connected to the TPA code through a preprocessor so that the interface between these two codes can easily be achieved by modifying the preprocessor if and when changes are made to EBSPAC. Like other modules of the TPA code, EBSPAC must execute in an independent mode implying no data feedback from the TPA code during a stand-alone execution. The functional requirements for EBSPAC were determined and described elsewhere (Mohanty et al., 1996).

With this overall strategy in mind, this report first describes the processes and models incorporated or to be incorporated in EBSPAC. This is followed by the description of the current version of EBSPAC which includes a discussion on code structure and code capabilities. An example problem is also presented that provides guidance to the user through data inputs and result outputs.

2 DESCRIPTION OF PROCESSES AND MODELS IN EBSPAC

This chapter presents various models used in EBSPAC to represent underlying processes that govern the failure of the WP and ultimately the release of radionuclides. Well established models, such as convective and diffusive flow, are briefly discussed. In contrast, the processes that are either heretofore not taken into account or lack adequate experimental support are discussed in detail to highlight the choice of associated models and parameters. Some models, though not used in this version of EBSPAC, are presented for the sake of completeness and future references. Although the determination of thermohydrological conditions or the definition of the environment in the vicinity of the EBS are not intrinsic to the EBSPAC, they are presented in this chapter to emphasize their significance and influence on WP failure and source-term calculation.

2.1 GENERAL OVERVIEW OF PROCESSES AND MODELS

An important consideration is the modification with time after waste emplacement of the physical and physicochemical characteristics of the environment surrounding the WP. Figure 2-1 shows a simplified conceptualization of the processes occurring in the vicinity of a WP, which is horizontally emplaced on top of a concrete invert in a drift instead of the vertical emplacement in a borehole considered in SOTEC and in SCCEX codes (Sagar et al., 1992; Cragnolino et al., 1994).

As schematically indicated in Figure 2-1, water can reach the drift walls from the ground surface through infiltration in the rock by matrix and fracture flow. Water percolating through the backfill material (e.g., crushed tuff) can contact the WP surface. However, as a result of the heat generated by the radioactive decay of the waste, groundwater in the backfill and the rock media surrounding the drift will be vaporized initially and driven away from the vicinity of the WPs, leading to the formation of a dry-out zone. Condensation of water vapor may occur at a certain distance from the drift walls, reestablishing partially saturated conditions. Backflow through fractures of this condensate, enriched in salts due to rock-water interactions affected by the increase in temperature over long periods of time, may lead to corrosion and subsequent failure of the outer steel overpack and, eventually, to penetration of the inner container. Upon breaching of the containers, solutions concentrated with respect to the original groundwater and modified by the presence of soluble corrosion products, will interact with the waste form leading to the release of radionuclides that can be transported to the water table, as schematically illustrated in Figure 2-1.

All the processes succinctly described above are incorporated through simplified models into the EBSPAC code, as illustrated in the flow chart shown in Figure 2-2. The temperature evolution at the WP surface is obtained from the thermal model and the time at which this surface begins to be covered with a water film is calculated by modeling the near-field environment. The environment model provides the relative humidity (RH) reached at a given temperature of the WP. In addition, the pH and chemical composition of the liquid phase contacting the WP is calculated, mainly in terms of predominant anionic species such as Cl^-. Because the onset of aqueous corrosion is dictated by the WP surface conditions, especially the presence of a water film, the time at which the surface is covered by a water film (i.e., the surface wetting time) is an important parameter to be calculated. This time can be determined by using either the critical RH approach adopted by the DOE in TSPA-95 (TRW Environmental Safety Systems, Inc., 1995) or the vapor-pressure gradient model developed by Walton (1993) and used previously in the SCCEX code (Cragnolino et al., 1994). Only the first option has been implemented in this version of EBSPAC.

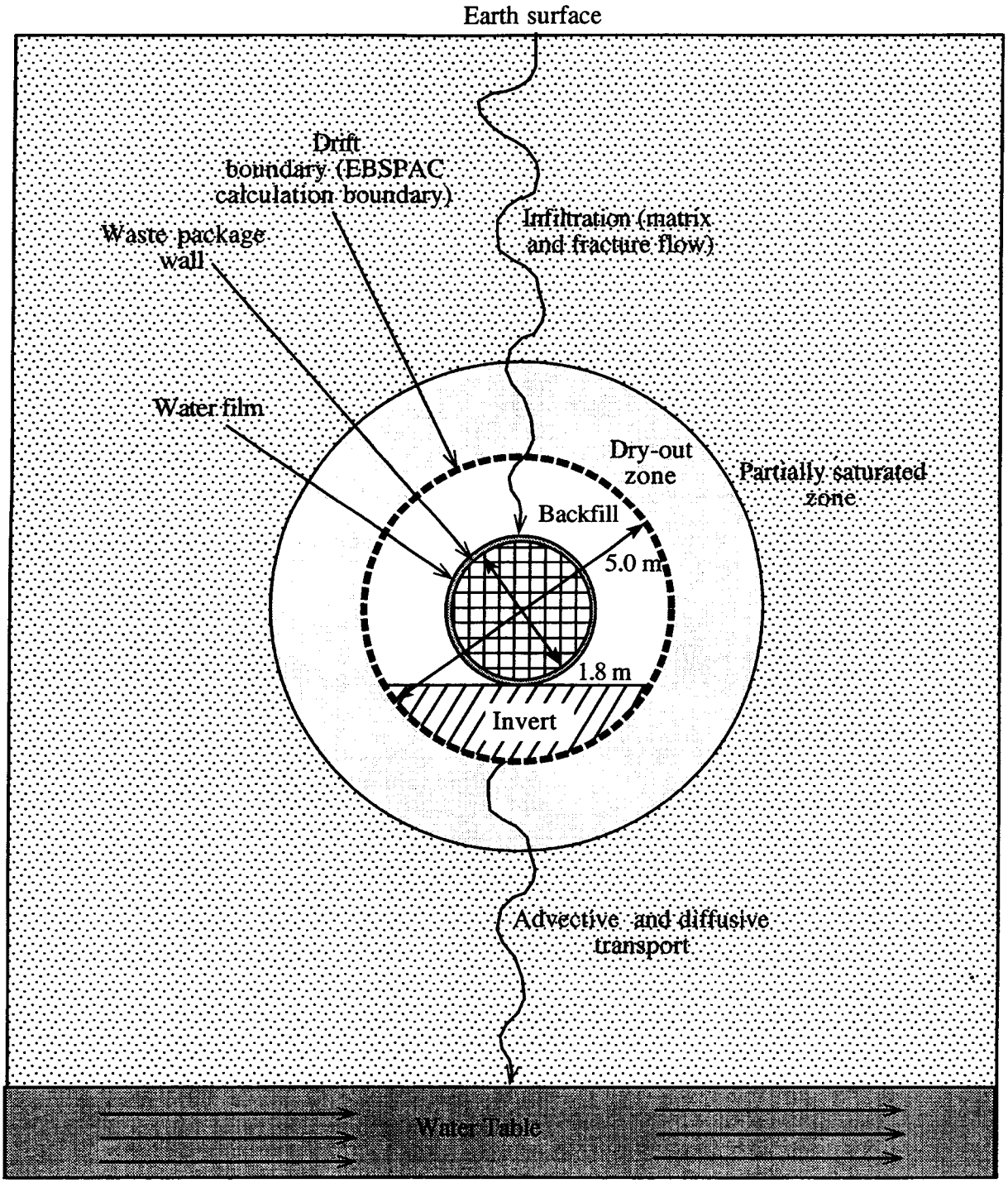

Figure 2-1. Conceptualization of the radionuclide release from waste packages emplaced in a horizontal drift. The thick broken circle represents the EBSPAC boundary. Processes outside this boundary are not modeled in EBSPAC but are represented as inputs.

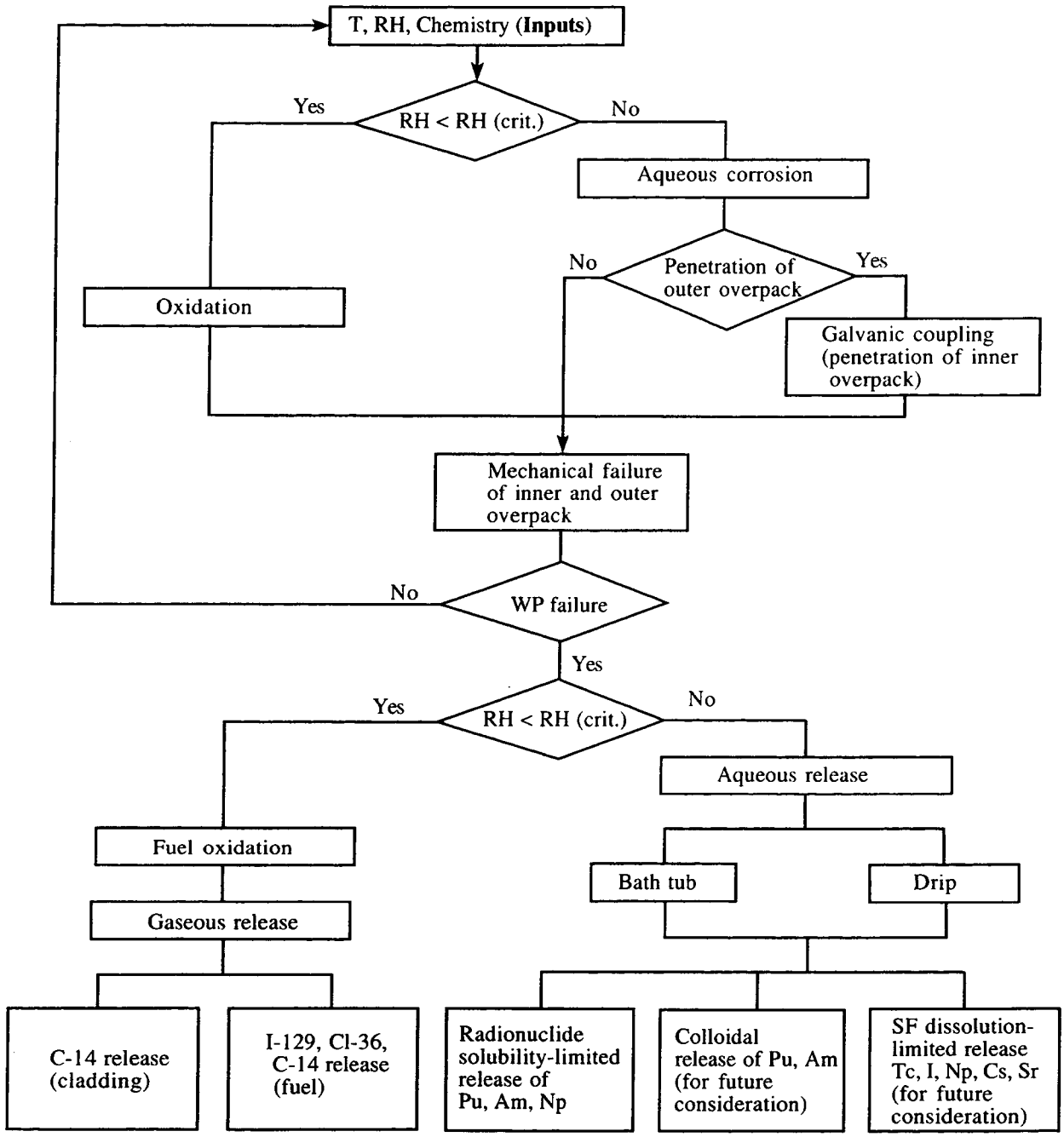

Figure 2-2. Flow chart showing various components considered in the source-term calculations

In the flow chart (Figure 2-2), it is shown that the conditions for the formation of a water film are determined by a critical value of RH. Below this value, air oxidation in the presence of water vapor is modeled as the dominant process for the steel overpack in parallel with the evaluation of mechanical failure as a result of thermal embrittlement of the steel promoted by long-term exposure to temperatures above 150 °C. If the RH is higher than the critical value, the occurrence of aqueous corrosion of the steel overpack is evaluated. The corrosion models calculate the rates of uniform and localized corrosion. The corrosion process at any given time period depends on the corrosion potential and the critical potential required to initiate a particular localized corrosion process. Following penetration of the outer container, electrical contact of the inner and outer container coupled to the presence of an electrolyte path such as that provided by modified groundwater promotes galvanic coupling. The galvanic corrosion model evaluates whether penetration of the inner container by localized corrosion is possible or otherwise mechanical fracture becomes the predominant failure mechanism.

Once penetration of the inner container occurs, containment is assumed to be lost. The RH criterion is then applied to determine whether air oxidation or aqueous dissolution of the SF is the subsequent process to be evaluated. Air oxidation of SF leads to gaseous release of C-14 predominantly from the fuel cladding, whereas I-129, Cl-36, and C-14 are released as gases from the fuel pellets and the pellet-cladding gap. Two models are considered for aqueous release of radionuclides. One is the "bathtub" model and the other is based on modified groundwater dripping on the SF. Only the bathtub model is included in this version of EBSPAC. Finally, three plausible mechanisms for the aqueous release of transuranics and certain fission products are considered, including solubility limited release, colloidal release, and dissolution rate limited release. However, the mechanism for colloidal-controlled release is not implemented in this version of EBSPAC.

2.2 THERMAL MODEL

As a set of external calculations to EBSPAC, the thermal model provides the temperature distribution as a function of time and position within the EBS as well as in the surrounding geosphere. In particular, the temperature and RH at the WP surface as functions of time are used to predict the rate of corrosion and subsequent release of radionuclides. In this section, the method and data used to predict the thermohydrologic environment of a representative WP are briefly described. The method used has been described in detail elsewhere (Manteufel, 1996). The thermal model was developed within the Thermal Effects on Flow (TEF) KTI, to be used as a module in TPA.

The thermal model is based on a plan view of the repository, as shown in Figure 2-3. Waste packages are assumed to reside evenly spaced in parallel emplacement drifts. The periodic elementary unit (EU) identified in Figure 2-3 has a dimension of half of the drift spacing and half of the WP spacing. The WP spacing within a drift and the spacing between drifts are used to affect the areal mass loading (AML) of the repository which is currently a design variable. Low AML designs spread the waste to minimize the thermal impact on the host rock, while high AML designs concentrate the waste in order to vaporize and drive away the water from the vicinity of the WP. The purpose of increasing the thermal loading is to extend the time interval under which dry conditions can be maintained to avoid aqueous corrosion of container materials.

Assuming each WP has the same thermal output, the edges of the EU in Figure 2-3 represent symmetry boundaries. The EU identified in Figure 2-3 is then extended up to the ground surface and down into the saturated zone deep below the repository to construct a 3D model, as shown in Figure 2-4.

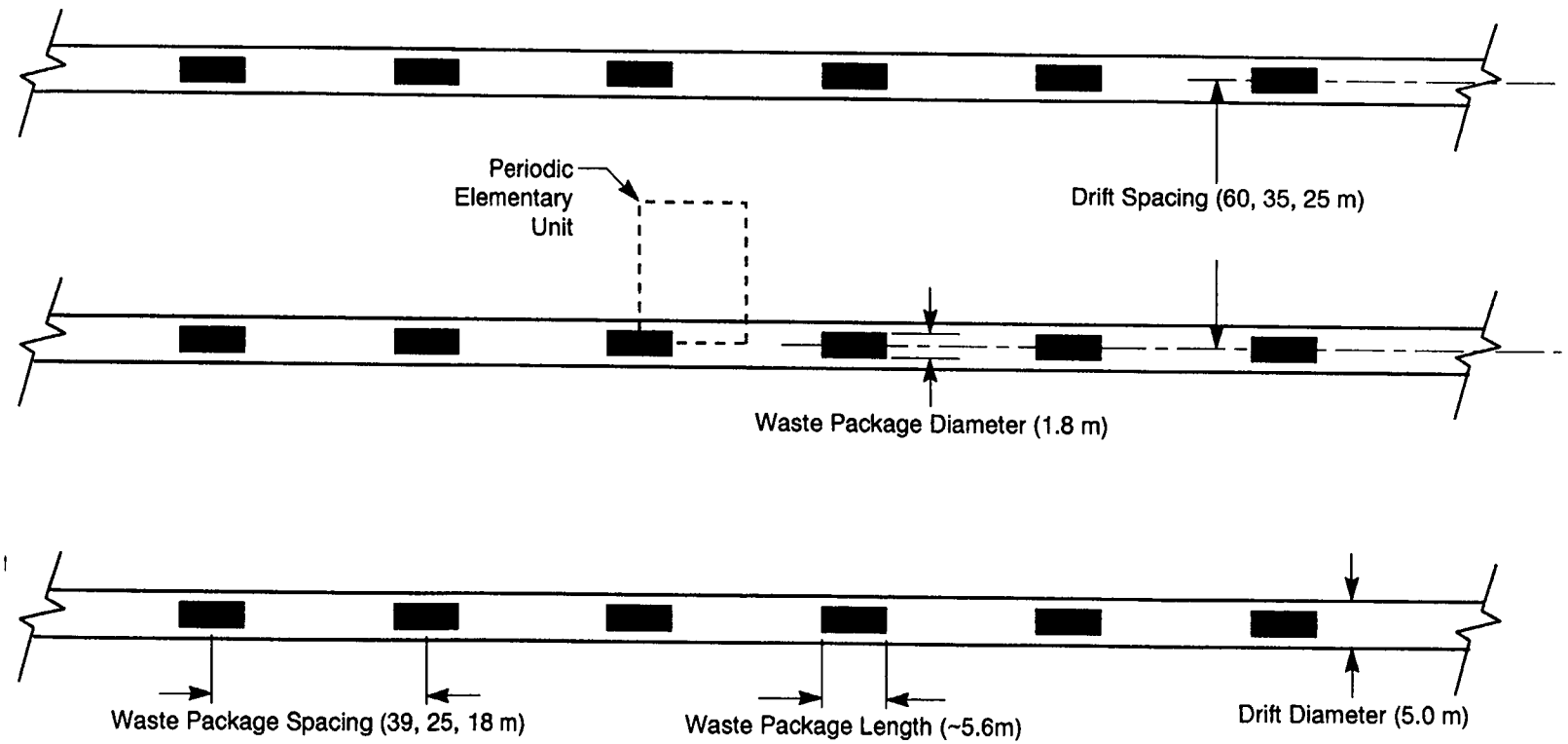

Figure 2-3. Plan view of emplacement drifts

Finite elements are used to discretize the model and describe the WP, invert, backfill, and surrounding geologic media. Only the elements immediately surrounding the WP are shown in Figure 2-4. Backfill elements exist in the model but are not shown in the figure for clarity. Symmetry principles are used to limit the size of the model so that only one-quarter of a package is actually discretized.

The dimensions of the system are design variables and based primarily on the ACD proposed by the DOE (TRW Environmental Safety Systems, Inc., 1996), as discussed in Section 1.2. Only the large WP containing either 21 PWR fuel assemblies or 40 BWR fuel assemblies emplaced inside a MPC, as shown in Figure 1-1, is considered. The packages reside in 5 m diameter drifts. The drift spacing can be either 60, 35, or 25 m, which combined with decreasing WP spacing of 39, 25, or 18 m, yield AMLs of 20, 40, or 80 MTU/acre, respectively. The mesh for the 40 MTU/acre case is shown in Figure 2-4 as an example.

Six distinct thermohydrologic units (e.g., Topopah Spring, Calico Hills) are included in the model which extends from the ground surface (350 m above the repository horizon), to the water table (250 m below the repository), and beyond (750 m below the water table). The elevations and thermophysical properties are listed by Manteufel (1996) and included in Section 5, Table 5-2. They are consistent with those used in other studies (Wilson et al., 1994; TRW Environmental Safety Systems, Inc., 1995).

In this work, three major factors are varied to affect the thermohydrologic environment of the WP: (i) AML, (ii) ventilation during the operations period, and (iii) emplacement of backfill after the operations period. During the operations period, which covers the first 100 yr following emplacement of the waste, the drifts are not backfilled and ventilation may or may not be employed. If ventilation is employed, a steady flow of relatively cool, dry surface air would flow through the emplacement drifts and be exhausted through vertical ventilation shafts. This air flow will remove some heat and moisture from the subsurface facility. At 100 yr, ventilation is anticipated to be halted and the repository permanently closed. At this time, backfill material may or may not be used to fill the emplacement drifts. The backfill material is assumed to be a crushed, unconsolidated rock (presumably Topopah Spring tuff) which would have a relatively low bulk thermal conductivity.

The ABAQUS code (Hibbitt, Karlson & Sorenson, Inc., 1994) is used to simulate the heat transfer. Models of both sensible and latent heat removal, as well as groundwater vaporization and removal, are implemented in the model. In the emplacement drifts, effective thermal conductivity models are used for both backfilled and unbackfilled cases. The unbackfilled thermal conductivity model is based on both thermal radiation and natural convection heat transfer from the WP to the drift wall surface. The heat transfer is dominated by thermal radiation, especially as the ambient temperature within the drift increases above 100 °C. The unbackfilled effective thermal conductivity, based on previous work (Manteufel, 1996), is estimated to be given by:

$$k_{eff} = 30\ k_a + 2\ \epsilon\ D_{wp}\ \sigma\ T^3 \ln\left(\frac{D_d}{D_{wp}}\right) \qquad (2\text{-}1)$$

where

k_{eff} = effective thermal conductivity [W m^{-1} $°K^{-1}$]

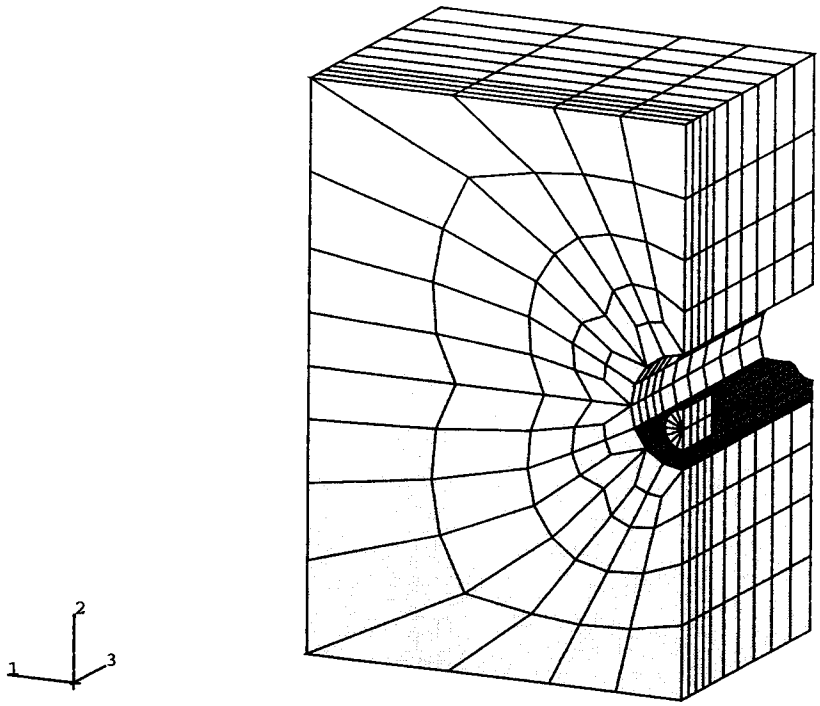

Figure 2-4. Three-dimensional model used to predict waste package thermohydrologic environment

k_a = thermal conductivity of air [W m^{-1} $°K^{-1}$]
ϵ = emissivity of surface of the WP
D_{wp} = WP diameter [m]
σ = Stefan-Boltzmann constant [5.67×10^{-8} W m^{-2} $°K^{-4}$]
D_d = drift diameter [m]
T = local absolute temperature [°K]

The backfill thermal conductivity is assumed to be that of loose, crushed rock. The effective conductivity model includes both stagnant conduction and thermal radiation. The stagnant conduction model is based on Hadley's model (1986) for granular, unconsolidated, two-phase mixture, in which solid grains represent one of the phases. In addition, an effective radiative conductivity model based on models developed for packed particle beds is used. The backfilled effective conductivity model is estimated to be given by:

$$k_{eff} = \frac{\phi f k_a + (1 - \phi f) k_m}{1 - \phi(1 - f) + \phi(1 - f) k_m / k_a} + 4 \epsilon d_p \sigma T^3 \qquad (2\text{-}2)$$

where

ϕ = porosity of crushed backfill

f = a model parameter (=0.8 based on Hadley, 1986; Verma et al., 1994)

k_m = matrix conductivity of intact rock particles [W m^{-1} $°K^{-1}$]

ϵ = emissivity of rock particle surfaces

d_p = mean size of intact rock particles [m]

Both effective conductivity models are temperature dependent and range from 5 to 20 W m^{-1} $°K^{-1}$ for temperatures varying from 20 to 220 °C for the unbackfilled case, and from 0.2 to 0.6 W m^{-1} $°K^{-1}$ from 20 to 320 °C for the backfilled case. The backfilled values are consistent with those published by Ryder et al. (1996), who report measurements from 0.58 to 0.74 W m^{-1} $°K^{-1}$ for temperatures up to 700 °C.

The thermal output of the WP is based on the type, amount, and age of the waste. As noted in Section 1.2, the largest WP currently being considered in designs would have the capacity to carry either 21 PWR assemblies or 40 BWR assemblies. A representative PWR assembly contains about 0.45 metric tons of uranium (MTU) and has experienced an average burnup in the reactor of 42 GWd/MTU. A representative BWR assembly contains 0.19 MTU and has a burnup of 32 GWd/MTU. The age of either fuel is assumed to be about 26 yr from the time of removal from the reactor to that of emplacement. Based on the number and types of reactors currently operating, it is expected that about 65 percent of the waste will be PWR and 35 percent will be BWR. For analysis purposes, a blended representative package is used for the thermal output of the WP. This simulated package has an average of 8.8 MTU of waste with 38.5 GWd/MTU burnup. The thermal output of the WP is based on published data (U.S. Department of Energy, 1987). The thermal output is applied as a time-dependent volumetric heat source to the WP.

The strength of the volumetric heat source is calculated as:

$$Q'''(t) = \frac{1}{V_{wp}} \left[Q_{wp}(t) - \frac{\dot{m}_a c_a \left(T_{a,o} - T_{a,i} \right)}{N_{wp}} - \frac{\dot{m}_v h_{fg}}{N_{wp}} \right] \qquad (2\text{-}3)$$

where

$Q'''(t)$ = effective volumetric heat source [W m^{-3}]

$Q_{wp}(t)$ = radiogenic heat output of the WP [W]

V_{wp} = volume of WP within which heat output is modeled [m^3]

$\dot{m}_a$ = mass flow rate of ventilation air through repository [kg s^{-1}]

c_a = specific heat of air [J kg^{-1} $°K^{-1}$]

$T_{a,o}$ = outlet air temperature [°K]

$T_{a,i}$ = inlet air temperature [°K]

N_{wp} = number of WPs in repository

$\dot{m}_v$ = groundwater vaporization and removal rate from repository [kg s^{-1}]

h_{fg} = heat of vaporization of water [J kg^{-1}]

The thermal model has three components: (i) internal radiogenic heat generation rate, (ii) heat removal by sensible heating of ventilation air, and (iii) heat removal by latent heating of vaporized groundwater. The groundwater vaporization rate depends on the extent of the dryout which is discussed elsewhere (Manteufel, 1996). If ventilation is used, then a portion of the thermal energy will be removed from the repository. If ventilation is not employed, then there is no removal of heat and the volumetric heat source has only the first term of Eq. (2-3) due to radiogenic heat.

The model is used to predict the WP temperature, the drift wall temperature, and the RH at the WP surface. The WP temperature and RH are required inputs for the corrosion and release models. The RH is defined as the ratio of the actual vapor pressure to the maximal vapor pressure at the WP surface:

$$RH = \frac{P_v(\min[T_b, T_w])}{P_v(T_{wp})} \tag{2-4}$$

where

P_v	=	vapor pressure which is a function of temperature [Pa]
T_b	=	boiling point temperature [~370 °K at repository]
T_w	=	drift wall temperature [°K]
T_{wp}	=	WP surface temperature [°K]
min[,]	=	minimum of two values

Below boiling conditions, the definition of RH used in Eq. (2-4) is equivalent to the mole fraction definition of RH frequently found in thermodynamic textbooks (e.g., van Wylen and Sonntag, 1978; Moran and Shapiro, 1992). RH is often defined as the actual mole fraction of water vapor in the air, divided by the maximal mole fraction of water vapor in the air *at the same temperature and pressure* conditions. Below boiling conditions, the mole fractions are related to the vapor partial pressures so that this definition is equivalent to that of Eq. (2-4). Above boiling conditions, the vapor partial pressure can not exceed the atmospheric pressure at the location of interest. When the WP temperature exceeds the boiling point, then it is preferable to define RH as a ratio of vapor pressure, which is consistent with much of the literature (Hartman, 1991; Bejan, 1988; Fyfe, 1994). For both above and below the boiling point, RH is defined as shown in Eq. (2-4). More detailed thermal results are described in Section 5.1.1 for the example problem calculations.

2.3 ENVIRONMENT MODEL

The chemical composition of fluid which is able to come in contact with the WP is an important consideration in modeling WP integrity and radionuclide transport. The environmental model, developed within the Evolution of the Near Field Environment (ENFE) KTI, provides the chemical environment as a function of time in the immediate neighborhood of the WP. These chemical parameters, which include solution pH, oxygen fugacity, chloride and bicarbonate concentration, dissolved silica, and alkalinity among other environmental factors, can have important consequences on the rate of corrosion of the WP, dissolution of SF, and the formation of alteration products. Of special concern in terms of chemical composition in a partially saturated environment are evaporative effects produced by the heat released from the WP.

To estimate the expected changes in chloride concentrations due to evaporation, a simple upper bound on the chloride concentration may be derived by assuming equilibrium with halite for example. As evaporation takes place, the sodium and chloride concentrations must remain approximately proportional to one another. Therefore,

$$a_{Na^+} = \alpha a_{Cl^-} \tag{2-5}$$

where α is the constant of proportionality and a_{Na^+} and a_{Cl^-} are sodium and chloride activities. Equilibrium with halite implies:

$$K = a_{Na^+} a_{Cl^-} = \alpha a_{Cl^-}^2 \tag{2-6}$$

where K is the equilibrium constant. Therefore,

$$a_{Cl^-} = \sqrt{\frac{K}{\alpha}} \tag{2-7}$$

The log K for halite at 100 °C is equal to 1.578. Taking $\alpha = 11.11$, derived from J-13 well-water (see Table 2-1), it follows that $a_{Cl^-} = 1.85$ molal and $a_{Na^+} = 20.5$ molal. To estimate concentrations, activity coefficient corrections, which could be substantial at these relatively large concentrations, must be taken into account. If the sodium concentration is lowered by precipitation of other Na-bearing solids, the chloride concentration in equilibrium with halite could be substantially increased and the concentration of sodium reduced.

The maximum silica concentration estimated from equilibrium with quartz, chalcedony and cristobalite gives, respectively, $a_{SiO_2} = 0.000835$, 0.00137, and 0.00218 molal. By contrast, J-13 well water has a silica concentration of 0.0011 molal.

Table 2-1. Initial fluid composition and pH corresponding to J-13 well-water (adapted from Harrar et al., 1990)

Species	Molality
Ca^{+2}	2.9e-4
Na^+	2.0e-3
K^+	1.4e-4
HCO_3^-	2.7e-3
SiO_2(aq)	1.1e-3
Cl^-	1.8e-4
pH	6.9

Bounds on the pH are more difficult to obtain. Likewise calcium and carbonate have no obvious upper bounds since their concentrations will be pH-dependent.

In order to provide a more precise estimate of the near-field fluid composition, the computer code MULTIFLO, developed within the ENFE KTI, was used to provide quantitative data in tabular form for the EBSPAC code. The code MULTIFLO takes into account transport of reacting chemical constituents coupled to evaporation and condensation processes involving two-phase fluid flow (Lichtner and Seth, 1996; Seth and Lichtner, 1996). The code sequentially couples two-phase fluid flow of liquid water, water vapor, and air, with reactive transport of aqueous and gaseous species. Homogeneous

reactions in the aqueous phase and heterogeneous reactions between the aqueous and gaseous phases are assumed to be in local equilibrium. Mineral reactions are treated irreversibly through prescribed kinetic rate laws.

The environmental model computes temperature as a function of time and the associated moisture redistribution independently, using a repository scale model in contrast to the drift-scale model used by the thermal model described in Section 2.2. In the environmental model, the repository is represented as a single disk-shaped uniform heat source. Therefore, the detailed geometry of the WPs is consequently lost. The fractured YM tuff host rock is described using the equivalent continuum model (ECM) in which fracture and matrix properties are averaged into a single continuum representation. Model predictions indicate the formation of zones of enhanced liquid saturation above and below the repository during the dryout period following emplacement of the waste. As capillary suction draws liquid water towards the heat source, evaporation takes place resulting in an increase in salinity and pH as CO_2 is degassed from solution. In the cooler condensate region, the salinity is expected to decrease as the dilute condensing solution is mixed with the ambient groundwater.

Within the confines of the repository-scale model and the ECM approximation of fracture-matrix interaction, it is not possible to model the eventual return of liquid water from the enhanced saturated zone lying above the repository to the WP. This flow would most likely take place along open fractures in the form of gravity driven flow manifested as dripping. The aim of the MULTIFLO calculations is to estimate the composition of the fluid that could come in contact with the surface of the WP.

During the first phase of work in applying MULTIFLO to estimate the near-field environment, a 1D, repository-scale calculation was performed with an AML of 80 MTU/acre based on 26-yr-old fuel with a mix of 65 percent PWR and 35 percent BWR SF. With this heat load, the calculations show that a liquid phase is always present and complete dryout does not occur following emplacement of the waste. A schematic diagram of the conceptual model used in the calculations is shown in Figure 2-5a. The initial fluid composition corresponds to J-13 well-water as given in Table 2-1. The YM host rock is modeled in these preliminary calculations as pure quartz with 10 percent porosity. This assumption is considered reasonable for the purpose of the calculations presented here which is to estimate the change in salinity and pH caused by evaporation and condensation process. Future work will consider the geostratigraphy used in the thermal model as described in Section 2.2 and, to the extent possible, the compositional differences of the different stratigraphic layers. The temperature profile shown in Figure 2-5b is computed at different times as indicated in the figure. The plateau at approximately 100 °C indicates the presence of a heat pipe effect. The saturation profile is shown in Figures 2-6a and 2-6b for various times varying from 10 to 10,000 yr. Above and below the repository horizon, zones of enhanced moisture form as vapor condenses. Results for pH and chloride concentration are shown in Figures 2-6c and 2-6d plotted as a function of distance for times of 10, 50, 250, and 500 yr. The pH increases to approximately 10 in the vicinity of the repository at 250 yr and then begins to decrease as the repository cools. The chloride concentration increases by an order of magnitude before it begins to decrease. The calculated pH values and chloride concentrations are provided as look-up tables for the EBSPAC calculations.

Future work will consider the very-near-field environment at the drift scale, as well as 2D calculations at the repository scale. Sensitivity analyses will be performed to investigate the effect of different heat loads, host rock compositions and mineral reaction rates, and initial fluid compositions.

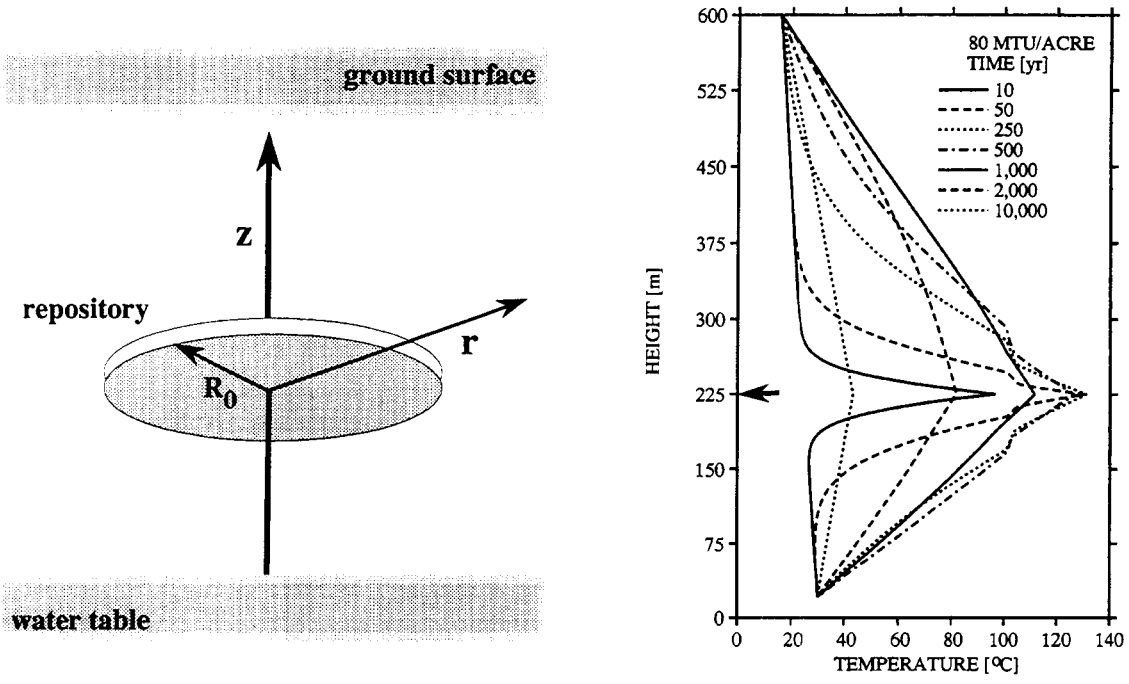

Figure 2-5. (a) Conceptual model of the repository and near field used in the environment model and (b) computed temperature profile at different times. The arrow indicates the repository level.

2.4 AIR OXIDATION MODEL

The DOE concluded that the oxidation of the outer steel container by hot air will be negligible at the YM repository site (TRW Environmental Safety Systems, Inc., 1995). Oxidation of steel can take place under relatively dry conditions in the presence of air at relative humidities lower than 70 percent and temperatures up to 200 to 250 °C. The oxide layers formed under such conditions are considered to protect the container against further oxidation. However, the possibility exists that the oxide will grow continuously at a constant rate and that oxidation will become highly localized. Unprotective or localized, dry air oxidation may lead to a much deeper oxidation than the current DOE assessment, which may adversely affect the long-term container integrity in a dry air environment.

The lack of protection by the oxide layers as it grows may be due to its porous, amorphous, defective, or transformed crystalline structure. These changes may accelerate transport of metal cations, oxygen anions and vacancies for the continuous oxide growth. Localized dry oxidation includes internal oxidation and intergranular oxidation. In the case of internal oxidation, the oxide forms as islands in the metal underneath the uniform oxide layer whereas in intergranular oxidation, the oxide forms preferentially along grain boundaries. Localized dry oxidation takes place by mass transport through short-circuit diffusion paths, such as interfaces between metal and oxide (or other inclusions and

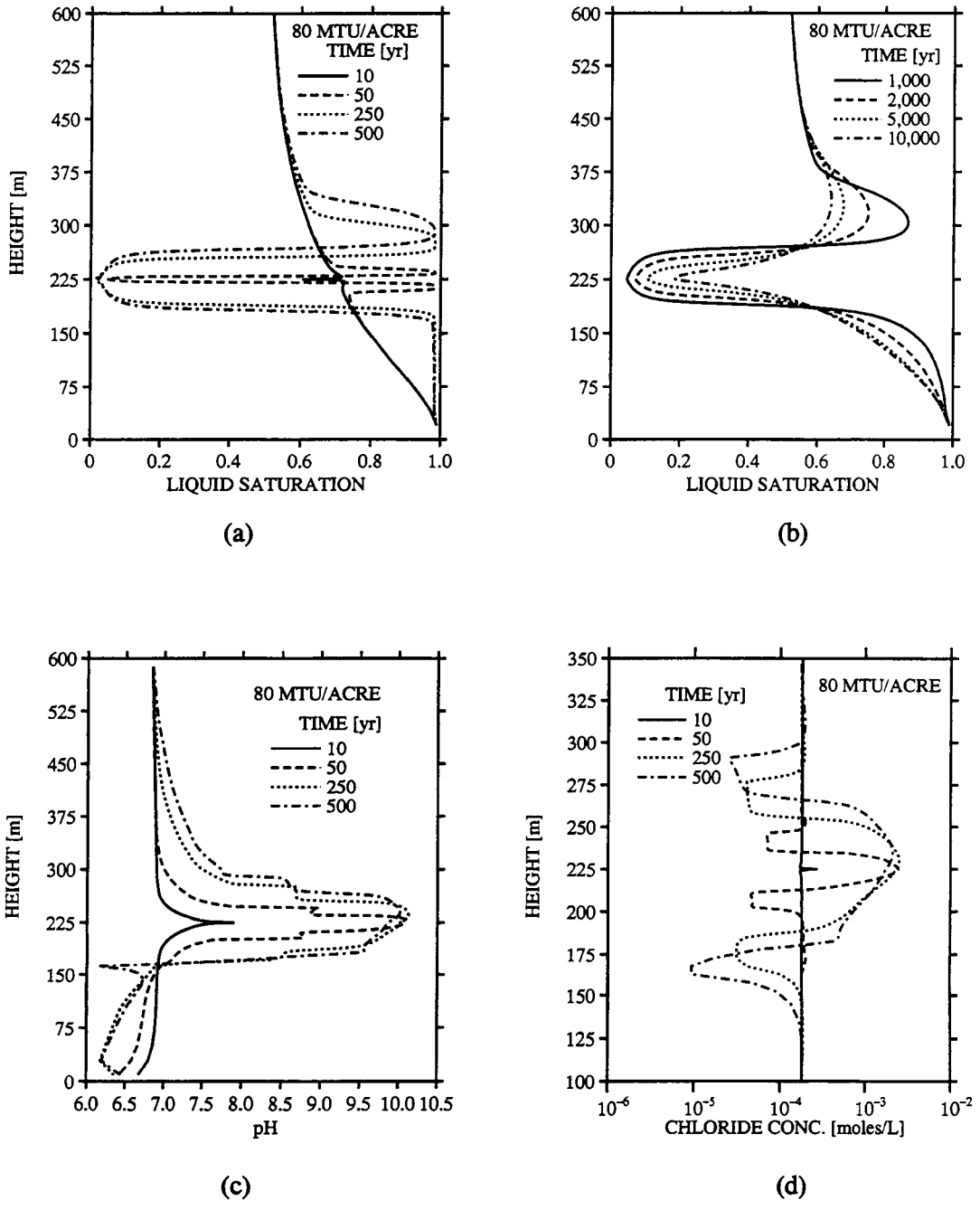

Figure 2-6. Computed MULTIFLO calculations at different times: (a) and (b) saturation profiles, (c) pH profile, and (d) chloride concentration profile

precipitates) or grain boundaries. Therefore, localized dry oxidation can penetrate into the metal deeper than uniform dry oxidation. These characteristics of dry-oxidation have been recently discussed in detail (Ahn, 1996).

Literature data for the candidate carbon and low-alloy steels, listed in Table 1-1, is sparse but is available for other iron-based alloys indicating the existence of unprotective oxides and the occurrence of internal oxidation and intergranular oxidation (Grabke et al., 1991; References in Table 2-2). Data summarized in Table 2-2 (Ahn, 1996) were mostly obtained in tests conducted at temperatures above 600 °C. Based on these data, bounding estimates of the dry oxidation of candidate overpack materials such as C-Mn (A516 Grade 55) steel and 3Cr-0.5Mo (A387 Grade 22) low-alloy steel can be made for up to 10,000 yr at 100 to 200 °C. The evaluation assumes that iron oxides themselves are not protective after extended oxidation times. Due to the lack of relevant data for the candidate alloys, other steels with higher concentrations of alloying elements were evaluated instead.

Stresses associated with volume expansion as a result of oxide formation are calculated using a linear elastic formula (McClintock and Argon, 1966). The volume expansion is about 30 percent in iron-based alloys. The calculated stresses exceed fracture stresses of the alloys and their oxides. At lower temperatures, this tendency is more likely because of less stress recovery. The original and modified Wagner criteria (Nesbitt, 1989) suggest easier internal oxidation at lower temperatures, or with less amounts of alloying elements. Shida and Moroishi (1992) suggest that the tendency to intergranular oxidation could be insensitive to temperature. However, the extent of intergranular oxidation in the candidate materials as a consequence of the lower Cr content is unclear. Less Cr in the alloy will deplete Cr along grain boundaries faster, which, in turn, may allow faster oxygen transport and, as a result, enhance internal and intergranular oxidation. On the other hand, in iron and low-alloy steels, oxidation may not involve inward diffusion of oxygen but outward diffusion of cations.

Internal oxidation and intergranular oxidation can be predicted semiquantitatively. For the predictions, kinetic data obtained for Fe-1Mn and Fe-1Mn-1C alloys, alloy 800 (Fe-10Cr-32Ni), and stainless steels at temperatures above 600 °C are extrapolated to 150 and 200 °C to calculate penetration depths after 10,000 yr of exposure, as shown in Table 2-2. The parabolic law derived from Wagner's theory was used in the extrapolation. An activation energy of 84.6 kJ/mol (20.2 kcal/mol) was selected as a lower bound for the grain boundary diffusion of oxygen. This value corresponds to one half of the activation energy for matrix diffusion of oxygen in γ-iron (Bergner, 1983) and it was selected based on assumptions of Shida and Moroishi (1992), Whittle et al. (1982), and Shewmon (1963) regarding enhanced diffusion of interstitial impurities along grain boundaries. Table 2-2 shows the results of these calculations in which penetrations up to 188 μm in 10,000 yr were estimated.

However, the data quoted in Table 2-2 was obtained above 600 °C, temperatures at which mobile species include not only interstitial oxygen ions but also substitutional metal ions. At lower temperatures, substitutional metal ions are expected to be practically immobile. If only interstitial oxygen ions had been allowed to move, the actual penetration could have been deeper than the case of simultaneous diffusion of oxygen ions and metal ions.

For the calculations of the formation of intergranular oxide in EBSPAC, a mathematical model developed by Oishi and Ichimura (1979) is used, in which oxygen diffusion in the matrix and along the grain boundary in an infinite 1D body are calculated simultaneously. The main assumptions in the calculations are: (i) effects of external oxide are negligible; (ii) oxygen diffuses in metallic phases near

Table 2-2. Data on internal and intergranular oxidation of various alloys and extrapolated penetration depth values at typical repository temperatures (Ahn, 1996)

Materials	Mode	Temperature (°C)	Time (hr)	Penetration Depth (μm)	Reference	Extrapolated Penetration* (μm)	
						200 °C	150 °C
Stainless Steels	Internal	700	1000	100	Otsuka and Fujikawa, 1991	123	35
Fe-1Mn and Fe-1Mn-1C	Internal	1000	30	90	Mayer and Smeltzer, 1973	188	53
Fe-10Cr-34Ni	Intergranular	600	1000	40	Newcomb and Stobbs, 1991	89	25
Fe-21Cr-32Ni (varying Al addition)	Internal (a) Intergranular (b)	900	3000	20 (a) 90 (b)	Shida and Moroishi, 1992	7 (a) 32 (b)	2 (a) 9 (b)
Stainless steels Fe-20Cr-19Ni-4Al and type 314 SS	Internal	1100	360	30	Tasovac et al., 1989	14	4
* — 10,000 yr							

the interface between grain boundary oxide and metal; and (iii) oxygen also diffuses into metallic matrices from grain boundaries. The distance of oxygen penetration in the metal is then represented by

$$Y_p = \left[\frac{4\ D_l}{r_g\ \delta\ D_g} \sum_{n=1}^{\infty} \exp\left(- \frac{D_l\ n^2\ \pi^2\ t}{r_g^2} \right) \right]^{-1/2} \qquad (2\text{-}8)$$

where

D_l = matrix diffusivity [cm^2/s]
D_g = grain boundary diffusivity [cm^2/s]
δ = the thickness of grain boundary ($\approx$0.7 nm, based on Lobnig et al., 1992)
r_g = the grain radius ($\approx$10 μm for cast steel, based on Ahn and Soo, 1983; 1984)

The value of D_l can be calculated from

$$D_l = 5.75\ \exp\left(- \frac{169.1}{RT} \right) \qquad (2\text{-}9)$$

where T is in $°K$, and R is in kJ mol^{-1} $°K^{-1}$. This expression is obtained from measurements of diffusion of oxygen in γ-iron (Kedves and Beke, 1983).

A range of D_g values can be estimated by assuming that the activation energy for D_g may vary from 0.5 to 0.8 of that for D_l as expected by comparing data for various metals (Shida and Moroishi, 1992; Whittle et al., 1982; Shewmon, 1963). Because oxygen is an interstitial element, the difference between D_g and D_l is expected to be less significant than if it were a substitutional element. Nevertheless, the lower-bound value of 0.5 is included because grain boundaries can open up due to stress buildup. The pre-exponential term of D_g is determined assuming that the values of D_g and D_l have a certain ratio at high temperatures. The (D_g/D_l) ratio has been observed to vary from 1 to 10^5 (Lobnig et al., 1992; Whittle et al., 1982) at 1,000 °C. This variation determines the pre-exponential term, D_{go}, in the grain boundary diffusivity of oxygen. The range of pre-exponential terms arises strictly from data uncertainties rather than from uncertainties associated with diffusion processes.

While Eq. (2-8) yields penetration distance of oxygen along grain boundaries, it does not directly address oxide formation. There are several uncertainties in estimating intergranular oxide depth: (i) oxygen diffusion may simply cause oxygen embrittlement due to oxygen segregation to grain boundaries without the formation of an oxide, (ii) the kinetics of oxide formation are not well known at lower temperatures, (iii) oxygen consumption as a result of oxide formation could diminish the localized penetration, and (iv) there would be some retardation of oxygen diffusion by the external oxide. To bound these uncertainties, an extremely simple diffusion distance (square root of diffusivity $\times$ time) can be calculated. Assuming a value of D_{go} equal to 2.0 cm^2/s, a penetration distance of 5.4 cm is obtained after 10,000 yr exposure at 150 °C using an activation energy of 84.6 kJ/mol, which decreases to approximately 40 μm if an activation energy of 134.8 kJ/mol is used.

2.5 MODEL FOR HUMID AIR AND AQUEOUS CORROSION

Corrosion of steel containers in the presence of air at a high RH, as expected under repository conditions, bears certain similarities with atmospheric corrosion. For this reason, corrosion of WPs in humid air has been evaluated in TSPA-95 (TRW Environmental Safety Systems, Inc., 1995) using data from atmospheric corrosion tests as the main database and making allowance for the time of wetness. However, there are significant differences that must be noted. First, in addition to the effect of seasonal fluctuations in temperature and RH which is related to the time of wetness (Fyfe, 1994), corrosion under outdoor atmospheric conditions exhibits a quasi-periodic variation in the environmental parameters, characterized by daily, alternating wet and dry periods (Mattsson, 1982). On the other hand, humid air corrosion under repository conditions may exhibit very irregular, and difficult to predict, wet and dry periods, until a liquid film is stabilized on the metal surface, above a critical RH, when the temperature of the surface drops below 100 °C. Second, after the dry period has lapsed, temperatures decreasing from around 100 °C can be expected under repository conditions whereas outdoor atmospheric corrosion occurs at temperatures that reach at the most 40 °C. Third, although the container surface is only exposed to humid air under almost-stagnant conditions prior to backfilling, particles of a solid phase in contact with the metal surface after backfilling increase the complexity of the metal/air interface, affecting the corrosion behavior by creating crevices and other irregularities. Finally, unlike atmospheric corrosion specimens from which the TSPA-95 corrosion model was derived, the container surface is a heat-transfer surface with an outward flux of heat over long periods of time.

Atmospheric corrosion takes place only when the metal surface is covered by a water film. Water can be physically adsorbed to the metal surface in molecular form or it can be chemically bonded in a dissociated form which results in the formation of metal-hydroxyl bonds (Leygraf, 1995). Both molecular and dissociative bonding occur on metal oxides. The metal-hydroxyl film is actually quite protective and can be formed at low values of RH (approximately 20 percent). As shown in Table 2-3, RH determines the characteristics and thickness of the water film.

Table 2-3. Approximate number of water monolayers versus relative humidity (Leygraf, 1995)

RH (%)	Number of Water Monolayers
20	1
40	1.5–2
60	2–5
80	5–10

At approximately 40 percent RH, an additional highly immobile water layer is adsorbed onto the metal-hydroxyl film. The critical RH above which atmospheric corrosion of most metals occurs closely coincides with the RH necessary for the formation of multiple water monolayers and the liquid film behaves in a manner similar to bulk water. Under these conditions, atmospheric corrosion is governed by the same electrochemical laws which are applicable to corrosion of metals immersed in an aqueous electrolyte.

However, several factors can decrease the critical RH required to form a multilayer surface water film. Particulate matter from the air can deposit on the surface and promote the adsorption of water (a similar effect can be expected from particles of backfill material). Similarly, the deposition of hygroscopic salts on the metal surface can substantially decrease the critical RH necessary to form a water film. A list of hygroscopic salts and the RH of air in equilibrium with their saturated salt solutions is given as an example in Table 2-4 (Fyfe, 1994; Lide, 1990). Lastly, capillary condensation of water can occur in the pores of a thick oxide layer according to the following expression (Fyfe, 1994):

Table 2-4. Relative humidities of air in equilibrium with various saturated solutions of salts relevant to the near-field environment (Fyfe, 1994; Lide, 1990)

Solid Salt Phase	Temperature (°C)	Relative Humidity (%)
$Na_2SO_4 \cdot 10H_2O$	20	93
$Na_2CO_3 \cdot 10H_2O$	18.5	92
$FeSO_4 \cdot 7H_2O$	20	92
$Na_2CO_3 \cdot 10H_2O$	24.5	87
KCl	20	86
NaCl	20	76
$NaNO_2$	20	66
$FeCl_2$	20	56
$CaCl_2 \cdot 6H_2O$	5	39.8
$CaCl_2 \cdot 6H_2O$	10	38
$CaCl_2 \cdot 6H_2O$	18.5	35
$CaCl_2 \cdot 6H_2O$	20	32.3
$CaCl_2 \cdot 6H_2O$	24.5	31
NaCl, KNO_3, and $NaNO_3$	16.39	30.49
$LiCl \cdot H_2O$	20	15

$$p = p_0 \exp\left(-\frac{2\sigma M}{dRTr}\right) \qquad (2\text{-}10)$$

where

p = saturated vapor pressure in the pores
r = pore radius
p_0 = saturated vapor pressure above a plane surface
σ = surface tension of the liquid
T = absolute temperature
R = gas constant
d = density of the liquid

M = molecular weight of the liquid

Iron and steel exhibit a primary critical RH of around 60 percent, similar to most metals (Fyfe, 1994). Above 60 percent RH, corrosion proceeds at a slow rate, but at 75–80 percent RH the corrosion rate sharply increases. This secondary critical RH is attributed to capillary condensation of water in the pores of the solid corrosion products. The water films that form on the metal surface usually contain a variety of contaminants, including trace amounts of Cl^- and other soluble species such as CO_2 that increase the electrical conductivity and decrease the pH of the film, leading to an increase in the dissolution of the iron or steel (Leygraf, 1995).

Initially the dry steel surface is oxidized in air and a mixture of oxides (Fe_2O_3 and Fe_3O_4) and oxyhydroxides (FeOOH) can be formed. The main products are γ-FeOOH (lepidocrocite) and α-FeOOH (goethite), that by aging can be transformed into $Fe_2O_3 \cdot xH_2O$. When exposed to water the Fe(III) species in the oxide scale are reduced by Fe^{2+} cations, creating a semiconducting layer of magnetite (Fe_3O_4) rich in Fe^{2+} species (Stratmann et al., 1990). The electrochemical nature of this process is well established and involves an autocatalytic process that can be expressed in simple terms as

$$4\ Fe_2O_3 + Fe^{2+} + 2\ e^- = 3\ Fe_3O_4 \qquad (2\text{-}11)$$

followed by the electrochemical oxidation of magnetite by oxygen

$$3\ Fe_3O_4 + 0.75\ O_2 = 4.5\ Fe_2O_3 \qquad (2\text{-}12)$$

The net result is the formation of loosely attached corrosion products enriched in Fe^{3+} cations. Oxygen, diffusing through the electrolyte layer, is reduced at the oxide solution interface according to the following reaction

$$O_2 + 2H_2O + 4e^- \Rightarrow 4OH^- \qquad (2\text{-}13)$$

Under acidic conditions the reduction of hydrogen ions also takes place as follows

$$2H^+ + 2e^- \Rightarrow H_2 \qquad (2\text{-}14)$$

These cathodic reactions [(2-11), (2-13), and (2-14)] are coupled to the anodic dissolution of iron to Fe^{2+} cations

$$Fe \Rightarrow Fe^{2+} + 2e^- \qquad (2\text{-}15)$$

followed by their hydrolysis

$$Fe^{2+} + H_2O \Rightarrow Fe(OH)^+ + H^+ \qquad (2\text{-}16)$$

The reaction (2-16) promotes acidity in the liquid film which becomes enriched in soluble corrosion products. Anodic dissolution proceeds at a rate controlled by the diffusion of oxygen through a thin electrolyte layer, followed by its reduction. However, as the surface dries the thickness of the water layer decreases, and hence, the diffusion path for oxygen decreases whereas the ionic strength of the

electrolyte increases. The consequent increase in the oxygen reduction rate anodically polarizes the actively corroding surface and increases the corrosion rate. Further hydrolysis of $Fe(OH)^+$ leads to the formation of insoluble corrosion products which precipitate out of the electrolyte layer (Stratmann et al., 1990). As noted above, upon drying the Fe(II) corrosion products are slowly oxidized to Fe(III) by air and when rewetting occurs, the entire process is repeated. Numerous wet and dry cycles increase the formation of corrosion products which initially contain Fe(II) species that are subsequently oxidized to Fe(III) species (Misawa et al., 1971). The corrosion rates after numerous wetting and drying cycles has been reported to be 0.2 mA/cm^2 (2.1 mm/yr) during drying and as high as 0.5 mA/cm^2 during the reduction of Fe(III) to Fe(II) immediately after rewetting (Nishikata et al., 1994; Tsuru et al., 1995). Numerous corrosion products can be formed including oxides, hydroxides, sulfates, and carbonates depending on the contaminants in the water film (Graedel and Frankenthal, 1990). The presence of Cl^- in the environments promotes the formation of β-FeOOH (akaganeite) and greatly enhances the corrosion rate. If a backfill is present the formation of pits or other irregularities in the corroding surface may increase substantially, particularly under slightly alkaline conditions ($pH > 8.0$).

In the presence of an aqueous phase, corrosion of steels is an electrochemically controlled process which could be relatively uniform at pH lower than neutral or localized under slightly alkaline conditions promoting passivity. It must be noted that in EBSPAC, in contrast to the approach used by DOE in TSPA-95 (TRW Environmental Safety Systems, Inc., 1995), for simplicity no distinction is made between humid air corrosion and aqueous corrosion. It is assumed that after a liquid film is stabilized on the metal surface, depending on the chloride concentration and pH, corrosion can occur uniformly or become localized under slightly alkaline conditions ($pH > 8.0$) once a critical potential is reached. In this latter case, the integrity of the container is affected by the occurrence of localized corrosion and the rate of penetration of the container wall.

The corrosion models calculate the rates of uniform corrosion and localized corrosion following the approach adopted previously in the SCCEX code (Cragnolino et al., 1994). The dominant corrosion process at any given time is dictated by the corrosion potential and the appropriate critical potential for that process. The corrosion potential is the mixed potential established at the metal/solution interface when a metal is immersed in a given environment. For example, if the corrosion potential exceeds the critical potential for pit initiation, pits are assumed to initiate and grow. If the corrosion potential falls below the repassivation potential, previously growing pits are assumed to cease growing and the material passivates, corroding uniformly at a very low rate through a passive film. On the basis of experimental evidence obtained for alloy 825 in simulated groundwater containing 1,000 ppm Cl^- (Dunn et al., 1996), it can be concluded that the potential measured for the initiation of localized corrosion tends to decrease with increasing test time and the repassivation potential can be considered as a lower limit for localized corrosion initiation. No distinction is made between the repassivation potentials for pitting and crevice corrosion. This is justifiable based on literature data (Sridhar et al., 1993) which suggest that critical potentials for the two localized corrosion processes tend to coincide at temperatures higher than 20 °C. The concept of repassivation potential as a threshold condition for the initiation of localized corrosion has been shown to be consistent with a number of field observations (Sridhar et al., 1995).

2.5.1 Model for Determining Corrosion Potential

The corrosion potential is defined as the potential at which the current due to all the cathodic processes is equal to the current due to all the anodic processes including the electrochemical dissolution of the metal (Vetter, 1967), as indicated by

$$\sum_{j=1}^{n} I_{a,j} - \sum_{j=1}^{n} I_{c,j} = 0 \qquad (2\text{-}17)$$

where

$I_{a,j}$ = anodic (oxidation) currents including that of the metal dissolution, which is called the corrosion current, I_{corr}

$I_{c,j}$ = cathodic (reduction) currents

If the anodic and cathodic processes occur uniformly throughout the surface of interest, then Eq. (2-17) can be written in terms of appropriate current densities. However, once localized corrosion initiates, this assumption is no longer valid since physical separation of anodic and cathodic areas occurs. The areas of passive corrosion, in which cathodic reactions take place, must be considered separately from the areas of active corrosion. In the following sections, prior to the occurrence of localized corrosion, uniform distribution of cathodic and anodic areas is assumed for simplicity. Once localized corrosion occurs, it is reasonable to assume that the cathodic reaction takes place on the whole available surface because the pitted area is comparatively very small.

The two cathodic reactions assumed in EBSPAC are the oxygen reduction and hydrogen evolution reactions as given by Eqs. (2-13) and (2-14), respectively. The oxygen reduction reaction is assumed to be a mixture of activation-controlled charge transfer and molecular diffusion-controlled transport processes. As discussed elsewhere (Sridhar et al., 1993b; Cragnolino et al., 1994), the resulting current density can be written as

$$i_{O_2} = -k_{O_2} C_{O_2}^{bulk} \frac{\exp\left(-\dfrac{z_{O_2}\beta F E_{corr}}{RT}\right)}{\left[1 + \left(\dfrac{k_{O_2}\delta \exp\left(-\dfrac{z_{O_2}\beta F E_{corr}}{RT}\right)}{4FD_{O_2}}\right)\right]} \qquad (2\text{-}18)$$

where

k_{O_2} = reaction rate constant for the oxygen reduction reaction

E_{corr} = corrosion potential

F = Faraday constant

β = charge transfer coefficient

R = gas constant

T = temperature in °K

z_{O_2} = number of electrons involved in the process per mole

D_{O_2} = diffusivity of oxygen in aqueous solution

δ = thickness of the diffusion layer (e.g., water film)

$C_{O_2}^{bulk}$ = bulk concentration of oxygen in solution

For the oxygen reduction reaction, the bulk concentration is related to the partial pressure through Henry's law

$$C_{O_2}^{bulk} = K_H p_{O_2} \tag{2-19}$$

where

p_{O_2} = partial pressure of oxygen over the solution

K_H = Henry's law constant for oxygen solubility

The reaction rate constant is not usually measured directly but can be calculated from the exchange current density (Vetter, 1967; Bockris and Reddy, 1970) using the following equation

$$i_{O_2}^0 = k_{O_2} C_{O_2}^{bulk} \exp\left(-\frac{z_{O_2}\beta_{O_2}F}{RT} E_{eq}^{O_2}\right) \tag{2-20}$$

where

$i_{O_2}^0$ = exchange current density

$E_{eq}^{O_2}$ = equilibrium potential for the oxygen evolution reaction

where this equilibrium potential is given by the Nernst equation as

$$E_{eq}^{O_2} = E_0^{O_2} - 2.303 \frac{RT}{F} pH - 0.576 \frac{RT}{F} \log p_{O_2} \tag{2-21}$$

where

$E_0^{O_2}$ = standard electrode potential

For the hydrogen evolution reaction or the water reduction reaction, the cathodic current is assumed to be dictated only by the charge transfer process (Sridhar et al., 1993b; Cragnolino et al., 1994). The cathodic current density is given by

$$i_{H_2O} = -k_{H_2O} \exp\left(-\frac{\beta_{H_2O} z_{H_2O} F}{RT} E_{corr}\right) \tag{2-22}$$

where

k_{H_2O} = reaction rate constant for the water reduction reaction

E_{corr} = corrosion potential

The reaction rate constant can be calculated from the appropriate exchange current density for the hydrogen evolution reaction similar to that shown in Eq. (2-20). The equilibrium potential for water reduction/hydrogen evolution will depend on the bulk concentration of the H^+ ion, which is related to the pH. The temperature dependence of the reaction rate constants for the oxygen evolution and the water reduction reactions are assumed to be given by an Arrhenius-type relationship as shown in Eq. (2-23).

$$k = k_o \exp\left[\frac{E_a}{R}\left(\frac{1}{T_o} - \frac{1}{T}\right)\right] \tag{2-23}$$

where

E_a = activation energy for the particular cathodic reaction

k_o = reaction rate constant at T_o, which is usually 298 °K

The anodic current density is assumed to be equal to the passive current density of the steel and independent of the potential. A survey of the literature on passive metals indicated that the passive current density can be considered independent of temperature, at least as a first approximation, up to approximately 100 °C (Sridhar et al., 1993b). The corrosion potential is then calculated by solving simultaneously for E_{corr} using the passive current density and Eqs. (2-18) and (2-22).

The same approach can be used to calculate the corrosion potential of the inner container of a bimetallic structure. In this case, the galvanic effects due to the anodic polarization of the external corrosion-allowance type material must be included in the calculations. For a WP with two container materials wherein the outer container is assumed to develop through-wall defects, the areas of the outer container and the exposed inner container must be considered in Eq. (2-17). Such analyses of the effects of through-wall penetrations of various sizes on the outer container will be performed in future versions of the EBSPAC code.

In Version 1.0β of EBSPAC, a simplified approach is used to account for galvanic coupling effects between the outer and inner containers. The corrosion potential of the galvanic couple formed when the outer container is penetrated by a pit, E_{corr}^{wp}, is estimated by using experimentally measured values of the potential of the bimetallic couple, E_{couple}, for a well-defined area ratio between both components. Then E_{corr}^{wp} is determined through a linear combination of E_{couple} and E_{corr} of the outer container, as calculated by the code at the time of through-wall penetration of the outer container, according to the following expression

$$E_{corr}^{wp} = (1-\eta)\, E_{corr} + \eta\, E_{couple} \tag{2-24}$$

where

η = efficiency of the galvanic coupling (which must fulfill the condition $0 \le \eta \le 1$)

2.5.2 Models for Pitting and Crevice Corrosion

Empirically derived equations are used in EBSPAC for the dependence of critical potentials on environmental parameters. The pit initiation and repassivation potentials are assumed to depend only on the chloride concentration and temperature. Experimental results (Sridhar et al., 1993a) have shown that the dependence of critical potentials on pH, bicarbonate, and silica is negligible for alloy 825. Both nitrate and sulfate can act as inhibitors if the ratio of nitrate to chloride or sulfate to chloride is sufficiently high (Sridhar et al., 1993a). However, in the current calculations, the effects of these anionic species are not considered. The dependence of the critical potentials on chloride concentration and temperature is given by

$$E_{crit} = E^{\circ}_{crit}(T) + B(T) \log [Cl^-] \quad (2\text{-}25)$$

where the constants $E^{\circ}_{crit}(T)$ and $B(T)$, which are dependent on the material, were considered as linear functions of temperature. It should be noted that $E^{\circ}_{crit}(T)$ is the value of $E_{crit}(T)$ for a Cl^- concentration equal to 1 M. The constants were evaluated for A516 steel and alloy 825 from literature and CNWRA data for initiation and repassivation potentials for both pitting and crevice corrosion (Sridhar et al., 1993a; 1995; Dunn et al., 1996b).

The propagation of pits was considered in a simplified manner by introducing an empirical equation developed by Marsh and Taylor (1988) for carbon steel. In this equation, pit penetration is time dependent and given by

$$P = At^n \quad (2\text{-}26)$$

For the corrosion-resistant material, a constant rate of penetration was considered for pit growth. Recent experimental results (Dunn et al., 1996a) have shown that this is quite conservative since a parabolic rate law was found to apply.

2.6 MECHANICAL FAILURE MODEL

Fracture, as a result of thermal embrittlement of the steel overpack, is an important failure mode to be considered for the new WP design. Thermal embrittlement of low-alloy steels occurs as a consequence of prolonged exposure at elevated temperatures and results in a substantial degradation of specific mechanical properties. One of the important mechanical properties required for a material to be used as a component of the WP is toughness, which is the ability to absorb energy in the form of plastic deformation without fracture. However, toughness is significantly affected by thermal embrittlement, a phenomenon closely related to temper embrittlement. This type of embrittlement is characterized by an upward shift in the ductile-brittle transition temperature (DBTT), measured by the variation of the impact fracture energy for notch specimens as a function of test temperature, as a result of material exposure to the temperature range of 350 to 575 °C through isothermal heating or slow cooling (Vander Voort, 1990). The possibility of thermal aging at temperatures above 100 °C and its potential effect on mechanical properties and embrittlement of disposal steel overpacks has been recently assessed (Cragnolino et al., 1996).

Segregation of impurities, such as Sb, P, Sn, and As, along prior austenite grain boundaries is the main cause of temper embrittlement (Briant and Banerji, 1983). The segregation of P, which in the case of commercial steels is the predominant impurity, promotes fracture of notched specimens upon impact and leads to a change in the low-temperature fracture mode from transgranular cleavage to intergranular fracture. Empirical equations relating embrittlement with chemical composition of steels, in which the effect of alloying elements and detrimental impurities is included, have been reviewed (Cragnolino et al., 1996).

The degree of P segregation can be calculated by applying the McLean's equilibrium segregation theory (McLean, 1957) as a function of bulk phosphorous content and temperature. The fractional monolayer coverage of segregant, X_b, after reaching equilibrium at the grain boundary, is given by the following expression

$$\frac{X_b}{\left(X_b^0 - X_b\right)} = \left[\frac{X_c}{\left(1 - X_c\right)}\right] \exp\left(-\frac{\Delta G_b}{RT}\right) \tag{2-27}$$

where

X_b^0 = fractional coverage at saturation
X_c = concentration in the bulk
R = gas constant
ΔG_b = free-energy for equilibrium segregation at grain boundaries

Druce et al. (1986) found that ΔG_b for pressure vessel steels can be expressed by the following equation

$$\Delta G_b\ (J/mol) = -63{,}000 + 21.0\ T(^\circ K) \tag{2-28}$$

within the range of temperatures of 450 to 550 °C over which equilibrium was rapidly established. At lower temperatures, when the segregant atoms have insufficient time to reach equilibrium, transport by diffusion over the period of thermal aging is considered. The kinetics of segregation, as developed by McLean (1957), can be expressed by

$$\frac{\left[X_b(t) - X_b(0)\right]}{\left[X_b(\infty) - X_b(0)\right]} = 1 - \exp\left(\frac{4Dt}{\beta_b^2 f^2}\right) erfc\left(\frac{4Dt}{\beta_b^2 f^2}\right)^{1/2} \tag{2-29}$$

where

$X_b(0)$ = grain boundary content at t=0 (e.g., in the as-annealed condition)
$X_b(t)$ = grain boundary content at time t
$X_b(\infty)$ = grain boundary content at equilibrium
D = diffusion coefficient at the temperature

The factor $f=a^3b^{-2}$ is related to the atom sizes of the solute and matrix elements, b and a, respectively, and the grain boundary enrichment ratio, β, is defined as the ratio of the solute in the grain boundary to that in the adjacent atom layer of the bulk.

The diffusion coefficient of P in the matrix was derived (Druce et al., 1986) from a compilation of high temperature diffusion data for iron and various steels as

$$D = 0.25 \exp\left[-\frac{200}{RT}\right] \tag{2-30}$$

where D is in cm^2/s, T is in °K, and R is in kJ mol^{-1} $°K^{-1}$.

The modeling results clearly indicate that the equilibrium level of P segregation increases and the rate of segregation decreases as the temperature is decreased, resulting in a maximum P concentration for a given time at an intermediate temperature. The predicted grain boundary segregation can be combined with the embrittling potency of P to predict the kinetics of embrittlement. The amount of P segregation was found by Druce et al. (1966) to be linearly related to the susceptibility to embrittlement as measured through the shift in the DBTT. As discussed in detail (Cragnolino et al., 1996), a predictive approach based essentially on the detrimental role of P segregation seems to be appropriate to assess the long-term effects of thermal aging on mechanical properties at temperatures below 350 °C. This is similar to the approach adopted by Druce and coworkers (Druce et al., 1986; Hudson et al., 1988; Vatter et al., 1993) in their extensive investigation on thermal embrittlement of low-alloy steels, such as A508 and A533B steels, which are used as pressure vessel materials in nuclear power plants. Hudson et al. (1988) have applied this approach for predicting the propensity to thermal embrittlement of 2.25Cr-1Mo (A387 Grade 22) steel, one of the candidate overpack materials. By establishing an acceptance criterion based on a Charpy impact energy level and evaluating the degree of P segregation which corresponds to this energy level, the acceptable bulk P levels of the material for a given exposure time can be estimated as a function of the operating temperature. By assuming a critical value of the impact energy, the expected lifetime for 2.25Cr-1Mo steel with a given P content after isothermal exposure can be determined. The estimation can be extended to account for nonisothermal exposure over a range of temperatures as is the case for the WPs under repository conditions.

Correlations used to estimate fracture toughness, K_{Ic}, based on values of impact energy obtained with Charpy V-notched specimens, have been reviewed (Cragnolino et al., 1996). Using these correlations, it is possible to estimate the fracture toughness values at various temperatures. The consequence of toughness degradation is that the tolerable crack size for a given stress level is reduced. The fracture criterion based on linear elastic fracture mechanics (LEFM) can be expressed in the form

$$K_{Ic} = Y\sigma(a_{cr})^{1/2} \tag{2-31}$$

where Y is a flaw shape parameter which depends on the crack geometry and load distribution. The interaction of material properties, such as the fracture toughness, with the design stress (σ) and critical crack size (a_{cr}) controls the fracture conditions in a component. The critical crack size may decrease during service as a result of the decrease in fracture toughness of the materials and lead to premature failure of components. Calculation based on bounding values of residual stresses or sudden loads associated to seismic events should provide the stress level and, hence, the size of a tolerable crack. This

flaw size can then be compared to the detection limits of nondestructive examination techniques and monitored during the period before permanent closure.

The concept of life assessment has recently been reviewed by Viswanathan (1989). Measurements of subcritical crack growth rate and experimental data on the degree of temper embrittlement and toughness degradation after long-term exposure have been generated and analyzed for use in remaining life prediction models for reactor pressure vessels (Iwadate et al., 1985) and turbine rotors (Swaminathan et al., 1991). Application of these life assessment techniques can be extended to the assessment of the thermal stability and mechanical properties of WP containers.

A successful thermal stability assessment requires sufficient information for the specific material conditions to fully define both the segregation model parameters and the embrittlement potencies. Therefore, to validate the proposed procedure for the thermal stability assessment of the WP containers all of the pertinent material property data necessary to perform the thermal stability assessment should be generated for specific container materials. However, preliminary calculations can be made with the data for pressure vessel steels to introduce the proposed methodology in the assessment of the potential for mechanical failure of the steel disposal overpack. This mechanical failure model is only valid for the outer overpack. For the inner overpack, the LEFM approach may not be valid because of extremely high fracture toughness values. In Version 1.0β of EBSPAC, a simple fracture criterion based on yield strength has been implemented.

2.7 MODELS FOR RADIONUCLIDE RELEASE

The calculation of radionuclide release in EBSPAC is similar to the approach adopted in SOTEC (Sagar et al., 1992) as used in the NRC Iterative Performance Assessment Phase 2 (IPA Phase 2) (Nuclear Regulatory Commission, 1995). However, several modifications have been introduced to simplify models used to describe gaseous and aqueous release. It should be noted that Version 1.0β of EBSPAC only considers radionuclide release from burned-up but intact SF. Since WPs are assumed to contain only SF, no consideration of radionuclide release from glass waste form is made in this analysis.

2.7.1 Gaseous Release

For the sake of simplicity, gaseous release is treated separately from aqueous release. Three different modes of release are included in the calculations of gaseous release.

2.7.1.1 Prompt Release

The prompt release mechanism accounts for C-14 loosely-held in the cladding, the pellet/cladding gap, and the crystallite (grain) boundaries of the irradiated UO_2 pellets. This also accounts for I-129 present in the gap and the pellet intercrystallite boundaries. The prompt release fraction of the inventory of C-14 and I-129 is rapidly released following container failure.

The fraction of C-14 held in the cladding will be released promptly from the ZrO_2 and crud formed during reactor operation. Smith and Baldwin (1993) derived an expression for diffusion out of a layer of finite thickness in a semi-infinite body to obtain the rate of cumulative C-14 release as

$$\frac{dR_z}{dt} = \left(\frac{D_z}{\pi t}\right)^{1/2} C_z \qquad (2\text{-}32)$$

where

R_z = cumulative C-14 release in Ci cm^{-2} sec^{-1}
D_z = effective C-14 diffusivity in cm^2/sec
C_z = C-14 inventory in Ci/cm^3

A regression fit, using data for post-transition oxides, was used to obtain an expression for D_z as follows:

$$D_z \simeq 0.79 \exp\left[-\frac{94.2}{RT}\right] \qquad (2\text{-}33)$$

where D_z is in cm^2/s, T is in °K, and R is in kJ mol^{-1} $°K^{-1}$. In this version of EBSPAC, Eqs. (2-32) and (2-33) are not used because separate calculations demonstrate that release is extremely rapid. Thus, in order to simplify the code, a fixed amount of C-14, which is present in the pellet-cladding gap (Sagar et al., 1992), is allowed to undergo release instantaneously.

2.7.1.2 Oxidation of Cladding

The Zircaloy-2 or Zircaloy-4 cladding of the SF contains C-14 in solid solution as a radionuclide formed by the reaction $^{14}N(n,p)^{14}C$, in which thermal neutrons are captured by nitrogen, usually present as an impurity in zirconium alloys. Most of this C-14 will be released slowly over time because diffusion of C-14 in unoxidized cladding is considered to be very slow (Ahn, 1994). However, C-14 release will be rapid once the cladding is oxidized. Therefore, the rate-limiting step for C-14 release from cladding is cladding oxidation. Recent reviews of the dry oxidation of Zircaloy (Einziger, 1994) suggest that the long-term oxidation kinetics reported by Rothman (1984) would be best described by the following expression:

$$\Delta w = 1.12 \times 10^8 \exp\left[-\frac{12{,}529}{T}\right] t \qquad (2\text{-}34)$$

where

Δw = weight gain in mg/dm^2
t = time in days

By knowing the initial weight of the cladding and surface area, the corresponding C-14 release is determined.

2.7.1.3 Oxidation of UO_2

Oxidation of UO_2 will account for the largest amount of the inventory of the C-14 which is contained in the form of solid solutions, elemental carbon, carbides, and oxycarbides. Separate models for dry oxidation are used for temperatures above and below 250 °C, respectively.

Dry Oxidation of Spent Fuel Matrix to $UO_{2.4}$ Below 250 °C

The SF matrix is oxidized by oxygen in the air from UO_2 to $UO_{2.4}$ at temperatures below 250 °C (Einziger et al., 1992) in a process known as lower oxidation. Moisture in air (dew point $\leq$ 80 °C) has little or no effect on dry oxidation. The lower-oxidation kinetics determine: (i) the surface area of the SF matrix which governs radionuclide release in both dry and aqueous environments; and (ii) the kinetics of C-14 release in dry environments.

Lower oxidation is accompanied by about 3 percent volume contraction which promotes the opening of grain (crystallite) boundaries (Einziger et al., 1992). In dry environments, partially open grain boundaries do not retard the release of radionuclides, mainly C-14, diffusing out from the matrix. Aqueous environments completely disintegrate partially open grain boundaries (Lawrence Livermore National Laboratory, 1995). Consequently, a large surface area from individual grains can be exposed to groundwater promoting matrix dissolution for liquid releases.

Following solid-state atomic diffusion in the unoxidized SF matrix, C-14 can be released to both dry and aqueous environments. Carbon diffusivity in the SF matrix has not been measured to date, but it is considered close to that of oxygen diffusivity because their atomic numbers (i.e., atomic radii) are relatively close. Oxygen diffusivity can be estimated from lower oxidation kinetics because oxygen diffusion is rate-limiting in this case. As a conservative approximation, therefore, lower oxidation kinetics can be regarded as carbon diffusion kinetics (Ahn, 1994). Once the SF matrix oxidizes to $UO_{2.4}$, C-14 release is considered very rapid. Therefore, lower oxidation kinetics are rate-limiting for the kinetics of C-14 release. Although it is assumed that C-14 is present and diffuses as an atomic species, it may also be present in the form of immobile compounds. In this case, no contribution to release can be expected.

The lower oxidation kinetics has been measured experimentally (Einziger et al., 1992). The width of the oxidized zone assuming spherical grains is given by

$$w = (2kt)^{1/2} \tag{2-35}$$

$$k = 1.04 \times 10^8 \exp\left[-\frac{100.5}{RT}\right] \tag{2-36}$$

where

t = time [hr]
k = rate constant [μm^2/hr]
T = temperature [°K]
R = universal gas constant [kJ mol^{-1} $°K^{-1}$]
w = width of the oxidized zone [μm]

In Eqs. (2-35) and (2-36), the mass transport within the SF matrix is not coupled with grain boundary diffusion. The grain boundary diffusion is so rapid that it is essentially instantaneous, and thus Eqs. (2-35) and (2-36) represent only the oxidation kinetics of individual grains. The surface area of the SF matrix is the total surface area of all individual grains in the volume. Conservatively, the amount of C-14 released is equal to the total C-14 inventory in the same volume of the oxidized phase. In reality, C-14 diffusion in the unoxidized matrix will be slower than oxygen diffusion in the oxidized phase. This is because oxide formation consumes oxygen, and oxygen diffuses faster in the oxidized phase. On the other hand, C-14 has a finite diffusivity in the oxidized phase and, hence, is not expected to be released instantaneously. Equation (2-35), as implemented in EBSPAC, may represent a conservative upper bound for the kinetics because of large scatter of experimental data.

Dry Oxidation of Spent Fuel Matrix to U_3O_8 Above 250 °C

At temperatures above 250 °C, the SF matrix is oxidized from UO_2 through $UO_{2.4}$ to U_3O_8 ($UO_{2.67}$) (Einziger et al., 1992). This oxidation is called higher oxidation. The higher-oxidation kinetics determines (i) further increase of the surface area of the SF matrix and (ii) release of C-14, Cl-36, Tc-99, I-129, and Cs-135 by solid-state diffusion.

Higher oxidation results in about 36 percent volume expansion, creating large stresses and causing inter- and intra-granular fractures to relieve the stresses (Ahn, 1995a). As a consequence, small individual subgrains will be exposed to air or groundwater, increasing the total reactive surface. The subgrains are assumed to be spherical. As the SF matrix is oxidized to a higher oxidation state such as U_3O_8, not only C-14 but also the heavier radionuclides, such as Cl-36, Tc-99, I-129, and Cs-135, can be released by solid-state diffusion.

These radionuclides can be released either instantaneously (Stacy and Goode, 1978; Stone and Johnson, 1978) or following diffusion kinetics in a sphere (Crank, 1975). The latter is given by the following equation

$$\frac{M_t}{M_\infty} = \frac{6}{\pi^2}\sum_{n=1}^{\infty}\left[\frac{1}{n^2}\exp\left(-\frac{D_m n^2 \pi^2 t}{r_t^2}\right)\right] \qquad (2\text{-}37)$$

where

M_t = total amounts of diffusing species at time t
M_∞ = total amounts of diffusing species at time $t = \infty$
D_m = diffusivity of oxygen in unoxidized matrix [cm^2/s]
r_t = subgrain radius [μm]

In evaluating Eq. (2-37), the C-14 diffusivity can be obtained experimentally from the time required to complete the lower oxidation (Ahn, 1995a). The estimated value of D_m can be expressed as

$$D_m \simeq 0.6\, r_g^2 \left\{ 9.4 \times 10^{-6} \exp\left[\frac{111.3}{RT} \right] \right\}^{-1} \qquad (2\text{-}38)$$

where r_g is the grain radius of SF. In Eq. (2-38), D_m is in cm^2/s, r_g is in μm, R is in kJ mol^{-1} $°K^{-1}$, and T is in °K.

The oxygen diffusivity is expected to decrease sequentially from that of the lower oxide, to the higher oxide, and to the unoxidized matrix (Ahn, 1994; Kofstad, 1972). Therefore, this diffusivity could be considered a lower bound in relation to the upper bound of instantaneous release.

The diffusivities of Cl-36, Tc-99, I-129, and Cs-135 have not been measured. However, the Xe-133 diffusivity has been measured in the higher oxide (Lindner and Matzke, 1959). The Xe-133 diffusivity is presumably slower than or close to the diffusivities of Cl-36, Tc-99, I-129, and Cs-135 because the atomic radius of Xe-133 is larger than or similar to the rest. The value of D_m for Xe-133 is given by

$$D_m \simeq 1.5 \times 10^{-10} \exp[-77.8/RT] \qquad (2\text{-}39)$$

where D_m is in cm^2/s, R is in kJ mol^{-1} $°K^{-1}$, and T is in °K.

This approximation assumes that all these radionuclides exist in solid solution. Some Tc-99 is likely to be present as intermetallic compounds (Thomas and Guenther, 1989), which will be essentially immobile. In addition, if the radionuclides diffusing to the SF surface do not react with air or groundwater, they may diffuse back into the matrix. Tc-99 is likely to be oxidized by air (Gray and Wilson, 1995) but reactions of other radionuclides with air or moisture are not known.

The initiation time for the higher oxidation to U_3O_8 has been determined experimentally by considering that it is approximately equal to the splitting time of the cladding after U_3O_8 formation. As discussed elsewhere (Ahn, 1995a), the initiation time is given by the following expression

$$t_{2.4} + \Delta = 1.56 \times 10^{-19}(yr) \exp[184.5(kJ/mol)/RT] \qquad (2\text{-}40)$$

This time includes the cladding fracture time in addition to the U_3O_8 formation time. However, because the fracture time is relatively short, Eq. (2-40) is used as the time for the full conversion to U_3O_8. It is likely that a threshold temperature exists below which the initiation time becomes infinite (Ahn, 1995a). Therefore, Eq. (2-40) provides a conservative estimate of the time required for the oxidation to U_3O_8. For convenience, EBSPAC uses the criterion that U_3O_8 will form above 250 °C instead of using Eq. (2-40). In Version 1.0β, for simplicity, the temperature of the SF is assumed to be that of the WP surface.

2.7.2 Liquid Release

No radionuclides other than gaseous radionuclides such as C-14 and Cl-36, can leave the WP until it is breached or perforated, and water can contact the waste. Upon failure, the water flowing into the WP could lead to the release of radionuclides through different mechanisms. In the current version

of EBSPAC, it is assumed that liquid release of radionuclides from the SF includes only congruent release of the radionuclides contained in the irradiated UO_2 matrix. Liquid release accounts for the radionuclides released from the fuel, produced from radioactive decay of another radionuclide in a chain, losses from radioactive decay, advective flow, and diffusion. The advective mass transfer is a simple mass balance (i.e., amount out=concentration×water flow rate out of the container). The diffusive mass transfer is assumed to be taking place from a spherical source, as implemented in SOTEC (Sagar et al., 1992). The diffusion model considers radioactive decay but, for simplicity, the chains are not considered (Sagar et al., 1992). A simplified model for colloids transport may be considered at a later phase of EBSPAC development.

Figure 2-7 presents a schematic of a horizontally emplaced WP with two conduits, one representing the inlet and the other representing the outlet. In this schematic, the conduit for liquid entry is shown on the upper half of the WP and the conduit for the liquid exit is shown on one of the sides. Liquid water will accumulate in between the SF rod and in the pore space until its level rises to the level (solid parallelogram) of the exit conduit (dashed parallelogram). Thus, in the bathtub model, the maximum volume of water that is available for UO_2 matrix dissolution is the level shown by the dotted parallelogram. All SF above this level is assumed to remain dry and contributes to gaseous releases. The following section presents the mass balance of the radionuclides in the accumulated water shown in Figure 2-7.

2.7.2.1 Mass Balance of Radionuclides in the Waste Package

When liquid water enters into the WP following its failure, the mass balance for the radionuclide inventory in liquid water contacting a failed WP leads to a differential equation of the form

$$\frac{\partial m_i}{\partial t} = w_{li}(t) - w_{ci}(t) - w_{di}(t) - m_i \lambda_i + m_{i-1} \lambda_{i-1} \qquad (2\text{-}41)$$

where

m_i = mass of radionuclide i in the WP water at time t
w_{li} = rate of mass transfer from the solid fuel into the resident water in the WP due to leaching of the SF
w_{ci} = rate of advective mass transfer out of the WP
w_{di} = rate of diffusive mass transfer out of the WP
λ_i = decay constant of radionuclide i
m_{i-1} = mass of the daughter product of i at time t
λ_{i-1} = decay constant of the daughter product $i-1$

The product, $m_i\lambda_i$, is the mass loss due to decay, and $m_{i-1}\lambda_{i-1}$ represents mass generation of the daughter products as a consequence of the decay of the parent radionuclide i. These mass transfer processes are discussed individually in the following sections.

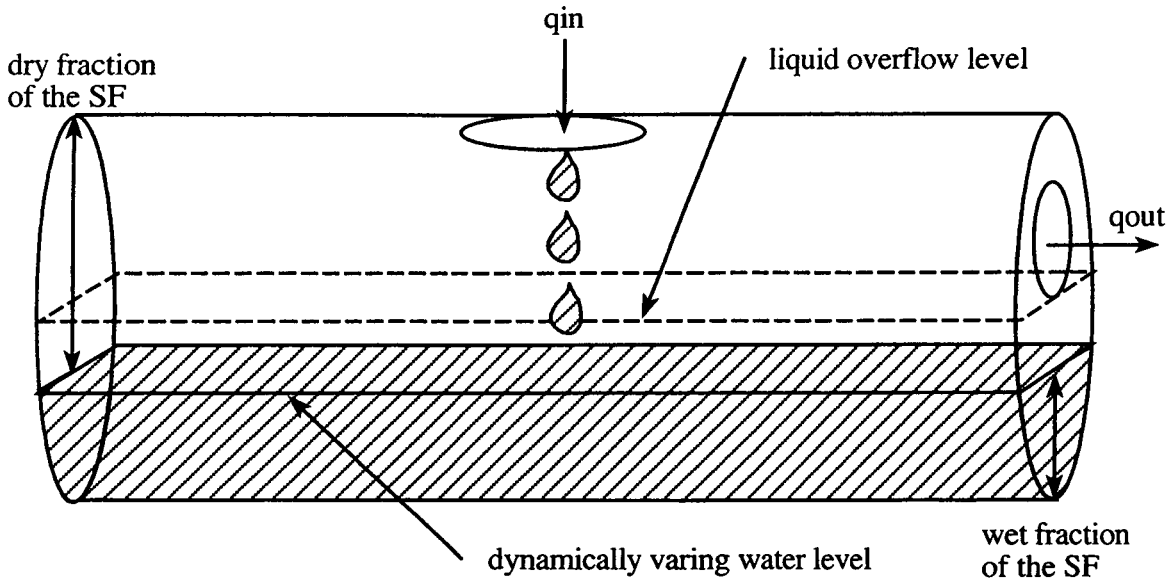

Figure 2-7. Schematic of the bathtub concept inside the waste package. Water encroachment (q_{in}) and withdrawal (q_{out}) points on the horizontally emplaced waste package are chosen to be on the top and side, respectively.

2.7.2.2 Advective Mass Transfer

The advective mass transfer out of the WP can be represented by (Nuclear Regulatory Commission, 1995)

$$w_{ci}(t) = C_i(t)\, q_{out}(t) \tag{2-42}$$

and

$$q_{out}(t) = q_{in}(t)\, k_q \left(\frac{V}{V_{max}}\right)^2 \tag{2-43}$$

where

C_i = concentration of radionuclide, i, in the WP water
V = volume of water in the WP at time t
V_{max} = maximum volume of water that the WP can hold before water overflow
k_q = "Weir coefficient" (arbitrarily chosen)
q_{in} = water entering into the WP at time t
q_{out} = water leaving the WP at time t

The Weir coefficient is a damping factor that allows a transient flow system to reach steady state according to its magnitude. Advective mass transfer is considered from the inside to the outside of the WP but not into the material surrounding it, as schematically shown in Figure 2-7. The only mass transfer process through the medium surrounding the WP that is considered consists of diffusive mass transfer as discussed in the following section.

2.7.2.3 Diffusive Mass Transfer

Once the water leaves the WP, it is assumed to envelope the whole outer surface of the WP. As a result, the radionuclides are present in uniform concentration. Then, assuming that the WP can be represented by a sphere with equal surface area, the diffusive loss due to the molecular diffusion of a radionuclide into the porous medium can be represented by

$$w_{di}(t) = 4\pi r^2 \phi D \left.\frac{\partial C}{\partial r}\right|_{r = r_0} \tag{2-44}$$

where

D = diffusion coefficient of the radionuclide in the medium surrounding the WP
r = radius of the medium surrounding the WP
ϕ = porosity of the medium surrounding the WP

$\left.\frac{\partial C}{\partial r}\right|_{r = r_0}$ can be obtained by solving the following boundary and initial value problem:

$$K \frac{\partial C}{\partial t} = D \frac{1}{r^2} \frac{\partial}{\partial t}\left(r^2 \frac{\partial C}{\partial r}\right) - \lambda K C \tag{2-45}$$

$$C|_{t = t_0} = C_0 \tag{2-46}$$

$$C|_{r = \infty} = C_0 \tag{2-47}$$

$$C|_{r = r_0} = C(t) \tag{2-48}$$

where

K = retardation coefficient
C = concentration
t = time
λ = decay coefficient

This formulation accounts for molecular diffusion, retardation of radionuclides, and radioactive decay, but not the generation of radionuclides from chain decay. For simplicity, it is assumed that D is independent of the species. The diffusion model is presented for spherical geometry. Thus, the inner-boundary condition is maintained at a distance that is equivalent to the radius of a sphere with the same surface area as a single WP. Although the outer boundary is defined at infinity, the numerical solution

of these sets of equations requires that a finite distance be assigned. A distance beyond the drift wall is considered sufficient for this.

The spherical configuration was chosen for the sake of simplicity and lends itself to simple one-dimensional analytical or numerical solution. The solution may be conservative (Nuclear Regulatory Commission, 1995) because:

- The $C|_{r = r_0}$ takes the value of $C(t)$ inside the container, which implies that the radionuclide concentration at the outside wall of the WP is the same as that inside the container.
- A steep concentration gradient results from the absence of the generation of daughter products in the chain, contributing to faster diffusive release.
- $C|_{r=\infty} = C_0$ results in a steeper concentration gradient than expected when all WPs in all cells are considered together for diffusive release calculation. The steeper gradient results in a faster release, thus rendering the assumption conservative.

2.7.2.4 Waste Dissolution Rate

Fission products and activated radionuclides normally have high solubility limits. The solubilities do not limit the release of these radionuclides in the anticipated groundwater. These radionuclides include Tc-99, I-129, Cs-135, C-14, and Cl-36. Np-237 may belong to this category also, depending on the chemistry and the flow rate of groundwater. These radionuclides are understood to be released congruently to the dissolving SF matrix. Gray and Wilson (1995) have determined the intrinsic dissolution rate of the SF matrix from flow-through tests. The flow-through tests use artificially high flow rates to eliminate the precipitation of secondary phases on the SF surface. The secondary phases may modify the intrinsic dissolution rate of the SF matrix by altering the area of the reactive surface.

The dissolution rate in solutions containing carbonate anions, which are representative of altered groundwaters present in the near field, was expressed by Gray and Wilson (1995) as

$$\log r = 9.310 + 0.142 \log\left[CO_3^{2-}\right] - 16.7 \log p_{O_2} + 0.140 \log\left[H^+\right] - \frac{2130}{T} + 6.81 \log(T) \cdot \log\left(p_{O_2}\right) \quad (2\text{-}49)$$

where

r = dissolution rate [mg m^{-2} d^{-1}]
$\left[CO_3^{2-}\right]$ = carbonate ion concentration [mol/L]
p_{O_2} = oxygen partial pressure [atm]
$\left[H^+\right]$ = concentration of hydrogen ions [mol/L]

Normally, the groundwater at the YM repository site contains Si and Ca ions. In the presence of these species, the dissolution rate decreases about 100 times (Gray and Wilson, 1995). In J-13 well water containing these ions

$$r = (1.4 \sim 5.5) \times 10^4 \exp\left[-\frac{34.3}{RT}\right] \tag{2-50}$$

with R in kJ/mol · °K. This equation was obtained from data reported by Gray (1992) at 25 and 85 °C (Ahn, 1995b). The rate increases by a factor of 10 as temperature increases from 25 to 85 °C.

The secondary phases deposited on the surface may result in the slow release of dissolved ions by diffusion constraint across the secondary-phase layer. In this case of retardation, the dissolution rate may be written as

$$r = k\,(t + a)^{-1/n} \tag{2-51}$$

where k, a, and n are constants that can be determined by more rigorous methods (Lichtner, 1994).

Actual calculations can choose between Eqs. (2-49), (2-50), and (2-51). Equations (2-49) and (2-51) are not implemented in the current version of EBSPAC. In more general terms, these three equations can be combined in series such that the one corresponding to the slowest rate controls the overall kinetics.

In deriving these equations, radiation effects have not been considered explicitly. On the SF surface, α-radiolysis may play a role in the matrix dissolution. Ahn (1995b) compared the dissolution rate measured in flow-through tests to that obtained from semi-static tests, suggesting that a slight increase of release occurs in semi-static tests. More pronounced radiolysis effects can be expected in drip tests. Presumably, stronger radiolysis effects can be observed in drip tests because the leachate is present as a thin layer on the SF surface. However, no radiolysis effects have been noted at a high drip rate of 0.75 mL/3.5 d (Bates et al., 1995).

2.7.2.5 Treatment of Colloids

Actinides such as Pu-239, Pu-240, and Am-241 have low solubility limits. In TSPA-95, it was assumed that the dissolved actinides are positively charged and their sorption capacity is large enough to be retarded in the host rock during their transport (TRW Environmental Safety Systems, Inc., 1995). It appears that no dissolved actinides may be released to the accessible environment. However, recent experimental and analytical assessments suggest that this assumption may not be valid (Kim, 1986; Ahn, 1995b; Manaktala et al., 1995). Actinide ions may be present as colloidal suspensions of complexes or particles. Colloids are not always positively charged. Consequently, the sorption coefficients can be very small. The actinide inventory in the SF is very large in terms of potential dose. Even if a small fraction of this inventory is released, the contribution to the dose in the accessible environment can be significant. The contribution of actinides can be dominant over that of other radionuclides.

Three different processes for colloid formation are associated with SF dissolution (Ahn, 1995b):

(i) Condensation Process—Condensation denotes the formation of nuclei when the groundwater becomes supersaturated with respect to a given species. Often, the groundwater replenishment induces this imbalance because the replenishment decreases the surface areas for the growth of radionuclide layers on existing colloids. Therefore, nuclei can form continuously. The condensation can take place homogeneously in leachates or heterogeneously on the fresh surface of groundwater colloids.

(ii) Dispersion Process—Dispersion involves the breakup of solid (or condensed) material. This process may occur during physical and chemical weathering. Among vastly different mechanisms involved in dispersion, two types of disintegration have been considered in SF dissolution. The first arises from the disintegration of unstable precipitates of secondary phases. The second arises from the intergranular preferential dissolution of SF matrices, leaving individual grains in leachates.

(iii) Pseudo-Colloid Formation—Pseudo-colloids form by radionuclides released from SF sorbing onto groundwater colloids. Traditionally, instantaneous reversible linear sorption has been considered to determine the total amount of radionuclides sorbed onto the colloidal phase. J-13 well water is generally known to have 0.01 to 1 μg/mL groundwater colloids (Manaktala et al., 1995). Additional pseudo-colloids may form from the above (i) condensation process. Radionuclides can nucleate heterogeneously and grow on the surface of groundwater colloids. The heterogeneous nucleation and growth can result in much more radionuclides associated with groundwater colloids than the sorption does.

Currently, it is well accepted (Manaktala et al., 1996) that colloids form during SF dissolution. However, it is unclear whether colloidal suspensions are stable and mobile. As time elapses, colloids may flocculate or grow and may settle out of the transporting medium.

Colloid transport also has many uncertainties. In the laboratory column tests, more than 70 percent penetration of colloids through host rocks has been observed (Kim et al., 1996). Because colloid transport depends largely on surface charge properties, colloids may behave differently at the YM site. Additionally, colloids formed from the condensation or the sorption process may redissolve to be absorbed in host rocks. Nevertheless, the current uncertainties should not preclude the consideration of colloid issue in performance assessment.

Quantitative assessment of colloidal release requires numerical solution of mass balance equations over long periods of time. For the present, estimates of radionuclides associated with colloids (Ci/mL) are obtained from drip tests (Bates et al., 1995) and immersion tests (Wilson, 1990) at laboratory time scales. No consideration of colloidal transport is made in Version 1.0β of EBSPAC.

2.7.2.6 Water Infiltration

The infiltration of meteoric water and its arrival at the WP is a function of the hydrostratigraphic conditions above and below the repository horizon. The carrying capacity of the fractures and matrix above the repository, as well as horizontal diversion depending on the dip of the bedding planes, and thermal conditions will dictate the rate of infiltration into the EBS. In some instances

the infiltrating water may reach the EBS by matrix-only flow (Nuclear Regulatory Commission, 1995). EBSPAC uses the funnel flow concept adopted in SOTEC to represent flow into the EBS. The funnel flow concept assumes that flow through fractures over a wide area will converge to focused spots on the drift and will result in dripping of water on the WP. Therefore, the dripping flow can be represented as

$$q = A_e I_f \tag{2-52}$$

where

q	=	water influx into a cell
I_f	=	average fracture infiltration rate
A_e	=	largest cross-sectional area of the WP

The average fracture infiltration rate can be specified as a function of time for more realistic input of infiltration data. Detailed calculations of infiltration performed elsewhere (Stothoff, 1996; Stothoff et al., 1996) will provide average fracture infiltration rate. The chemical composition of this water and its effect on radionuclide dissolution and release is not explicitly considered in the present version of EBSPAC. It is postulated that the meteoric water has the same composition as the groundwater, which is assumed to be represented by that of J-13 well water.

2.7.2.7 Inventory Model

The inventory in the failed WP is monitored by performing material balance calculation at specified time steps. The mass balance calculation includes depletion due to decay, generation of daughter products, and mass depletion due to diffusive and advective releases. For the case where $w_{li}(t) = w_{ci}(t) = w_{di}(t) = 0$, Eq. (2-41) reduces to

$$\frac{\partial m_i}{\partial t} = -m_i \lambda_i + m_{i-1} \lambda_{i-1} \tag{2-53}$$

$$m_i\big|_{t=0} = m_{i0} \tag{2-54}$$

Equation (2-53) represents a set of coupled, linear-ordinary differential equations, generally known as the Bateman equation, with Eq. (2-54) as boundary conditions. This set of differential equations is also used to determine the remaining solid mass of the radionuclides in a chain at a given time t. The analytical solution to this initial value problem is given by

$$N_{ij} = \prod_{k=1}^{j-1} \lambda_k N_{i0} \sum_{l=1}^{j} \frac{e^{-\lambda_l t}}{\prod_{\substack{m=i \\ m \neq l}}^{j} (\lambda_m - \lambda_m)} \tag{2-55}$$

where

N_{ij} = contribution from the ith chain member to the jth chain member

N_{i0} = initial mass of ith member of chain

λ_j = decay coefficient of jth member of the chain

It may be noted that the dimension of the mass N_{i0} becomes the dimension of N_{ij} and does not depend on any other term in Eq. (2-55). The total amount of the jth chain member at any time is

$$N_j = \sum_{i=1}^{j} N_{ij} \tag{2-56}$$

In the above equations, $m_i = N_i$ except that N_i is used to represent radionuclide mass under conditions where no injection or production of mass occurs, except due to its own decay.

2.8 SOURCE TERM

The solution to Eq. (2-41) provides the mass of radionuclides in the WP water as a function of time. This information is used as the boundary condition for advective and diffusive mass fluxes. On the other hand, the source term w_{si} is defined as the mass flow rate of radionuclides at the outer surface of the WP and is represented by

$$w_{si}(t) = w_{ci}(t) + w_{di}(t) \tag{2-57}$$

w_{si} is the information to be passed on to the TPA code to determine the transport of the radionuclides from the EBS to the far field.

2.9 NUMERICAL SOLUTION METHOD

A numerical solution is implemented to solve Eqs. (2-42) through (2-45) representing diffusive flow equations with specified boundary conditions. Although an analytical solution can be obtained for this boundary value problem, for generality purposes, a finite difference scheme with varying grid spacing is chosen to solve this equation. The main advantage of this numerical method for the diffusion equation is that heterogeneities can be specified by assigning different diffusion coefficient, retardation factor, and porosity to different numerical grid blocks. The system of algebraic equations obtained from the finite difference scheme are solved for each time step by using Thomas algorithm. Thomas algorithm (Lapidus, 1962) provides a quick and efficient algorithm for solving tridiagonal matrices as obtained in diffusion problems of the above kind (Sagar et al., 1992).

Differential equation presented in Eq. (2-41) must be integrated to obtain the mass of individual radionuclides in the WP. Similar calculations are needed to determine the WP outer overpack penetration depth from the penetration rate equations presented in Section 2.5.2. These initial value problems can be solved by many different methods. Fifth-order Runge-Kutta method (Press et al., 1992) that uses auto-adjusted time stepping has been used in EBSPAC because of its robustness.

3 SOFTWARE DESCRIPTION

3.1 EBSPAC CODE CAPABILITIES

EBSPAC was developed following the framework of existing codes, such as SOTEC (Sagar et al., 1992) and SCCEX (Cragnolino et al.,1994), in order to minimize code development time. In a departure from SOTEC, however, EBSPAC performs calculations only for a single cell or a sub-area and not for the whole repository. An attempt is made in EBSPAC to improve the numerical calculations, thus reducing mass balance errors. Although no specific unit system is required by EBSPAC, the International Systems of Units (SI) (American Society for Testing and Materials, 1992) has been used to the extent possible.

The flow chart for EBSPAC is shown in Figure 2-2, where two distinctive parts appear, the upper part representing the WP failure calculations and the lower part the release calculations. As shown in Figure 3-1, the WP failure calculations are performed using *ebspac_fail.f* and the release calculations using *ebspac_release.f*. For clarity, these two sections of EBSPAC have their independent main input files, *ebspac_fail.inp* and *ebspac_release.inp*, respectively. No feedback from the release part into the failure part exists, as illustrated in Figure 3-1. Since these two parts exist essentially as two separate codes in EBSPAC, they are discussed separately in the following sections.

3.1.1 Waste Package Failure Calculations

Three different failure modes of the WP are considered in EBSPAC: (i) initial failure, (ii) disruptive scenario failure, and (iii) corrosion and mechanical failures. In this report, these three failures are also referred to as Type 1, Type 2, and Type 3 failures, respectively. In Type 1 failure, a portion of the WPs in a cell are specified to have failed at time t=0 yr as a result of initial defects. These WPs are assumed to have been damaged prior to or during emplacement and are specified in the input data as a fraction of the total containers in a cell. The scenario failure option allows the user to specify the time of occurrence of a disruptive event and the number of WPs failed by Type 2 failure as a result of that disruptive event. The scenario events may include events such as fault-movement, seismic events, and volcanic events. Multiple scenarios disrupting the cell at different times cannot be represented separately. An approximation can be made by averaging all failure times and summing the number of failed WPs from multiple disruptive events.

All WPs in a cell that have not undergone Type 1 and Type 2 failures are potentially subjected to corrosion and mechanical (Type 3) failures. This implies that corrosion is assumed to affect all WPs equally in a cell so that when one WP fails, then all WPs in the same cell that have not already failed under Type 1 and 2 modes will fail simultaneously. For simplicity, failure of the WP is defined as the through-wall penetration of the outer and inner overpack by a single pit. Failure can also occur by brittle fracture due to mechanically dominated processes. No credit is given in the current version of EBSPAC to the protection ability of the MPC or the fuel cladding against corrosion or mechanical failure following the criterion adopted by the DOE in TSPA-95 (TRW Environmental Safety Systems, Inc., 1995). Once the outer and inner overpack are penetrated or failed by fracture, the SF is considered to be completely exposed to the near-field environment. Also, no consideration is given to the existence of "leaked" fuel rods that exist as part of the SF inventory.

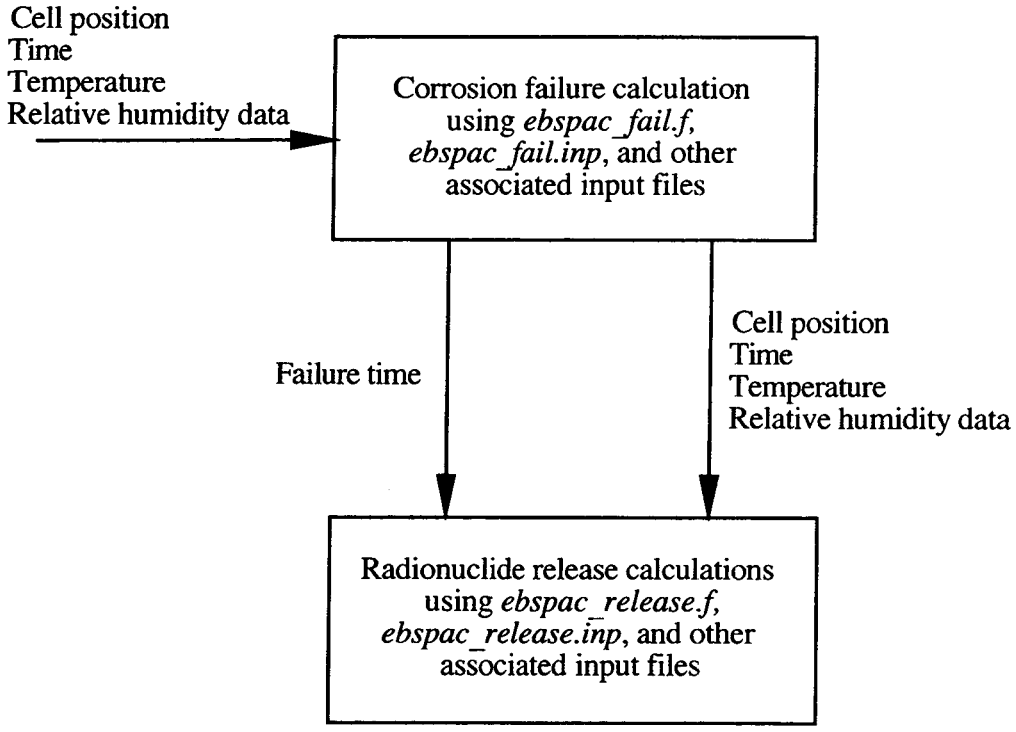

Figure 3-1. Flow diagram showing data transfer from waste package failure module to the radionuclide release module. The waste package failure module uses time, temperature, and relative humidity data and transfers this information, along with the waste package failure time, to the radionuclide release module.

Two types of near-field environments are considered, leading to different corrosion processes. One is dry, hot air that promotes the oxidation of the outer steel overpack and the other is air at a high RH that induces wet, aqueous corrosion. Dry air oxidation occurs over a time interval that ends when water condenses on the WP. Water condensation begins when the temperature at the WP surface decreases to a value at which the RH of the environment surrounding the WP reaches a threshold RH specified by the user. The water available at the WP surface is the result of the condensation of water vapor following the decrease in the temperature at the surface of the WP. In order to simplify calculations while simultaneously preserving conservatism, no background flow of water is considered for corrosion failure calculation. The conservativeness is based on the assumption that a thin layer of water, in which high concentration or fast transport of electroactive species occurs, tends to enhance corrosion processes more than a thick water layer or water flowing around the WP.

The thickness of the liquid layer is assumed to be the same regardless of the presence or absence of backfill material around the WP and the nature of the contact between particles of backfill and the WP surface. It is assumed that the wettability of this surface is such that water droplets impinging on it or condensing nuclei of water vapor can spread immediately to form a layer of uniform thickness. The water layer is thin and defined by an arbitrary, specified thickness. No consideration is given to the contact between the WP and the invert in the drift (Figure 2-1).

At every time step, a calculation is conducted to determine if the RH has reached the critical or threshold value. The environment surrounding the WP is dry air if the RH is lower than the threshold, and, hence, a calculation of the amount of outer overpack material consumed by oxidation is done to

determine the penetration of the oxidation front. In the same time interval, a mechanical failure test is conducted for the new thickness resulting from metal oxidation to evaluate if failure due to fracture occurs. If the WP does not fail under a predetermined external load, then the time is advanced and the same test is repeated. If at any time step condensation of water takes place, then the calculation of oxidation in dry air is interrupted and the aqueous corrosion calculation is initiated. The mechanical failure test is performed at all time intervals until failure takes place, no matter whether the WP is undergoing dry or wet oxidation. Aqueous corrosion could be uniform or localized. If it is localized because the corrosion potential is above the critical potential, the calculation of penetration is initiated in the form of pit growth.

When the depth of the pit is greater than the initial thickness of the WP outer overpack, the potential of the galvanic couple formed by the outer and inner container is calculated. If the potential of the couple is lower than the critical potential for the inner container, penetration of the inner container is computed as uniform corrosion under passive conditions. Otherwise, pit growth of the inner overpack begins and continues until the depth of the pit becomes equal to the inner overpack wall thickness. Then, the calculation is stopped and the lesser of the two times constituting a time step is recorded as the time to failure of the WP when corrosion failure took place. As long as there is one or more intact WP in the cell, the failure calculation focuses only on the fate of one initially intact container and is independent of the total number of containers in the cell, initially failed containers, and scenario failure.

Integration of the penetration rate equation [Eq. (2-26)] included in the numerical calculation of the code is time consuming. A fifth-order Runge-Kutta method is used for this calculation in EBSPAC.

3.1.2 Radionuclide Release Calculations

The release calculations are performed by the code *ebspac_release.f*. The release calculation is essentially confined to the radionuclides being released just outside of the WP. Both gaseous and liquid release calculations are carried out in this part of EBSPAC. Complexities in model considerations include the incorporation of radionuclide decay, generation of daughter products in the chains, temporal variation of inventory in the WP, and spatial variations in the properties of the surrounding material. However, the degree of the complexity incorporated varies from model to model in order to accomplish necessary simplifications, while ensuring conservatism, in the calculation of radionuclide release. In the release code, the cumulative release histories for all specified radionuclides are calculated at all time steps for the three failure modes. In the case of gaseous release, the calculations are performed for C-14 and Xe-133.

First, the number of WP to be considered for each failure mode is determined. While the number of WP undergoing Type 1 and Type 2 failure are read from the input file, the number of WP actually being considered for Type 2 failure is recalculated based on the corrosion failure time and the onset of wet conditions on the WP. If the Type 3 failure occurs before the Type 2 failure, then the number of WP undergoing Type 2 failure is reset to zero. If the Type 3 failure occurs after the Type 2 failure and wet conditions simultaneously exist, then calculations of release from Type 2 failure is performed using the specified number of failed WPs. In summary, gaseous release begins as soon as a WP fails, but two conditions must be satisfied for liquid release: (i) WP must fail, and (ii) a liquid environment must be available around the WP.

For Type 1 failure, gaseous release begins at t=0 whereas liquid release begin at $t=t_{wet}$, where t_{wet} is the time to wetness. For Type 2 and 3 failures, however, gaseous release begins at $t=t_{fail}$, which is the WP failure time, and liquid release begins at the longest of two times, t_{fail} and t_{wet}, because both conditions (failure and wetting) must be fulfilled. In all cases, the gaseous release calculations may continue until the final time ($t=t_{end}$) even if the wet condition may have arisen much earlier because the fuel in the WP may not be completely wet. In EBSPAC, gaseous and liquid releases are calculated for each failure type and later summed to obtain total releases from all failure types. Perhaps a more efficient approach is to perform the release calculations in a single sweep that includes all failure types, by keeping track of the lag time among failure types. For simplicity, however, the former option was chosen in which calculations are performed over three passes and in each pass it is assumed that the other failure types are absent.

For simplicity, all gaseous releases, such as those of C-14 and Xe-133, are lumped together. Gaseous releases include the releases from cladding oxidation, lower fuel oxidation ($UO_2 \rightarrow UO_{2.4}$), and higher fuel oxidation ($UO_2 \rightarrow U_3O_8$). Each of these processes is implemented in a separate subroutine in *ebspac_release.f*, making provisions for future modifications. Simple analytical solutions are used in gaseous release calculations, avoiding the use of time consuming numerical integrations. While gaseous release from U_3O_8 is presented in Eq. (2-34) in terms of mass fraction, gaseous release from $UO_{2.4}$ is presented in terms of the thickness fraction of the oxidized zone in a fuel matrix pellet [Eq. (2-32)]. This thickness must therefore be converted to mass of the gaseous release. Considering that the mass of gas release from $UO_{2.4}$ formation is proportional to the oxidized width, the total mass release can be represented by

$$m_{C\text{-}14} = \frac{1}{R^3}\left(3R^2w - 3Rw^2 + w^3\right) M_{C\text{-}14} \qquad (3\text{-}1)$$

where

$m_{C\text{-}14}$ = mass of C-14 gas released at time t
R = fuel matrix pellet radius
w = width of the oxidized zone
M_{C14} = initial inventory of C-14 gas

While release from $UO_2 \rightarrow UO_{2.4}$ conversion is computed at all time steps vis-a-vis all temperatures, the release from U_3O_8 formation begins only when the WP temperature reaches 250 °C. Because $UO_2 \rightarrow U_3O_8$ conversion forms $UO_{2.4}$ as an intermediate product, gaseous release from U_3O_8 is therefore simply added to the gaseous release associated to $UO_{2.4}$ formation. For reporting purposes, only the cumulative gaseous release at the end of the maximum time is stored whereas the time history of gas evolution is not stored.

Liquid release calculations, as performed for the gaseous release, focus on release from a single WP. It is assumed that the release environment within the cell is not affected by the location or the geometric configuration associated to the location of other WPs. However, to obtain the total release in the final calculations, the release from one WP is multiplied by total number of WPs. While the thermal model provides the specifics of backfill emplacement, in Version 1.0 β, it is assumed that the backfill is always present in the release calculations.

Once the condition of wetting arises on the basis of the critical RH, the liquid enters into the WP. It is assumed that at the failure time, there are at least two pits acting as conduits in a horizontally emplaced WP located in a manner such that water enters through one pit and exits through the other one. In the absence of a model relating water encroachment rate in the WP (q_{in}) to background flow, condensing water flow, pit position, number of pits, and pit size, the user must specify q_{in}. This code assumes a steady encroachment of water into the WP. The water entering into the WP could be considered to be the background flow, as well as that originated by condensation of water vapor. Because the condensation process is transient, a provision is built in the code to handle tabular data so that water encroachment can vary with time. It is assumed that one of the pits is located on the side of the WP at a level lower than that of the water entrance pit, which is situated at the top of the horizontally emplaced WP, as schematically illustrated in Figure 2-7. Once the water level in the WP rises to the user specified outflow position, water begins to flow out of the WP along with the dissolved radionuclides. The implementation of this position is rather indirect because the user only specifies the volume of water that the WP contains before overflow occurs. The fraction of fuel that becomes wet is also indirectly determined by the position of the overflow pit.

Liquid release arises only from the wetted fraction of the SF, whereas gaseous release originates from the remainder of the fuel. The wetted fuel matrix dissolves in the volume of water present in the WP as a function of time at a given temperature. The radionuclides are released congruently with the fuel matrix dissolution. Congruent release implies that the rate of release of the radionuclides into the contacting water is proportional to the rate of leaching of the fuel matrix. Two fuel matrix leaching models are implemented in a subroutine and the user must choose a model. The user must select a model based on the near-field chemistry, especially based on whether Ca and Si ions are present or absent. These two models provide leaching rate per unit area. Therefore, the leaching rate is multiplied by wetted surface area of the fuel. The surface area is calculated by assuming an assembly of spheres as a simulation of fuel pellets. For an assembly of uniform spheres, the specific internal surface area of a medium (i.e., surface area to volume) a_v can be represented by

$$a_v = \frac{6}{D_p} \tag{3-2}$$

where

D_p = sphere or particle diameter

By knowing the density, porosity, and particle diameter, the total surface area per unit volume is obtained. This equation assumes that the fuel pellets are not porous. However, from Section 2.7.1.3, we know that fragmentations caused in the process of conversion of UO_2 to $UO_{2.4}$ and U_3O_8 contribute to the porosity of the fuel matrix pellets. Porosity as a consequence of this fragmentation is expected to be very small and practically negligible compared to the inter-pellet porosity. However, in the future, a factor can be introduced so that the user can account for the additional effect of the fragmentation porosity.

The first task of the *ebspac_release.f* code is to initialize variables and parameters and read input parameters. Then, the number of WP failed under various failure types are determined. The gaseous release calculations are performed from $t=0$ to t_{end}. Following the gas release calculations, the liquid

release calculations are performed starting at $t=0$. The first step on these calculations is to determine whether liquid release is possible at a given time or not. If possible, the liquid release calculation at every time step includes the computation of the radionuclide inventory in the solid mass, radionuclide releases from the solid mass into the liquid surrounding the WP, the generation of the new radionuclide inventory in the chains in the liquid, convective release of mass from inside to the outside of the WP, and diffusive losses into the surrounding medium outside the WP.

At each time step, the inventory of the radionuclides in the water inside the WP is recorded, and the element inventory is computed as the sum of mass of all its isotopes. If the concentration of that element in the WP water exceeds its solubility limit, then the actual concentration value is discarded and the solubility limit is assigned to the concentration at that time step. At any given time, the concentration of a nuclide in the WP water is calculated from the element inventory by dividing by the volume of water in the WP. The release of an individual nuclide occurs at the rate that is proportional to its mass fraction among all the isotopes of an element.

To compute total mass release in a time interval, a fifth order Runge-Kutta integration (Press et al., 1992) of the mass rate equation is performed in which the time steps are automatically adjusted, thus reducing the impact of large time intervals. At every readjusted time step, the rate of change of mass in the WP water is computed as well as the diffusive losses to the surrounding. The diffusive loss is calculated by using a finite difference scheme and Thomas algorithm. For Runge-Kutta calculations, the total number of variables used is the sum of the number of radionuclides whose change of mass in the WP water with time is calculated, the number of nuclides corresponding to the mass flux out of the WP, and the change in the volume of WP water.

At the end of this calculation, the cumulative release is recorded for each nuclide, and then the time is advanced and the same calculation is repeated. The calculation continues until radionuclides are depleted from the SF solid and WP water or t_{end} is reached, whichever comes first. The code handles unequal time intervals and uses the time intervals at which temperature and RH values are available.

3.2 EBSPAC CODE STRUCTURE

As mentioned earlier, EBSPAC consists of two distinct programs: (i) *ebspac_fail.f* and (ii) *ebspac_release.f*. Tables 3-1 and 3-2 describe the subroutines used in these two codes. Some of the subroutines are repeated in both tables because the same subroutines exist in both programs. Because only a limited number of subroutines are used, all parameters and common statements are embedded in these codes instead of using include files as originally proposed in the Software Requirements Description (SRD) (Mohanty et al., 1996). The subroutines odeint, rk4, and rkqc, listed in Table 3-1, are used for integration purposes. In addition, another set of integration routines, namely, bsstep, mmid, and rzextr, are included, which could be used instead of the set of subroutines containing odeint, rk4, and rkqc.

The *ebspac_fail.f* code is executed before executing *ebspac_release.f*. The only information that the *ebspac_release.f* code requires from the *ebspac_fail.f* code is the failure time of a container, as noted in Figure 3-1. Other passive data transferred from the *ebspac_fail.f* code to the *ebspac_release.f* code include time, temperature, and RH, as well as the critical RH, as shown in Figure 3-1.

Table 3-1. List of subroutines used in ebspac_fail.f

Name	Function
bsstep	An alternate routine to rkqc for step size controlled Runge-Kutta method (will be implemented in the future)
corrode	Determines corrosion potential and critical potentials and calculates corrosion rate in the water film on the WP
dryoxdwp	Calculates the penetration depth due to dry air oxidation of the WP outer overpack
fracfail	Tests if fracture failure has occurred
input	Reads all input parameters required in the code
lint	Routine for linear interpolation
mech	Driver routine for fracfail
mmid	A routine to implement Runge-Kutta calculations; called by bsstep
odeint	A driver program for rkqc or bsstep; used for integration a given number of starting values from an initial to final value with specified accuracy; uses adaptive step sizes
rate	Calculates derivatives for the Runge-Kutta calculations
rk4	Performs integration using basic Runge-Kutta method
rkqc	Calculates step sizes for Runge-Kutta method
rzextr	A rational function extrapolation routine called by bsstep (for future implementation)
temphstry	Sets temperature and relative humidity as a function of time for EBSPAC by reading tabular data or by using empirical relationships

3.3 HARDWARE AND SOFTWARE REQUIREMENTS

The EBSPAC code is written in ANSI FORTRAN 77 language. The code has been developed and tested on a SUN IPX work station with the ANSI FORTRAN 77 compiler. To compile the code on a PC platform may require modifications to the current source code. Version 1.0β of EBSPAC consists of about 5,000 lines of code including the comment statements. The largest array used is about 4 Mb size. Therefore, the total disk space required is approximately 21 Mb.

Table 3-2. List of subroutines used in ebspac_release.f

Name	Function
decay	Routine to implement an analytical solution based on Bateman's equation to compute radionuclide decay of chains
derivs	Determines the rate of change of mass of each radionuclide in the water surrounding the WP
dflux	Calculates diffusive flux from the WP to the surrounding medium assuming spherical source
diag3	Solves tridiagonal matrix that implements Thomas algorithm
gasrel	Calculates gaseous releases due to fuel and cladding oxidation
init	Initializes parameters before subroutine input is called
input	Reads all input parameters
leachrt	Calculates UO_2 matrix leaching in the wetted portion of the fuel
liqrel	Calculates liquid release of all radionuclides at all time steps
odeint	Integrates a given number of starting values from an initial to final value with specified accuracy
opnfil	This module opens a formatted file on the unit specified with the attributes provided in the argument list
rdelem	A routine to read formatted file containing radionuclide-specific information
rk4	Performs integration using the basic Runge-Kutta method
rkqc	Calculates step sizes for Runge-Kutta method
setdif	Sets the coefficient matrices for the diffusion model assumes a spherical shell surrounding spherical source term
u3o8oxd	Routine to calculate C-14 and Xe-133 releases due to oxidation of $UO_2 \rightarrow U_3O_8$
uo24oxd	Routine to calculate C-14 releases due to oxidation of $UO_2 \rightarrow UO_{2.4}$
zircoxd	Routine to calculate C-14 releases from cladding oxidation

3.4 PRE- AND POST-PROCESSORS

No pre- or post-processors are being designed in this stage of the development of EBSPAC. The pre- and post-processors will be required, however, to incorporate EBSPAC into the TPA executive code.

3.5 EBSPAC COMPILATION AND EXECUTION

The code is run on a UNIX operating system by entering the command *ebspacrun*. The file contains the following statements:

f77 ebspac_fail.f -o ebspac_fail.x
f77 -r8 ebspac_release.f -o ebspac_release.x
time fail.x > echo.out
time ronj.x > echo.out

where the time command gives the execution time for the executions of *ebspac_fail.x* and *ebspac_release.x* separately. While the *ebspac_fail.f* is written in double precision, *ebspac_release.f* is written mostly in single precision. Therefore, the compilation statement uses -r8 extension to create double precision variables in *ebspac_release.f*. Extension -o is used to name the executable files *ebspac_fail.x* and *ebspac_release.x*.

The input files created by the user must be copied to *ebspac_fail.inp* and *ebspac_release.inp* before the program execution. To use the example problem data set, *example_fail.inp* and *example_release.inp* must be copied to *ebspac_fail.inp* and *ebspac_release.inp*, respectively.

3.6 GRAPHICS

No special graphics output devices are required. An ASCII file containing output data from *ebspac_fail.f* as a function of time is presented in the file *corrode.out*. The output data from *ebspac_release.f* is an ASCII file named *release.out*. These two files are presented in a spreadsheet-like format that can be read in by a user-preferred graphics software, such as MS Excel, Kaleidagraph, etc.

4 DESCRIPTION OF INPUT AND OUTPUT DATA

4.1 OVERVIEW

As noted in Section 3, there are two major codes in EBSPAC designated as *ebspac_fail.f* and *ebspac_release.f*, and dedicated to compute the WP failure time and the radionuclide releases from the WP, respectively. Each of these codes has separate main input files, *fail.inp* and *release.inp*, respectively. This separation was introduced to allow the user to focus either on the WP failure part or alternatively on the radionuclide release part. The *ebspac_fail.f* code can be run completely independent of the *ebspac_release.f* code. The independent execution of *ebspac_release.f* can be accomplished by using an output file from one particular run of *ebspac_fail.f*, and if desired, by subsequent modification of it.

Names of the auxiliary input files are specified in the main input files. Data input uses free format for all files except the auxiliary input file *ebspac.nuc* from which the nuclide names and nuclide-related data are read. A formatted file reader subroutine is used to read only the formatted data on nuclides. In the current version of EBSPAC, while free format is used, the input data must be read sequentially and from the appropriate data line (card). This approach has been adopted, at least temporarily, with the intention of keeping the code simple, non-cryptic, and compatible for Monte Carlo sampling options to be invoked by the Total Performance Assessment executive code.

4.2 DESCRIPTION OF INPUT DATA

The input parameters used for *ebspac_fail.f* and *ebspac_release.f* are presented in Tables 4-1 and 4-2, respectively. In these two tables, symbols used for representing the various parameters are presented in the first column of the table. In the second column, these parameters are briefly described. Values of these parameters, as examples, and the units that must be used to create data for EBSPAC, are given in the third and fourth columns, respectively.

Auxiliary files provide temperature, groundwater flow and radionuclide data. The temperature and RH data are calculated outside of *ebspac_fail.f* and *ebspac_release.f*, as described in Section 2.2. These data are required by both codes. However, the data are read by *ebspac_fail.f* first and then reformatted before being read by *ebspac_release.f*. The temperature file that is read by *ebspac_release.f*, designated *temphumd.dat*, can contain multiple data sets, with each set containing four columns representing time, WP temperature, drift wall temperature, and RH data. Different thermal loadings and environmental conditions correspond to different data sets. In addition, preceding the time column, the number of rows of temperature data provided in the file are indicated. The symbols for the parameters, a brief description, and the units are summarized in Table 4-3. The temperature file may contain extremely fine resolution of time that the external temperature calculation used to adequately resolve phase transitions. These time intervals are screened for new intervals in EBSPAC. In the absence of tabular data, or if the table does not contain information for times longer than a specified period (i.e., 10,000 yr), an approximate functional relationship can be used. Currently, the generic model developed in EBSPAC is the one based on the thermal loading adopted by the DOE in TSPA-1995 (TRW Environmental Safety Systems, Inc., 1995) to obtain data on drift wall temperature and RH. It is assumed that a constant temperature drop exists between the WP temperature and the drift wall temperature throughout the time period of interest.

Table 4-1. Nomenclature of input parameters used for waste package failure calculations in *ebspac_fail.f*

Line Number	Parameters	Parameter Description	Equation	Example Values	Unit
1	Header line				
2	Comment line				
3	Comment line				
4	tend	Simulation time length needed when empirical equations are used for temperature and relative humidity data (i.e., iflag=1)		10,000	yr
5	Comment line				
6	Comment line				
7	wplen	Length of WP		5.682	m
	wpdia	WP diameter		1.802	m
8	cthick1	Thickness of the outer overpack		0.1	m
	cthick2	Thickness of the inner overpack		0.02	m
9	Comment line				
10	iflag	iflag = 1 for using empirical equation for temperature and relative humidity history. iflag ≠ 1 for using tabulated data. Table must have data to tend years.		2	—
11	ntfile	Name of temperature file from external thermal module			

Table 4-1. Nomenclature of input parameters used for waste package failure calculations in *ebspac_fail.f* (cont'd)

Line Number	Parameters	Parameter Description	Equation	Example Values	Unit
12	nset	Temperature-relative humidity relationship to use. Various data sets (four columns of data in each set) can be provided in the same table representing various thermal loads, backfill—no-backfill, ventilation—no-ventilation cases. If the user has only one test case, the data must be placed in the first four columns of the table, and nset must be assigned as 1.		1	—
13	timintv	Time interval (>0) to be used when iflag$=1$. This value is used to screen out any time value (hence corresponding temperature and relative humidity values from ntfile) in the table that is smaller than timintv.		49.9999999	yr
14	nhista	Number of time steps at which temperature and relative humidity values are calculated when iflag$\neq 1$ ($<$dimension in program)		200	—
15	Comment line				
16	Comment line				
17	age	Age of fuel (not used in this version)		0	yr
18	Comment line				
19	Comment line				

Table 4-1. Nomenclature of input parameters used for waste package failure calculations in *ebspac_fail.f* (cont'd)

Line Number	Parameters	Parameter Description	Equation	Example Values	Unit
20	grainr	Average radius of the metal grains constituting the WP outer overpack. This is used in the model for calculating coupled oxygen diffusion along grain boundaries in metal	2-8	5	μm
21	nseries	Number of terms in the infinite series used in the model for calculating coupled oxygen diffusion along grain boundaries in metal	2-8	25	—
22	gbthick	Thickness of grain boundary used in the model for calculating coupled oxygen diffusion along grain boundaries in metal	2-8	0.7e-3	μm
23	constant	A constant relating matrix and grain boundary oxygen diffusivities in metal	2-8	1.e-2	—
24	Comment line				
25	Comment line				
26	humdc	Critical RH above which the water vapor condenses		0.65	—
27	filmthk	Thickness of water film on the WP surface. A uniform thickness all around the WP is assumed.		2.e-3	m
28	Comment line				
29	Comment line				

Table 4-1. Nomenclature of input parameters used for waste package failure calculations in *ebspac_fail.f* (cont'd)

Line Number	Parameters	Parameter Description	Equation	Example Values	Unit
30	betaox1	Transfer coefficient for oxygen reduction reaction (β_{O2}) for the WP outer overpack	2-20	0.75	—
	betahy1	Transfer coefficient for water reduction reaction (β_{H2O}) for the WP outer overpack	2-22	0.5	—
31	Comment line				
32	betaox2	Transfer coefficient for oxygen reduction reaction (β_{O2}) for the WP inner overpack	2-20	0.75	—
	betahy2	Transfer coefficient for water reduction reaction (β_{H2O}) for the WP inner overpack	2-22	0.5	—
33	Comment line				
34	rkox1	Rate constant for oxygen reduction in the WP outer overpack	2-20	3.8e12	C m mol^{-1} yr^{-1}
	rkhy1	Rate constant for water reduction in the WP outer overpack	2-22	1.6e−1	C m^{-2} yr^{-1}
35	gox1	Activation energy for oxygen reduction reaction for the WP outer overpack	2-20	37,300	J/mol
	ghy1	Activation energy for water reduction reaction for the WP outer overpack	2-22	25,000	J/mol
36	rkox2	Rate constant for oxygen reduction in the WP inner overpack	2-20	3.0e10	C m mol^{-1} yr^{-1}
	rkhy2	Rate constant for water reduction in the WP inner overpack	2-22	3.2	C m^{-2} yr^{-1}

Table 4-1. Nomenclature of input parameters used for waste package failure calculations in *ebspac_fail.f* (cont'd)

Line Number	Parameters	Parameter Description	Equation	Example Values	Unit
37	gox2	Activation energy for oxygen reduction reaction for the WP inner overpack	2-20	40,000	J/mol
	ghy2	Activation energy for water reduction reaction for the WP inner overpack	2-22	25,000	J/mol
38	aa(1,1)	Passive current density ilayer=1 (WP outer overpack)		3.15e5	C m^{-2} yr^{-1}
	aa(1,2)	Coefficient for the first order temperature correction to the passive current density for ilayer=1		0.0	—
	aa(1,3)	Coefficient for the second order temperature correction to the passive current density for ilayer=1		0.0	—
39	aa(2,1)	Passive current density ilayer=2 (WP inner overpack)		6.3e4	C m^{-2} yr^{-1}
	aa(2,2)	Coefficient for the first order temperature correction to the passive current density for ilayer=2		0.0	—
	aa(2,3)	Coefficient for the second order temperature correction to the passive current density for ilayer=2		0.0	—
40	xcouple	Factor, varying from 0 to 1, representing galvanic coupling between the outer and inner overpacks	2-24	0.95	—

Table 4-1. Nomenclature of input parameters used for waste package failure calculations in *ebspac_fail.f* (cont'd)

Line Number	Parameters	Parameter Description	Equation	Example Values	Unit
41	xread	Factor for defining critical potential range		0.0	—
42	clconc	Chloride concentration in water	2-25	3.e−1	mol/L
43	refph	pH		9.0	—
44	taus	Tortuosity of a porous layer scale deposited on the WP. Thickness does not change with time. In the case of no deposit, taus=1.0.		1.0	—
	spor	Porosity of the layer deposited on the WP. Porosity does not change with time. In the case of no deposit, porosity=1.0.		1.0	—
45	Comment line				
46	Comment line				
47	dtini	Runge-Kutta control parameter (smaller dtini may increase solver time greatly)			yr
	dtmax	Runge-Kutta control parameter (smaller dtmax may increase solver time greatly)			yr
48	errrel	Relative error for Runge-Kutta routines			—
	errabs	Absolute error for Runge-Kutta routines			—
49	Comment line				
50	Comment line				

Table 4-2. Nomenclature of input parameters used for radionuclide release calculations in *ebspac_release.f*

Line Number	Parameters	Parameter Description	Equation	Example Values	Unit
1	Comment line				
2	Comment line				
3	Comment line				
4	xcon	Number of waste packages in the cell	—	2,335	—
5	iscon	Number of containers affected by the failure scenario	—	1,000	—
6	sftime	Time of scenario failure	—	4,500	yr
7	deffrac	Fraction of initially failed containers in a cell		0.10	—
8	Comment line				
9	Comment line				
10	dintl	Internal diameter of WP	—	1.421	m
	xlintl	Internal length of WP	—	4.572	m
11	xvol	Internal WP volume where water can reside	—	7.83	m^3
12	Comment line				
13	Comment line				
14	temfil	Reformatted temperature and relative humidity file named *temphumd.dat* (output from *ebspac_fail.f*) (see Table 4-3)		—	—

Table 4-2. Nomenclature of input parameters used for radionuclide release calculations in *ebspac_release.f* (cont'd)

Line Number	Parameters	Parameter Description	Equation	Example Values	Unit
15	ctemp	Boiling point of water at atmospheric pressure		373.15	°K
16	Comment line				
17	Comment line				
18	rpor(1,2,3)	Porosity of the host rock divided into three layers corresponding to zones 2–4 (not used in this version)	2-45	0.14, 0.14, 0.14	—
19	Comment line				
20	Comment line				
21	ppor	Backfill porosity corresponding to zone 1	2-44	0.14	—
22	Comment line				
23	Comment line				
24	hydfil	Flow parameters file named *floebs.dat*		—	—
25	funnel	Funnel factor or fractional area for capture of darcy flow onto WP	2-43*	7	—
26	Comment line				
27	Comment line				
28	Comment line				
29	amassc	UO_2 mass per WP	2-49*	2.8e3	kg

* not used directly in the equation

Table 4-2. Nomenclature of input parameters used for radionuclide release calculations in *ebspac_release.f* (cont'd)

Line Number	Parameters	Parameter Description	Equation	Example Values	Unit
30	fuewt	SF molecular weight		250	g/mol
	fueden	SF density		3000	kg/m^3
	fuedif	Diffusion coefficient of gaseous radionuclides in SF		1.0e-08	m^2/s
	fuepor	SF pellet porosity; assumes granular porosity and porosity due to transgranular fracture are zero		0.3	—
31	Comment line				
32	Comment line				
33	imodel	Fuel leaching model type 1 — Eq. (3-18); 2 — Eq. (3-19)	3-18 3-19	2	—
	phvalue	pH for fuel leaching		9.0	—
	oxgnovpr	Oxygen over pressure for fuel leaching		0.2	atm
	cco3	Carbonate concentration in the surrounding water		2.e-3	mol/L
	wetfrac	Water level inside the WP expressed as a fraction of WP internal diameter		0.5	—
34	Comment line				
35	Comment line				
36	elefil	Nuclides file; named *ebspac.nuc* contains information on nuclide names, half life, inventory (details in Table 4-5)		—	—

Table 4-2. Nomenclature of input parameters used for radionuclide release calculations in *ebspac_release.f* (cont'd)

Line Number	Parameters	Parameter Description	Equation	Example Values	Unit
37	Comment line				
38	Comment line				
39	r0z	Initial radius of UO_2 particle		1.e-3	m
40	rhou	Density of UO_2		37.	kg mol m^{-3}
41	r1z	Radius of UO_2 grain	2-38	1.e-5	m
42	r2z	Subgrain fragment radius of UO_2 particle after transgranular fracture	2-37	1.e-6	m
43	thclad	Thickness of cladding	2-34*	6.1e-4	m
44	cfuel	C-14/kg of UO_2 fuel	3-1	7.2e-4	Ci
45	czmetal	C-14/kg of UO_2 fuel in Zircaloy cladding and other metals	2-37*	4.89e-4	Ci
46	czoxide	C-14/kg of UO_2 fuel in initial Zircaloy oxide and crud metals	—	2.48e-5	Ci
47	cgap	C-14/kg of UO_2 fuel in grain and pellet-cladding gap	—	6.2e-6	Ci
48	Comment line				
49	Comment line				
50	rdiff(1..4)	Diffusion coefficient for various layers of the surrounding medium (near-field transport parameter)	2-45 to 2-48	5.6e-5, 5.6e-5, 5.6e-5, 5.6e-5	m^2/yr

* not used directly in the equation

Table 4-2. Nomenclature of input parameters used for radionuclide release calculations in *ebspac_release.f* (cont'd)

Line Number	Parameters	Parameter Description	Equation	Example Values	Unit
51	Comment line				
52	Comment line				
53	Comment line				
54	Comment line				
55	imax,jmax	Number of grid nodes in x and y directions	2-45	10, 10	—
56	Comment line				
57	xcor (1...imax)	X coordinates for the numerical solution of diffusive flux out of the WP	2-45	.1, .5, 1.0, 2.0, 4.0, 5., 6., 7., 8., 9.	m
58	Comment line				
59	ycor (1...imax)	Y coordinates for the numerical solution of diffusive flux out of the WP	2-45	.1, .5, 1.0, 2.0, 4.0, 5., 6., 7., 8., 9.	m
60	Comment line				
61	Comment line				
62	nzones	Number of zones for material types (Note: zones apply to the above grid, zones are the same for all cell)	2-45	4	—
63–66	iz, (ib,jb) to (ie,je)	Zone identifications for material types. ib...ie are x coordinate indices, jb...je are y coordinate indices.	2-45	1 1 1 1 1 2 2 1 2 1 3 3 1 3 1 4 4 1 10 1	—

Table 4-2. Nomenclature of input parameters used for radionuclide release calculations in *ebspac_release.f* (cont'd)

Line Number	Parameters	Parameter Description	Equation	Example Values	Unit
67	Comment line				
68	Comment line				
69	dtinit	Runge-Kutta control parameter: initial guess of time step	2-41	25.	yr
	dtmin	Runge-Kutta control parameter: minimum time step allowed	2-41	1.	yr
	dtmax	Runge-Kutta control parameter: maximum time step allowed	2-41	50.	yr
70	eps	Relative error for Runge-Kutta routines	2-41	1.e−2	—
	tiny	Absolute error for Runge-Kutta routines	2-41	1.0e−10	—
71	Comment line				
72	Comment line				
73	bt	Size of time intervals in the output for preparing the data file for NEFTRAN code	—	100.	—
74	Comment line				
75	Comment line				

Table 4-3. Input file description: Temperature file *temphumd.dat*

Symbol	Description	Unit
ntemp	Number of temperature values (i.e., number of rows of data)	—
ttemp(it)	Time at which temperature values are provided; it is an index taking values from 1 to ntemp	yr
tcan(it)	Temperature at the container surface	°C
tave(it)	Temperature at the drift wall	°C
humd(it)	Relative humidity at temperatures tave(it)	—
cftime	Corrosion failure time	yr

The auxiliary flow file, *floebs.dat*, contains flow factor data to represent the variation with time of the flow. In this file, the flow rate can be expressed as a function of time. A shift of this data can be accomplished by multiplying the flow rate (infiltration) as a function of time by a load factor. Additional details of this auxiliary file are presented in Table 4-4 and in Section 5.

Another auxiliary file is the nuclides file, *ebspac.nuc*, which contains the initial radionuclide inventory. The subroutine *rdelem* is called to read this formatted file. The file provides information on the number and name of the chemical elements and their isotopes, number of chains in which a particular radionuclide appears, the position of the radionuclide in a chain, the solubility limit of the element in water, and its retardation in the backfill material or host rock. Then the file provides information on number of chains, and number of members in each chain including the parent. If an element is not present in any chain, then the element is considered to be a single-member chain. Following this, data are presented for each radionuclide, which include its name and half life, initial inventory, and fraction of the inventory in the fuel matrix gap or the gap between the cladding and the fuel matrix. Symbols of various parameters and a brief description are found in Table 4-5 and further clarification is presented in Section 5. Some conversion factors used in the code are listed in Table 4-6.

4.3 DESCRIPTION OF OUTPUT DATA

EBSPAC output data primarily consist of

— WP wetting time
— WP failure time
— Mass of parent nuclide and mass of daughter products
— Radionuclide release as a function of time
— Cumulative release at the end of program execution

The output from both codes include echoing of input data for verification purposes. The major output from *ebspac_fail.f* is the WP failure time. This single, real number output is directly fed into

Table 4-4. Input file description: Flow file *floebs.dat*

Symbol	Description	Unit
flowfactr	A multiplying factor to modify infiltration rate	—
tflo(i)	Time at which flow rate is provided	yr
floref(i)	Infiltration rate	m^3/yr

Table 4-5. Input file description: Nuclides file *ebspac.nuc*

Symbol	Description	Unit
nelem	Number of elements considered	—
elem(i)	Name of the element i	—
ncon(i)	Number of chains in which element i occurs	—
rde(i)	Retardation coefficient for the element i	—
kcon(i,l)	The chain number in which element i occurs. The argument l is an index identifying a chain among all chains in which element i occurs.	—
icon(i,l)	The position of element i in the chain kcon(i,l)	—
nchns	Number of chains	—
ni(i)	Size of the chain i	—
amall(k,i)	Molecular weight of the radionuclide in the chain k at position i	g/mol
namall(k,i)	Name of the radionuclide in the chain k at the position i	—
halflife(k,i)	Half life of the radionuclide in the chain k at the position i	yr
curall(k,i)	Initial inventory of the radionuclide in the chain k at the position i	Ci
fggap	Gap fraction of the radionuclide in the chain k at position i	—

Table 4-6. Some conversion factors used in the code

Conversion From	Conversion To	Formula
atoms	curies	$\frac{\text{atoms}}{\text{half life} \times 1.68340 \times 10^{18}}$
atoms	kg	$\frac{\text{atoms} \times \text{atomic weight} \times 0.001}{6.02 \times 10^{23}}$

ebspac_release.f as an input and printed to the same file that transfers input information, namely, time, temperature, and RH, from *ebspac_fail.f* to *ebspac_release.f*.

The output of the *ebspac_fail.f* code is listed in the output file *corrode.out*, which contains, in addition to the wetting time and the failure time, the remaining WP wall thickness and the values of corrosion and critical potentials as a function of time.

The output from *ebspac_release.f* is presented in two formats in two files. In the first format, data is presented in the input format of the NEFTRAN code (Nuclear Regulatory Commission, 1995). In the second format, the cumulative release of each radionuclide is presented as a function of time and this ASCII file can be imported by any graphics package for plotting.

5 EXAMPLE PROBLEM

An example problem is presented in this section to demonstrate an application of EBSPAC and the type of data and file requirements. For this purpose, the test case problem and associated data files are briefly described. Input and output data files are presented to illustrate the input file structure and output file format.

5.1 WASTE PACKAGE FAILURE CALCULATIONS

The main input data for running the *ebspac_fail.f* code are included in *ebspac_fail.inp* and listed in Table 5-1. A detailed description of the input data for the various models is included in the following sections.

5.1.1 Temperature and Relative Humidity Data

The example problem uses the stratigraphy of YM that includes the six thermohydrologic units shown in Table 5-2. The thicknesses and thermal properties of each stratigraphic unit are based on data from published sources (U.S. Department of Energy, 1993; Wilson et al., 1994). The decay characteristics of the thermal source are based on data published by DOE (1987). Details of the 3D thermal model are briefly discussed in Section 2.2.

The results of the calculations are shown in Figure 5-1. The results included the WP temperature, average drift wall temperature, and the RH. A total of twelve cases have been analyzed based on three values of the AML (20, 40, and 80 MTU/acre), with and without ventilation during the operations period, and with and without emplacement of backfill at the time of permanent closure of the repository (assumed to be 100 yr). It can be observed that AML has a strong effect on the temperatures as well as on the RH. In addition, ventilation has a strong effect but only for the high AML case. Backfilling always has a pronounced effect of rapidly increasing the WP temperature promptly after emplacement of backfill, but it has no effect on the average rock wall temperature. The RH near the WP is strongly influenced by the WP temperature so that it decreases significantly if backfill is emplaced. If ventilation is used then dry conditions are maintained up to 100 yr. It is important to note that for an AML of 80 MTU/acre, the value selected as a reference in TSPA-1995 (TRW Environmental Safety Systems, Inc., 1995) the lowest values of RH are attained after backfilling but the temperatures at the WP surface are above 200 °C over an extended period. The rate and extent of dryout surrounding WPs has been calculated for these cases, but is reported elsewhere (Manteufel, 1996).

The file *thermal.dat* has twelve sets of data and each set is identified by assigning a value to the parameter nset in *ebspac_fail.f*. Each set of data has WP surface temperature, drift wall temperature, and RH data as a function of time. The twelve sets represent the combinations shown in Table 5-3, corresponding to the cases illustrated in Figure 5-1.

For the TPA implementation, nset may be specified as 1, and for each realization, the thermal model will save data as only one set; the first set. Once *ebspac_fail.f* needs a particular set of temperature data, it reformats and saves the data in *temphumd.dat* for use by *ebspac_release.f*. The file *thermal.dat* may contain data at very small time intervals. Data is stored in unformatted form in the file *thermal.dat*.

Table 5-1. Input file *fail.inp*—Input file only for the waste package failure part of the EBSPAC

```
\input data file for ebspac fail code: ebspac_fail.f
|
\simulation time
10000.                                  ! tend: simulation time length [yr]
\                                       ! if iflag=1, table must have data to tend [yr]
\
5.682, 1.802                            ! wplen,wpdia: wp length and diameter [m]
0.1, 0.01                               ! cthick1,cthick2: wp layers 1&2 thicknesses [m]
|
\choose source of temperature data
2                                       ! iflag 1: emp. equation, 2: tab.data
1                                       ! nset (temp.-rel hum. relationship to use
49.9999999                              ! timintv (used when iflag=2)
200                                     ! nhista (used when iflag=1)
|
\other temperature parameters
0.                                      ! age of fuel (not used in this version)
|
\Dry oxidation of wp outer overpack
5.                                      ! grainr: metal grain radius [micrometer]
25                                      ! nseries: terms in the infinite series
0.7e-3                                  ! gbthick [micrometer]
1.e-2                                   ! constant1: used in the dry oxidation equn.
|
\evaporation-condensation
0.65                                    ! humdc: critical relative humidity
2.e-3                                   ! filmthk: thickness of water film [m]
|
\Corrosion Parameters
0.75, 0.5                               ! betaox1, betahy1: beta kinetics parameters
\                                         for oxygen and wateri for WP outer overpack
0.75, 0.5                               ! betaox2, betahy2: beta kinetics parameters for
\                                         oxygen and water for WP inner overpack
3.80e12, 1.6e-1                         ! rkox1 [c*m/y/m], rkhy1 [c/m2/yr]
37300., 25000.                          ! gox1 [J/mol], ghy1 [J/mol]
3.0e10, 3.2                             ! rkox2 [c*m/y/m], rkhy2 [c/m2/yr]
40000., 25000.                          ! gox2 [J/mol], ghy2 [J/mol]
3.15e5, 0.0, 0.0                        ! aa(1,1), aa(1,2), aa(1,3)
6.30e4, 0.0, 0.0                        ! aa(2,1), aa(2,2), aa(2,3)
0.06                                    ! xcouple, a fractional coupling strength
0.0                                     ! xread
3.e-1                                   ! clconc: chloride concentration [mol/L]
9.0                                     ! refph: reference pH
1.0, 1.0                                ! taus: deposit tortuosity, spor: deposit porosity
|
\Runge-kutta control parameters
1.e-3, 1.e0                             ! dtini, dtmax
1.e-2, 1.e-30                           ! errrel (same as eps), errabs (same as tiny)
|
\end
```

Table 5-2. Thermal properties of the various thermohydrologic units at Yucca Mountain

Thermohydrologic Unit	Elevation (m)	Thermal Conductivity ($W\ m^{-1}\ °K^{-1}$)	Density ($kg\ m^{-3}$)	Specific Heat ($J\ kg^{-1}\ °K^{-1}$)
TCw	310 to 350	1.69	2000	923
PTn	250 to 310	0.85	1640	1360
TSw	−70 to 250	2.10	2200	930
CHnv	−155 to −70	0.84	2100	1220
CHnz	−250 to −155	1.42	1890	1420
CHnz (Sat.)	−250 to −1000	1.56	2070	1230

TCw = Tiva Canyon welded
PTn = Paintbrush nonwelded
TSw = Topopah Spring welded
CHnv = Calico Hills nonwelded vitric
CHnz = Calico Hills nonwelded zeolitic

Table 5-3. Thermal model cases for several combinations of conditions

Set	AML (MTU/Acre)	Ventilation (up to 100 yr)	Backfill at 100 yr
1	80	N	N
2	80	N	Y
3	80	Y	N
4	80	Y	Y
5	40	N	Y
6	40	N	N
7	40	Y	N
8	40	Y	Y
9	20	N	N
10	20	N	Y
11	20	Y	N
12	20	Y	Y

Y: yes N: no

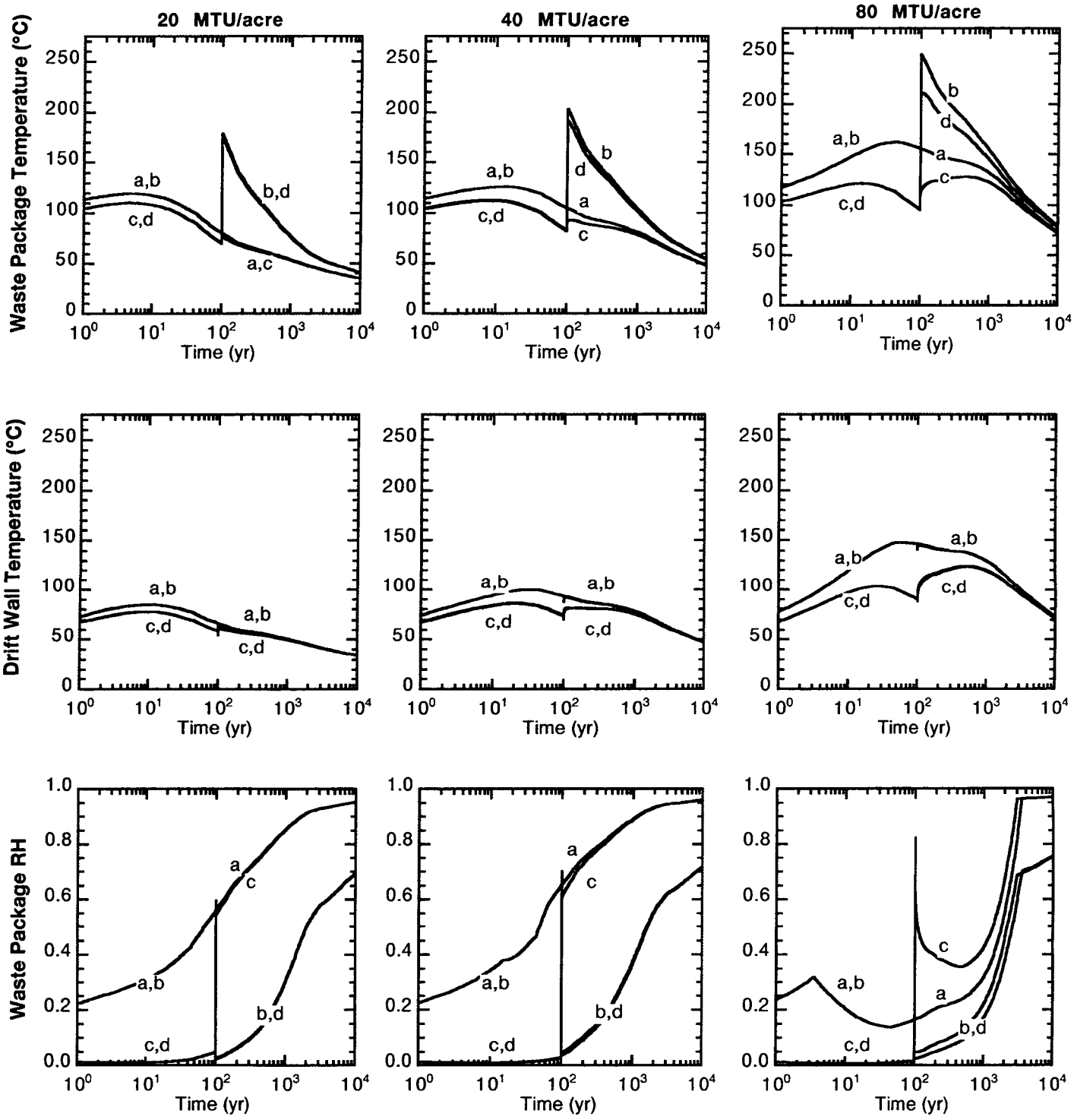

a = no ventilation, no backfill
b = no ventilation, backfill emplaced at 100 yr
c = continuous ventilation through 100 yr, no backfill
d = continuous ventilation through 100 yr, backfill emplaced at 100 yr

Figure 5-1. Temperature and relative humidity calculations for various values of the areal mass loading and different ventilation and backfilling conditions

The results from these simulations for an arbitrarily chosen interior cell have been formatted as input for EBSPAC. The file *thermal.dat* is first read by *ebspac_fail.f* for temperature and VPR data as a function of time. Then *ebspac_fail.f* creates an output file, *temphumd.dat*, that is required as an input for *ebspac_release.f*. The file *temphumd.dat* contains the number of rows of data that must be read where each row contains the row number, time, WP surface temperature, drift wall temperature, and VPR (or RH). The content of the file is shown in Table 5-4 for a limited number of rows. The data are presented in Table 5-4 at approximately 50 yr intervals where the unequal time intervals are noticeable. The last line of the file shows the WP failure time as computed by *ebspac_fail.f*, along with the temperature and RH data. A complete listing of the file *temphumd.dat* is presented in Appendix A.

5.1.2 Environment Data

Environment data as a function of time in the vicinity of the WP, such as Cl^- and CO_3^{2-} concentrations, O_2 overpressure, and pH values, required for WP corrosion and fuel matrix leaching calculations can be estimated by using MULTIFLO (Lichtner and Seth, 1996). Until MULTIFLO generates the full range of data compatible with the thermal model as functions of time and temperature, some representative values were calculated and assumed to remain constant with time as a first approximation in Version 1.0β of EBSPAC. Constant bounding values have been used for pH and Cl^- concentration of 10.0 and 3×10^{-3} M, respectively, as derived from MULTIFLO calculations. Despite the difference in the approach for calculating the temperature with respect to the thermal model, it should be noted that the maximum temperature in Figure 2-5b is close to the drift wall temperature shown in Figure 5-1, as calculated by the thermal model.

Future versions of EBSPAC will store the results of MULTIFLO calculations for **pH**, $\mathbf{f_{O_2}}$, $\mathbf{Cl^-}$, $\mathbf{Ca^{2+}}$, $\mathbf{SiO_2}$, and $\mathbf{CO_2(g)}$ in the file *environ.dat* at different times and at several distances above the repository horizon. Data will be stored in the file *environ.dat* in unformatted form beginning with two title lines, followed by the data entries:

TITLE1 number of time points
TITLE2
TIME PH CL- CA+2 SIO2 CO2(G) ...
.
.
.
The unit of time is in years, and concentrations of aqueous species are in units of molality, and gaseous species in bars. The file may be easily modified if additional species are required.

5.1.3 Waste Package Corrosion Data

An important group of parameters included in Table 4-1 is that related to the corrosion processes which can be classified in two subgroups. The first subgroup includes all the parameters needed for calculation of the corrosion potential.

The parameters in the numerator of Eq. (2-20), representing the current density as a function of potential for the oxygen reduction reaction under activation control, are the transfer coefficient (β), the rate constant (k_{O_2}), and the activation energy. A constant value of 0.75 was used for β on the basis

Table 5-4. Data file *temphumd.dat*—Input data file to *ebspac_fail.f* providing temperature and relative humidity with time

193

1	0.0002	21.8700	21.0000	0.5592
2	50.0900	109.9000	100.1000	0.0102
3	100.1000	103.8000	92.5300	0.6654
4	150.2000	123.2000	115.1000	0.4139
5	200.2000	124.9000	118.2000	0.3927
6	250.3000	126.1000	120.3000	0.3785
7	300.4000	127.0000	121.7000	0.3682
8	352.6000	127.6000	122.9000	0.3615
9	404.8000	128.0000	123.6000	0.3572
10	457.1000	128.2000	124.1000	0.3550
11	509.3000	128.0000	124.2000	0.3572
12	561.5000	127.6000	124.1000	0.3615
13	613.8000	127.0000	123.7000	0.3682
14	670.4000	126.4000	123.3000	0.3750
15	722.6000	125.7000	122.8000	0.3831
16	774.8000	125.1000	122.3000	0.3903
17	827.1000	124.5000	121.8000	0.3976
18	879.3000	123.8000	121.3000	0.4063
19	931.6000	123.2000	120.8000	0.4139
20	983.8000	122.5000	120.2000	0.4231
21	1036.0000	121.8000	119.6000	0.4324
22	1097.0000	120.9000	118.8000	0.4449
23	1149.0000	120.1000	118.1000	0.4563
24	1201.0000	119.3000	117.4000	0.4680
25	1254.0000	118.6000	116.7000	0.4786
26	1306.0000	117.8000	116.0000	0.4910
27	1358.0000	117.0000	115.3000	0.5038
28	1410.0000	116.3000	114.6000	0.5154
29	1463.0000	115.5000	113.9000	0.5289
30	1515.0000	114.7000	113.1000	0.5429
31	1567.0000	114.0000	112.4000	0.5555
32	1619.0000	113.2000	111.7000	0.5704
33	1672.0000	112.5000	111.0000	0.5837
34	1724.0000	111.8000	110.3000	0.5974
35	1776.0000	111.0000	109.7000	0.6136
36	1828.0000	110.3000	109.0000	0.6282
37	1881.0000	109.6000	108.3000	0.6431
38	1933.0000	108.9000	107.6000	0.6585
39	1985.0000	108.2000	106.9000	0.6744
40	2037.0000	107.6000	106.3000	0.6883
41	2089.0000	107.0000	105.7000	0.7025
42	2159.0000	106.2000	104.9000	0.7221
43	2229.0000	105.4000	104.2000	0.7423
44	2298.0000	104.7000	103.5000	0.7605
45	2368.0000	103.9000	102.8000	0.7820
46	2438.0000	103.2000	102.1000	0.8014
47	2507.0000	102.5000	101.4000	0.8213
48	2577.0000	101.8000	100.7000	0.8419
49	2647.0000	101.2000	100.1000	0.8599
50	2716.0000	100.5000	99.4400	0.8816
51	2786.0000	99.8700	98.8000	0.9016
52	2856.0000	99.2300	98.1800	0.9226
53	2925.0000.....			

A complete listing of this file is presented in Appendix A.

of experimental data for the reduction of oxygen on passivated iron in dilute alkaline solutions (Calvo, 1979; Calvo and Schiffrin, 1988). This value is equal to that used previously in the SCCEX Code (Cragnolino et al., 1994) for the reduction on stainless steel and half of the one suggested by Macdonald and Urquidi-Macdonald (1990). These authors indicate that, among other adjustments, the transfer coefficient for the oxygen reduction reaction was modified from 0.5 to 1.5 in order to obtain reasonable values of the redox potential, fulfilling the condition $-1.0 < E_{redox} < 1.0 V_{SHE}$ (Urquidi-Macdonald et al., 1990). The value of β is slightly higher than that of 0.5 reported by Vetter (1967), but lower than $\beta = 1.0$ as reported by Damjanovic (1969), in both cases for the reduction of oxygen on oxide-free platinum. Recent data of Okuyama and Haruyama (1990) for SS in a borate buffer solution exhibited a Tafel slope of 60 mV/decade for the reduction of oxygen which implies a transfer coefficient of 1.0. The use of $\beta = 0.75$ seems to be a reasonable compromise until more accurate data can be obtained.

The value adopted for the rate constant of the oxygen reduction reaction was 3.8×10^{12} C m mol^{-1} yr^{-1}. This value was calculated using Eq. (2-24) with the exchange current density, $i^0_{O_2}$, equal to 2.3×10^{-11} A/cm^2 as measured by Calvo (1979). This is a value close to those reported for noble metals in acidic media (10^{-10} to 10^{-12} A/cm^2), but more than two orders of magnitude larger than the values estimated for passive metals of the iron-group by Bockris and Reddy (1970). However, it was adopted because it represents the only experimentally measured value available in the literature for passive iron. A value of 37.3 kJ/mol was adopted for the activation energy as measured by Calvo (1979). This is a significant departure with respect to the value of 100 kJ/mol used in the SCCEX code (Cragnolino, 1994), on the basis of the activation energy suggested by Macdonald and Urquidi-Macdonald (1990).

For the overall equation describing the cathodic reduction of oxygen under mixed activation-diffusion control [Eq. (2-22)], the mass transport parameters of importance are the diffusion coefficient and the solubility of oxygen in solution, which are both functions of temperature. The oxygen solubility is expressed in terms of the Henry's law constant, which is given as a function of temperature by

$$\ln K_H = 0.2984 - \frac{5.59617 \times 10^3}{T} + \frac{1.04967 \times 10^6}{T^2} \qquad (5\text{-}1)$$

where K_H is the Henry's constant in mol kg^{-1} atm^{-1} and T is the temperature in °K, according to Battino (1981). The value of K_H is used to calculate the concentration of oxygen in the liquid layer using Eq. (2-23) assuming a partial pressure of oxygen equal to 0.21 atm. The diffusion coefficient of oxygen at any temperature was calculated from

$$D = 0.063 \exp\left\{\frac{14.612}{R}\left[\frac{1}{298.15} - \frac{1}{T}\right]\right\} \qquad (5\text{-}2)$$

where D is the diffusion coefficient in m^2/yr, and R is the ideal gas constant expressed in kJ mol^{-1} °K^{-1}. The pre-exponential coefficient, which represents the diffusivity of oxygen at 25 °C, is equal to 0.063 m^2/yr. For the activation energy a value of 14.612 kJ/mol was adopted. These two parameters were calculated from the experimental data reported by Case (1973).

For the cathodic reduction of water, as expressed by Eq. (2-26), a value of 0.5 was assigned to β, as commonly reported (Vetter, 1967; Bockris and Reddy, 1970) for the case of electrochemical discharge as the rate determining step followed by chemical desorption. The rate constant was calculated to be 1.57×10^{-1} C m^{-2} yr^{-1}, corresponding to a value of $i^0_{H_2O}$ of 5.97×10^{-23} A/cm^2, as derived from results by Turnbull and Gardner (1982). For the activation energy, a value of 25 kJ/mol was adopted, as reported by Heusler (1976) for Ni in alkaline solutions. This value is relatively close to 20 kJ/mol, which was suggested by Macdonald and Urquidi-Macdonald (1990) for the reduction on stainless steel and used in the SCCEX code (Cragnolino et al., 1994).

For consideration of the anodic corrosion process that occurs as soon as the container surface is wetted, a rate of dissolution in the presence of an aqueous solution equivalent to a passive current density of 1×10^{-6} A/cm^2 (approximately 10 μm/yr) was assumed for the steel overpack on the basis of the data from Alvarez and Galvele (1984) for iron in chloride-containing solutions at pH 10. This value represents a rate of 3.15×10^5 C m^{-2} yr^{-1}.

For consideration of localized corrosion, the dependence of the critical potentials for initiation (E_p) and repassivation (E_{rp}) on chloride concentration and temperature were previously discussed in detail (Sridhar et al., 1993b) and implemented in the SCCEX code (Cragnolino et al., 1994). A general expression for both parameters of the form

$$E_{crit} = E^0_{crit}(T) + B(T) \log [Cl^-] \tag{5-3}$$

was established on the basis of extensive literature data, in which the constants $E^0_{crit}(T)$ and $B(T)$ were found to be linear functions of the temperature expressed in °C (Sridhar et al., 1993b).

For A 516 steel, which is the primary candidate material for the outer overpack, on the basis of recent data (Dunn et al., 1996b), the following relationships were used for E_p at temperatures above 65 °C

$$E^0_p(T) = -584.8 + 3.92T;\ B_p(T) = -24.5 - 1.1T \tag{5-4}$$

and for E_{rp}

$$E^0_{rp}(T) = -620.3 + 0.47T;\ \ B_{rp}(T) = -95.2 + 0.88\ T \tag{5-5}$$

For alloy 825, considered the primary candidate material for the inner disposal overpack, on the basis of data already reported (Sridhar et al., 1995), the following parameters were used at temperatures above 50 °C for E_p

$$E^0_p(T) = 200;\ \ B_p(T) = -240 \tag{5-6}$$

and for E_{rp}

$$E^0_{rp}(T) = 422.8 - 4.1T; \quad B(T) = -64.0 - 0.8T \tag{5-7}$$

In all these equations, $E^0_{crit}(T)$ and $B(T)$ are expressed in mV_{SHE} (standard hydrogen electrode scale) and mV/decade, respectively, and the temperature in °C. The resulting values of E_p and E_{rp} are converted to V_{SHE} for comparison with E_{corr} values.

When the corrosion potential becomes higher than the critical potential for initiation of localized corrosion, it is assumed that localized corrosion of steel in the form of pitting occurs instantaneously without an induction time at pH values higher than 8. Pit penetration was calculated on the basis of experimental measurements conducted by Marsh and Taylor (1988). Experiments were conducted in 0.1 M $NaHCO_3$ solutions containing 1,000 ppm Cl^- (pH 8.4) at 90 °C to obtain cumulative pit size distributions. Using extreme value statistics and considering a return period of 40,000, which is defined as the surface area ratio between the overpack and the experimental specimen, the following expression for pit penetration as a function of time was obtained from the Marsh and Taylor (1988) data

$$P = 8.66\ t^{0.45} \tag{5-8}$$

where P is in mm and t is in yr. The correlation coefficient, R^2, was found to be 0.993. The differential form of Eq. (5-8) is used in the code to express the rate of penetration which is varying with time.

Once penetration of the outer overpack occurs, the potential of the galvanic couple established between the outer and inner overpacks, E^{wp}_{corr}, is calculated using Eq. (2-24). For that purpose, a value of E_{couple} equal to $-0.46\ V_{SHE}$ was adopted on the basis of results reported by Scully and Hack (1984) for galvanic couples with an area ratio 1:1 made of steel and alloy 625 (a nickel-base alloy with similar behavior to alloy 825) and exposed to sea water. If the E^{wp}_{corr} is lower than E_{rp} for alloy 825, a value of passive current density equal to 2×10^{-7} A/cm^2 (approximately 2 μm/yr) is adopted for the passive dissolution of the alloy. This value is typical of corrosion-resistant alloys (Sedriks, 1979) and similar to values measured in the CNWRA experimental program after long passivation times (Dunn et al., 1996a). For localized corrosion, no initiation time is assumed if E^{wp}_{corr} is greater than E_{rp}. In this case, a constant value of 6.3×10^6 C m^{-2} yr^{-1} (2×10^{-5} A/cm^2) is used for the pit propagation rate, which represents values typical of slow active dissolution.

In order to attain WP failure within the simulation time of 10,000 yr, the wall thickness of the inner container was reduced arbitrarily to 0.01 m in this example case. In addition, instead of using a chloride concentration of 3.0×10^{-3} mol/L as provided by MULTIFLO calculations, the concentration was arbitrarily raised to 3.0×10^{-1} mol/L. Nevertheless, this concentration level can be expected in certain circumstances in the near field, as discussed elsewhere (Sridhar et al., 1993a;b)

5.2 RADIONUCLIDE RELEASE DATA

As noted before, the main input data for the *ebspac_release.f* code is *release.inp*, which is presented in Table 5-5. A description of the various data files included in the *ebspac_release.f* code is presented in the following sections.

Table 5-5. Input file *release.inp*—Input file only for the release part of the EBSPAC

```
\input data file for ebspac release code: ebspac_release.f
|
\Cell information
2335.                                   ! xcon: number of WP
1000                                    ! iscon: # of WP in scenario failure
4500.                                   ! sftime: time of  scenario failure [y]
0.10                                    ! deffrac: defective fraction of WPs/cell
|
\WP information
1.421, 4.572                            ! dintl: internal WP diameter; xlintl: internal WP length [m]
7.83                                    ! xvol: internal WP volume in which water can reside [m^3]
|
\Thermal data
'temphumd.dat'                          ! temfil: temp. file (output from ebspac_fail.f)
373.15                                  ! ctemp: boiling point of water at atm. condition [K]
|
\Rock parameters
0.14, 0.14, 0.14                        ! rpor(1..3): rock porosities
\
\backfill parameters
0.14                                    ! ppor: packing porosity
|
\Flow parameters
'floebs.dat'                            ! hydfil: flow parameters file
7.                                      ! funnel: funnel factor
|
\SF  materials
\
2800.                                   ! amassc: SF mass [kg]
250., 3000., 1.0E-08, 0.3               ! fuewt,fueden,fuedif,fuepor
\
\Fuel leaching
2, 9.0, 0.2, 2.e-3, 0.50                ! imodel,phvalue,oxgnovpr [atm] ,cco3 [mol/L],wetfrac
|
\ Radionuclide inventory
'ebspac.nuc'                            ! elefil: nuclide names, halflife,inventory
|
\C-14 generation
1.e-3                                   ! r0z: initial radius of SF particle [m]
37.                                     ! rhou: density of SF [kg mole/m^3]
1.e-5                                   ! r1z: radius of the SF grain [m]
1.e-6                                   ! r2z: subgrain fragment radius after trans. frac. [m]
6.1e-4                                  ! thclad: thickness of cladding [m]
7.2e-4                                  ! cfuel: c-14 [ci] /kg SF
4.89e-4                                  ! czmetal: c-14 [ci] /kg SF in Zircaloy clad & other metals
2.48e-5                                 ! czoxide: c-14/kg SF in initial Zircaloy oxide & crud
6.2e-6                                  ! cgap: c-14/kg SF in grain and gap
|
```

Table 5-5. Input file *release.inp*—Input file only for the release part of the EBSPAC (cont'd)

```
\ Radionuclide transport
5.6e-5, 5.6e-5, 5.6e-5, 5.6e-5                ! rdiff(1..4): layers1..4 for diffusion
|
\NUMERICAL
\
\Grids
10, 10                                        ! imax,jmax: # of grid nodes in i,j directions
\X-COOR of grid nodes
.1, .5, 1.0, 2.0, 4.0, 5.0, 6.0, 7.0, 8.0, 9.0
\Y-COOR of grid nodes
.1, .5, 1.0, 2.0, 4.0, 5.0, 6.0, 7.0, 8.0, 9.0
\ Note: zones apply to the above grid, zones are the same for all cell
\ZONES
4                                             ! nzones: no. of zones for material types
1   1 1   1  1                               ! iz,ib,jb,ie,je: for zone 1
2   2 1   2  1                               ! iz,ib,jb,ie,je: for zone 2
3   3 1   3  1                               ! iz,ib,jb,ie,je: for zone 3
4   4 1   10 1                               ! iz,ib,jb,ie,je: for zone 4
|
\ Solution algorithm control parameters (Runge-Kutta)
25., 1., 50.                                  ! dtinit [yr], dtmin [yr], dtmax [yr]
1.0e-2, 1.0e-10                               ! eps, tiny
|
\output parameters
100.                                          ! ibt: number of bins for time values
|
\END
```

5.2.1 Nuclide Data

The nuclides data can be found in file *ebspac.nuc*. The content of this file is presented in Table 5-6. This file lists radionuclide elements, chains, solubility limit, retardation factor, molecular weight, half life, initial inventory, and gap fraction. A total of 21 radionuclides corresponding to 15 elements are considered. The elements included are Cm, Pu, U, Am, Np, Th, Ra, Pb, Cs, I, Tc, Ni, C, Se, and Nb. A total of 12 chains are considered with 3, 3, 2, 2, 4, 1, 1, 1, 1, 1, 1, and 1 chain members, respectively. Data for each element include the number of occurrences in various chains, solubility limit, and retardation factor. Then the chain number and chain position where this element occurs are presented. The atomic weights of 21 radionuclides from these 15 elements, corresponding half life, initial inventory, and fraction of the individual radionuclides present in the cladding-pellet gap are presented. The inventory and half life are presented in Ci/WP and yr, respectively. The list of parameters that describes this data set is presented in Table 4-5. The nuclide set and associated parameter values are the same as used in IPA Phase 2 activity (Nuclear Regulatory Commission, 1995).

5.2.2 Water Flow Data

The water flow data is found in *floebs.dat* and is presented as an example in Table 5-7. Through this file, the rate of infiltration into the EBS can be given as a function of time. In the example file shown in Table 5-7, the infiltration rate is kept constant between 0 and 10,000 yr (end of simulation) to invoke a steady-state condition. A flow factor is presented which is used as a multiplier such that the flow rate can be changed by that factor. A value of 1 assigned to the flow factor keeps the flow rate as specified. The use of this factor, which could be any positive number, is a convenient way to change the infiltration rate without having to change the infiltration data when it is presented at many time steps. For the example problem, the infiltration rate and load factor are chosen arbitrarily.

Table 5-7. Data file *floebs.dat*—Contains flow factor which can be a function of time to represent water entering into the EBS as a function of time (for future implementation)

```
1.00                    ! flowfactr: flow factor
0.        2.086E-03     ! time(yr) and infiltration(m3/yr)
10000.    2.086E-03     ! time(yr) and infiltration(m3/yr)
```

5.3 OUTPUT DATA

The output data from EBSPAC are presented in several files. Echoed input data and some intermediate printouts from the execution of *ebspac_fail.f* and *ebspac_release.f* can be found in *echo1.out* and *echo2.out*, respectively. The output file from *ebspac_fail.f* which is also an input file to *ebspac_release.f*, has already been discussed in the previous section. The penetration of the WP outer overpack as a function of time, followed by that of the inner overpack until either the time of failure or the maximum time has been reached, can be found in the file *corrode.out* and is presented as an example in Appendix B. A plot of the data is shown in Figure 5-2. In this figure, the WP surface temperature, drift wall temperature, and penetration depth expressed as remaining thickness are shown as functions of time. It is seen that penetration of the WP outer overpack begins when the temperature of the WP surface reaches about 108 °C. Initiation of localized corrosion occurs as soon as the surface becomes wet because E_{corr} is greater than E_{rp}.

Table 5-6. Data file *ebspac.nuc*—List of radionuclide elements, chains, solubility limit, retardation factor, molecular weight, half life, initial inventory, and gap fraction

```
 15
 CM      2 .24E-6    100.0
1 1
2 1
 PU      3 .01E-3    100.0
1 2
3 2
4 1
  U      3  0.95E-3  2.0
1 3
4 2
5 1
AM       2  .24E-6   200.0
2 2
3 1
NP       1  .237E-3  50.0
2 3
TH       1  2.3E-10  100.0
5 2
RA       1  6.8E-8   30.0
5 3
PB       1  1.       20.0
5 4
CS       1  1.       200.0
6 1
I        1  1.       1.0
7 1
TC       1  1.       1.0
8 1
NI       1  0.59E-3   2.0
9 1
C        1  1.       1.0
10 1
SE       1  7.9E-11   1.0
11 1
NB       1  1.       20.0
12 1
12 3 3 2 2 4 1 1 1 1 1 1 1
     246.0        CM246      4.73E03     0.07224     0.
     242.0        PU242      3.86E05     4.47857     0.
     238.0        U238       4.47E09     0.89038     0.
     245.0        CM245      8.50E03     0.35322     0.
     241.0        AM241      4.32E02     4590.53     0.
     237.0        NP237      2.14E06     0.8064      0.
     243.0        AM243      7.38E03     43.4528     0.
     239.0        PU239      2.41E04     862.391     0.
```

Table 5-6. Data file *ebspac.nuc*—List of radionuclide elements, chains, solubility limit, retardation factor, molecular weight, half life, initial inventory, and gap fraction (cont'd)

240.0	PU240	6.54E03	1422.21	0.
241.0	AM241	4.32E02	4590.53	0.
237.0	NP237	2.14E06	0.8064	0.
243.0	AM243	7.38E03	43.4528	0.
239.0	PU239	2.41E04	862.391	0.
240.0	PU240	6.54E03	1422.21	0.
236.0	U236	2.34E07	0.67178	0.
234.0	U234	2.45E05	5.283	0.
230.0	TH230	7.70E04	3.61E-4	0.
226.0	RA226	1.60E03	1.0E-6	0.
210.0	PB210	2.23E01	1.3E-7	0.
135.0	CS135	2.30E06	0.9796	0.0
129.0	I129	1.57E07	0.083	0.02
99.0	TC99	2.13E05	34.38	0.02
59.0	NI59	8.00E04	9.97	0.
14.0	C14	5.73E03	4.30	0.02
79.0	SE79	6.50E04	1.0663	0.02
94.0	NB94	2.03E04	2.2259	0.

1234567890123456789012345678901234567890123456789

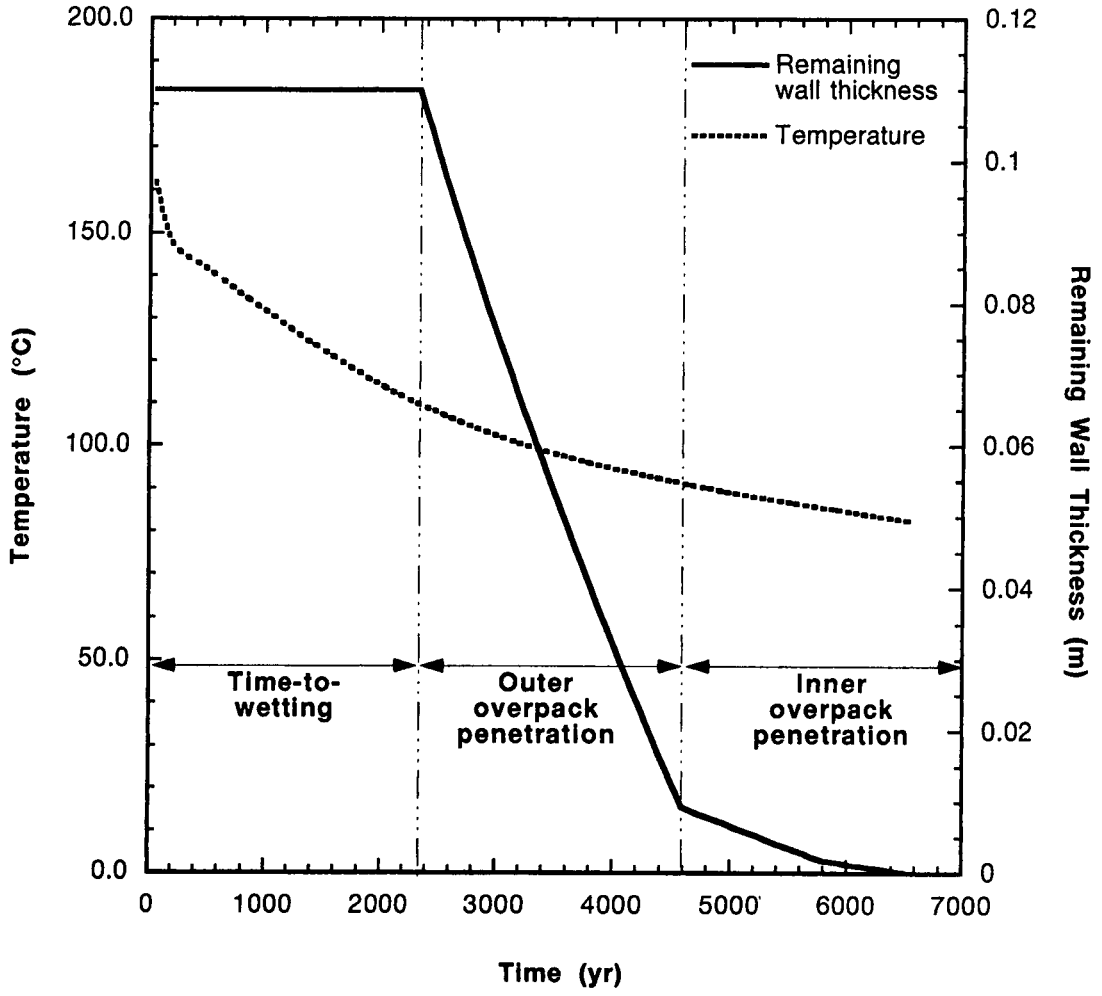

Figure 5-2. Temperature and remaining waste package wall thickness as a function of time

The cumulative release of radionuclides at the end of a 10,000-yr period (i.e., at t_{end}) can be found in the file *relcum.dat*. The content of this file in the case of the example is presented in Appendix C.

The cumulative release of radionuclides as a function of time is contained in the output file *release.out* and the results of the example case are presented in a plot-ready format in Appendix D. The first row contains the names of all the radionuclides whereas the first column provides the time in years. The cumulative release information for each radionuclide is presented in Ci. This file is portable to other computers for plotting purposes. The cumulative releases of the first 9 radionuclides are plotted against time using the data from this file as shown in Figure 5-3.

Finally, the output data that are likely to be used in the TPA calculations are presented in the output file *ebspacnef.dat*. The format used is the input file format specified by the NEFTRAN code which is used to compute radionuclide transport to the far field in the suite of TPA codes. In this file, information is presented for one nuclide at a time. First, the name of the radionuclide is presented, followed by the cumulative release as a function of time. A regular time interval is used for this output data.

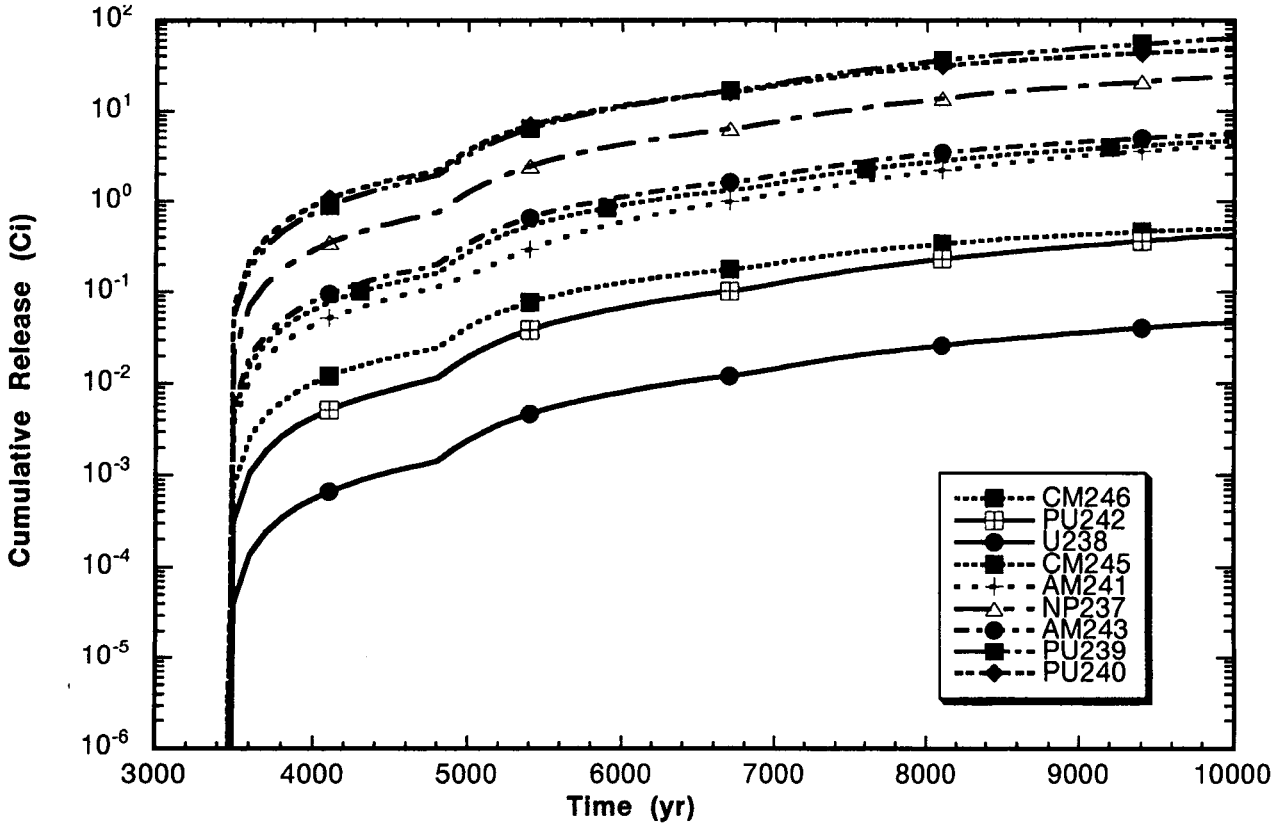

Figure 5-3. Cumulative release as a function of time for various radionuclides

6 SUMMARY AND FUTURE DEVELOPMENTS

EBSPAC has been developed for conducting performance assessments of the EBS taking into consideration the need to evaluate the failure of the WP and the subsequent release of radionuclides. It will be incorporated into the TPA code as the source term module. This report describes technical bases, computational approach, program flow and user interface, hardware and software requirements, graphics, and pre- and post-processors that are relevant to the development and use of EBSPAC.

Following an introduction, this report presents a brief description of several models used in EBSPAC, which essentially consists of two separate codes, one dealing with WP failure calculations (*ebspac_fail.f*) and the other with radionuclide release (*ebspac_release.f*). Thermohydrologic processes induced by the heat released by radioactive decay of the HLW and the consequent alteration of the environment surrounding the WPs are considered by separate models outside these two codes. Results of the corresponding calculations are then input into EBSPAC. The WP failure calculations are based on dry air oxidation of the outer disposal overpack, the aqueous corrosion of the outer and inner overpack, and mechanical fracture of the outer and inner overpack. The code related to radionuclide release is based on models for dry oxidation of the cladding and the fuel matrix (from UO_2 to $UO_{2.4}$ and to U_3O_8), dissolution of the fuel matrix as a function of temperature and chemical composition of the water, generation and dissipation in radionuclide chains, the mass balance of the radionuclides in the water in contact with the SF, and diffusive transport of radionuclides away from the WP. Simplifications and assumptions made in developing Version 1.0β of EBSPAC are explained in the text.

The EBSPAC code structure is described in detail, emphasizing the fact that there is no feedback from the code dealing with radionuclide releases into that dedicated to WP failure calculations. Therefore, the user can focus on developing or analyzing either part of EBSPAC. The functions of different subroutines used in both codes are briefly described. The computer code capability, compilation and linking, hardware requirements, and program execution procedures are discussed. Results from an example problem using this computer code are presented.

With minor modifications, EBSPAC is applicable to different designs of the EBS that involve different thermal and environmental conditions, distinct types of SF combinations, and dissimilar overpack materials and WP designs. Alterations in the radionuclide composition, including chains, can be accommodated by modifying the radionuclide input data file. However, the current version of the code needs additional modifications to be used for the vitrified HLW.

In order to keep the source term calculation simple, EBSPAC focuses on a single cell. However, post- and pre-processors can be written to integrate EBSPAC as a source term module into the TPA code for overall performance assessment studies.

It should be noted, however, that this version of EBSPAC has been developed mainly as an adequate framework for future developments. These developments will include:

- Implementation of the results of MULTIFLO calculations to obtain a better description of the evolution of the composition and variables of the near-field environment, such as pH and f_{O_2}, as a function of temperature and time.

- Implementation of future MULTIFLO calculations addressing the definition of the near-field environment at the drift scale, including the effects of various heat loads, host rock compositions, and initial fluid compositions.

- Incorporation of more developed corrosion models for the description of wet/dry periods, including the effect of through-wall penetrations of various sizes on the outer container and their related influence on galvanic coupling effects, as well as the consideration of stress corrosion cracking models.

- Improvement of the mechanical failure model through appropriate implementation of the methodology described for the analysis of thermal embrittlement of the steel outer overpack.

- Incorporation of a SF dissolution rate-limited model to address the release of relatively soluble radionuclides, such as Tc-99, I-129, Np-237, Cs-137, and Sr-90, and implementation of simplified models to account for colloidal transport of the actinides.

- Consideration of the effects of uranylsilicates as potential secondary alteration products of the spent fuel in the presence of high-silica concentration groundwater anticipated to be encountered by the WP because these alteration products could play an important role in dissolution of SF.

- Consideration of variable water infiltration into the EBS, which will require modification of modules where liquid release calculations are performed, to have a full implementation of the effect of time varying flow rate on radionuclide release from SF.

Eventually, the evaluation of the MPC performance can be incorporated to the code. It should be noted that the MPC performance is ignored in this version because the DOE is not taking credit for the MPC as a containment barrier.

In addition to the model developments listed above, the incorporation of different numerical solvers that may improve the efficiency of EBSPAC will be completed. Taking into consideration code architecture and efficiency, other modifications to the code will be implemented.

In the future, the implementation of FORTRAN 90 will be accomplished to develop modules for reading input data. FORTRAN 90 provides significant improvement in coding (i.e., uses fewer code lines) and simplifies input in a more readable manner. Unlike FORTRAN 77, FORTRAN 90 lends itself to a fully structured approach.

7 REFERENCES

Ahn, T.M. 1994. Long-term C-14 source term for a high-level waste repository. *Waste Management* 14: 393–408.

Ahn, T.M. 1995a. *Dry Oxidation and Fracture of LWR Spent Fuels*. NUDOC Accession Number: 9512220279. Washington, DC: Nuclear Regulatory Commission.

Ahn, T.M. 1995b. *Long-term Kinetic Effects and Colloid Formations in Dissolution of LWR Spent Fuels*. NUDOC Accession Number: 9508030112. Washington, DC: Nuclear Regulatory Commission.

Ahn, T.M. 1996. *Dry Oxidation of Waste Package Materials*. NUDOC Accession Number 9607290014. Washington, DC: Nuclear Regulatory Commission.

Ahn, T., and P. Soo. 1983. *Container Assessment—Corrosion Study of HLW Container Materials, Quarterly Progress Report, October-December 1983*. BNL-NUREG-34220. Upton, NY: Brookhaven National Laboratory.

Ahn, T., and P. Soo. 1984. *Container Assessment—Corrosion Study of HLW Container Materials, Quarterly Progress Report, January-March 1984, April-June 1984, July-September 1984*. (Informal Reports. Limited Distribution.) Upton, NY: Brookhaven National Laboratory.

Alvarez, M.G., and J.R. Galvele. 1984. The mechanism of pitting of high purity iron in NaCl solutions. *Corrosion Science* 24: 27–48.

American Society for Testing and Materials. 1992. *Standard Practice for Use of the International System of Units (SI) (the Modernized Metric System)*. E 380-92. Philadelphia, PA: American Society for Testing and Materials.

Bates, J.K., J.A. Fortner, P.A. Finn, D.J. Wronkiewicz, J.C. Hoh, J.W. Emery, E.C. Buck, and S.F. Wolf. 1995. *Yucca Mountain Project—Argonne National Laboratory Annual Progress Report, FY 1994*. ANL-94/42. Argonne, IL: Argonne National Laboratory.

Battino, R., ed. 1981. *International Union of Pure and Applied Chemistry (IUPAC) Solubility Data, Series: Oxygen and Ozone*. New York, NY: Pergamon Press: 7.

Bejan, A. 1988. *Advanced Engineering Thermodynamics*. New York, NY: John Wiley & Sons: p. 226.

Bergner, D. 1983. Diffusion of C, N and O in metals. *DIMETA-82. Diffusion in Metals and Alloys*. F.J. Kedves and D.L. Beke, ed. Bay Village, OH: Trans Tech Publications.

Bockris, J.O'M., and A.K.N. Reddy. 1970. *Modern Electrochemistry*. New York, NY: Plenum Press: 2.

Briant, C.L., and S.K. Banerji. 1983. Intergranular fracture in ferrous alloys in nonaggressive environments. *Treatise on Materials Science and Technology. Volume 25: Embrittlement of Engineering Alloys*. C.L. Briant and S.K. Banerji, eds. New York, NY: Academic Press: 21–58.

Calvo, E.J. 1979. *Study of the Electroreduction Reaction of Oxygen on Passive Metals in Different Aqueous Media*. (in Spanish). PhD Dissertation. La Plata, Argentina: Universidad Nacional de La Plata.

Calvo, E.J., and D.J. Schiffrin. 1988. The electrochemical reduction of oxygen on passive iron in alkaline solutions. *Journal of Electroanalytical Chemistry* 243: 171–185.

Case, B. 1973. The diffusivity of oxygen in dilute alkaline solution from 0 ° to 65 °C. *Electrochimica Acta* 18: 293–299.

Cragnolino, G.A., N. Sridhar, J. Walton, R. Janetzke, T. Torng, J. Wu, and P. Nair. 1994. *"Substantially Complete Containment"—Example Analysis of a Reference Container*. CNWRA 94-003. San Antonio, TX: Center for Nuclear Waste Regulatory Analyses.

Cragnolino, G.A., H.K. Manaktala, and Y.-M. Pan. 1996. *Thermal Stability and Mechanical Properties of High-Level Radioactive Waste Container Materials: Assessment of Carbon and Low-Alloy Steels*. CNWRA 96-004. San Antonio, TX: Center for Nuclear Waste Regulatory Analyses.

Crank, J. 1975. *The Mathematics of Diffusion*. 2nd edition. Oxford, UK: Clarendon Press.

Damjanovic, A. 1969. Mechanistic analysis of oxygen electrode reactions. *Modern Aspects of Electrochemistry*. J.O'M. Bockris and B.E. Conway, eds. New York, NY: Plenum Press: 5: 369-483.

Druce, S.G., G. Gage, G.R. Jordan, and J.A. Hudson. 1986. Effect of Ageing on the properties of pressure vessel steels. *Acta Metallurgical* 34: 641–652.

Dunn, D.S., G.A. Cragnolino, and N. Sridhar. 1996a. Localized corrosion initiation, propagation, and repassivation of corrosion-resistant high-level nuclear waste container materials. *CORROSION 96*. Houston, TX: NACE International. Paper No. 97.

Dunn, D.S., G.A. Cragnolino, H.K. Manaktala, P. Angell, Y.-M. Pang, and N. Sridhar. 1996b. Factors influencing the performance of carbon steel overpacks in the proposed high-level nuclear waste repository. *CORROSION 97*. Houston, TX: NACE International: Paper No. 99. To be published.

Einziger, R.E. 1994. Preliminary spent fuel oxidation source term model. *Proceedings of the Fifth International High-Level Radioactive waste Management Conference*. La Grange Park, IL: American Nuclear Society and New York, NY: American Society of Civil Engineer: 2: 554–559.

Einziger, R.E., L.E. Thomas, H.C. Buchanan, and R.B. Stout. 1992. Oxidation of spent fuel in air at 175 to 195 °C. *Journal of Nuclear Materials* 190: 53–60.

Fyfe, D. 1994. *Corrosion*. R.A. Jarman, and G.T. Burstein, eds. Oxford, U.K.: Butterworth Heinmann: 1: 2:31–2:42

Grabke, H., D. Wiemer, and H. Viefhaus. 1991. Segregation of sulfur during growth of oxide scales. *Applied Surface Science* 47: 243–250.

Graedel, T.E., and R.P. Frankenthal. 1990. Corrosion mechanisms for iron and low alloy steels exposed to the atmosphere. *Journal of the Electrochemical Society* 137: 2,385–2,394.

Gray, W.J. 1992. *Dissolution Testing of Spent Fuel.* Presentation to Nuclear Waste Technical Review Board, October 14-16, Las Vegas, NV. Richland, WA: Pacific Northwest National Laboratory.

Gray, W.J., and C.N. Wilson. 1995. *Spent Fuel Dissolution Studies FY 1991 to 1994.* PNL-10540. Richland, WA: Pacific Northwest National Laboratory.

Hadley, G.R. 1986. Thermal Conductivity of Packed Metal Powders. *International Journal of Heat Mass Transfer* 29(6): 909–920.

Harrar, J.E. (Chairman), J.F. Carley, W.F. Isherwood, and E. Raber. 1990. *Report of the Committee to Review the Use of J-13 Well Water in Nevada Nuclear Waste Storage Investigations.* UCID-21867. Livermore, CA: Lawrence Livermore National Laboratory.

Hartman, H.L. 1991. *Mine Ventilation and Air Conditioning.* Malabar, FL: Krieger Publishing Company: p. 8.

Heusler, K.E. 1976. Influence of temperature and pressure on the kinetics of electrode processes. *High Temperature, High Pressure Electrochemistry in Aqueous Systems.* D.deG. Jones and R.W. Staehle, eds. Houston, TX: National Association of Corrosion Engineers: 387–399.

Hibbitt, Karlson & Sorenson, Inc. 1994. *ABAQUS User's Manual, Version 5.3.* Pawtucket, RI: Hibbitt, Karlson & Sorenson, Inc.

Hudson, J.A., S.G. Druce, G. Gage, and M. Wall. 1988. Thermal aging effects in structural steels. *Theoretical and Applied Fracture Mechanics* 10: 123–133.

Iwadate, T., J. Watanabe, and Y. Tanaka. 1985. Prediction of the remaining life of high temperature/pressure reactors made of Cr-Mo steels. *Transactions of ASME. Journal of Pressure Vessel Technology* 107: 230–238.

Kedves, F., and D. Bebe, ed. 1983. *DIMETA-82 Diffusion in Metals and Alloys.* Bay Village, OH: Trans Tech Publications.

Kim, J. 1986. Chemical behavior of transuranic elements in natural aquatic systems. *Handbook on the Physics and Chemistry of the Actinides.* A.J. Freeman and C. Keller, ed. New York, NY: Elsevier Science Pub.

Kim, J.I., B. Delakowitz, P. Zeh, T. Probst, X. Lin, U. Ehrlicher, C. Schauer, M. Ivanovich, G. Longworth, S.E. Hasler, M. Gardiner, P. Fritz, D. Klotz, D. Lazik, M. Wolf, S. Geyer, J. L. Alexander, D. Read, and J. B. Thomas. 1996. *Colloid Migration in Groundwater:*

Geochemical Interactions of Radionuclides with Natural Colloids. EUR 16754. Bruxelles, Belgium: European Commission.

Kofstad, P. 1972. *Nonstoichiometry, Diffusion and Electrical Conductivity in Binary Metal Oxides*. New York, NY: Wiley-Interscience.

Lake, L.W. 1989. *Enhanced Oil Recovery*. Englewood Cliffs, NJ: Prentice Hall.

Lapidus, L. 1962. *Digital Computation for Chemical Engineers*. New York, NY: McGraw-Hill, Inc.

Lawrence Livermore National Laboratory. 1995. *Yucca Mountain Site Characterization Project (YMP) Status Report. April 1995*. Lawrence Livermore National Laboratory: Livermore, CA.

Leygraf, C. 1995. Atmospheric Corrosion. *Corrosion Mechanisms in Theory and Practice*. P. Marcus and J. Oudar, eds. Marcel Decker Inc., New York: 421–455.

Lichtner, P.C. 1994. *Engineered Barrier System Performance Assessment Codes (EBSPAC) Progress Report October 1, 1993, through September 25, 1994*. CNWRA 94-026. San Antonio, TX: Center for Nuclear Waste Regulatory Analyses.

Lichtner, P.C. 1994. *Multiphase Reactive Transport Theory*. CNWRA 94-018. San Antonio, TX: Center for Nuclear Waste Regulatory Analyses.

Lichtner, P.C., and Seth, M.S.. 1996. *User's Manual for MULTIFLO: Part II—MULTIFLO 1.0 and GEM 1.0, Multicomponent-Multiphase Reactor Transport Model*. CNWRA 96-010. San Antonio, TX: Center for Nuclear Waste Regulatory Analyses.

Lide, D.R., ed. 1990. *CRC Handbook of Chemistry and Physics*. 71st edition. Boca Raton, FL: CRC Press: 15–21.

Lindner, Von R., and Hj. Matzke. 1958. Diffusion von Xe-133 in uranoxyd verschiedenen sauerstoffgehaltes. *Zeitschrift für Naturforschung* 14a: 582–585.

Lobnig, R.E., H.P. Schmidt, K. Hennesen, and H.J. Grabke. 1992. Diffusion of cations in Chromia layers grown on iron-base alloys. *Oxidation of Metals* 37: 81–93.

Macdonald, D.D., and M. Urquidi-Macdonald. 1990. Thin-layer mixed-potential model for the corrosion of high-level nuclear waste canisters. *Corrosion* 46(5): 380–390.

Manaktala, H., D. Turner, T. Ahn, V. Colten-Bradley, and E. Bonano. 1995. *Potential Implications of Colloids on the Long-Term Performance of a High-Level Radioactive Waste Repository*. CNWRA 95-015. San Antonio, TX: Center for Nuclear Waste Regulatory Analyses.

Manteufel, R.D. 1996. Effects on ventilation and backfill on a mined waste disposal facility. *Nuclear Engineering and Design*. Submitted for publication.

Marsh, G.P., and K.J. Taylor. 1988. An assessment of carbon steel containers for radioactive waste disposal. *Corrosion Science* 28: 289–320.

Mattsson, E. 1982. The atmospheric corrosion properties of some common structural metals—A comparative study. *Materials Performance* 21(7): 9–19.

Mayer, P., and W. Smeltzer. 1973. Internal oxidation and decarburization properties of an Fe-1w/oMn and Fe-1w/oC alloy in carbon dioxide-carbon monoxide atmosphere at 1000 °C. *Canadian Metallurgical Quarterly* 12: 23–34.

McClintock, F., and A. Argon. 1966. *Mechanical Behavior of Materials*. Reading, MA: Addison Wesley Co.

McCright, R.D., W.G. Halsey, and R.A. van Konynenburg. 1987. *Progress Report on the Results of Testing Advanced Conceptual Design Barrier Materials Under Relevant Environmental Conditions for a Tuff Repository*. UCID-21044. Livermore, CA: Lawrence Livermore National Laboratory.

McCuen, R.H., and P. Albrecht. 1994. Composite modeling of atmospheric corrosion penetration data. ASTM STP 1194 *Application of Accelerated Corrosion Tests to Service Life Prediction of Materials*. G. Cragnolino and N. Sridhar, eds. Philadelphia PA: American Society for Testing and Materials: 65–102.

McLean, D. 1957. *Grain Boundaries in Metals*. Clarendon Press, Oxford, UK.

Misawa, T., T. Kyuno, W. Suetaka, and S. Shimondaira. 1971. The mechanism of atmospheric rusting and the effect of Cu and P on the rust formation of low alloy steels. *Corrosion Science* 11: 35–48.

Mohanty, S., T. Ahn, P.C. Lichtner, R.W. Janetzke, and G.A. Cragnolino. 1996. *Software Requirements Description for the Engineered Barrier System Performance Assessment Code (EBSPAC), Version 1.0*. San Antonio, TX: Center for Nuclear Waste Regulatory Analyses.

Moran, M.J., and H.N. Shapiro. 1992. *Fundamentals of Engineering Thermodynamics*. New York, NY: John Wiley & Sons, Inc.: p. 562.

Nesbitt, J. 1989. Predicting minimum Al concentrations for protective scale formation on Ni-base alloys. *Journal of Electrochemical Society* 136: 1,511–1,517.

Newcomb, S., and W. Stobbs. 1991. The effects of a grain-boundary on the compositional fluctuations inherent in the oxidation of Fe-10Cr-34Ni. *Oxidation of Metals* 35: 69–88.

Nishikata, A., T. Takahashi, H. Bao-Rong, and T. Tsuru. 1994. Monitoring of corrosion rate of carbon steel under wet/dry cycle conditions and its corrosion mechanism. *Corrosion Engineering* 43: 225–234.

Nuclear Regulatory Commission. 1995. *NRC Iterative Performance Assessment Phase 2*. NUREG-1464. Washington, DC: Nuclear Regulatory Commission.

Oishi, Y., and H. Ichimura. 1979. Grain-boundary enhanced interdiffusion in polycrystalline CaO-stabilized Zirconia system. *Journal of Chemical Physics* 71(12): 5,134–5,139.

Okuyama, M., and S. Haruyama. 1990. The cathodic reduction of oxygen on stainless steels in a neutral solution. *Corrosion Science* 31: 521–526.

Otsuka, R., and H. Fujikawa. 1991. Scaling of austenitic stainless steels and Nickel-base alloys in high-temperature steam at 973 K. *Corrosion* 47: 240–248.

Press, W.H., B.P. Flannery, S.A. Teukolsky, and W.T. Vetterling. 1992. *Numerical Recipes*. New York, NY: Cambridge University Press.

Ryder, E.E., R.E. Finley, J.T. George, C.K. Ho, R.S. Longenbaugh, and J.R. Connolly. 1996. *Bench-Scale Experimental Determination of the Thermal Diffusivity of Crushed Tuff*. SAND94-2320. Albuquerque, NM: Sandia National Laboratories.

Sagar, B., R.B. Codell, J. Walton, and R.W. Janetzke. 1992. *SOTEC: A Source Term Code for High-Level Nuclear Waste Geologic Repositories User's Manual: Version 1.0*. CNWRA 92-009. San Antonio, TX: Center for Nuclear Waste Regulatory Analyses.

Scully, J.R., and H.P. Hack. 1984. Galvanic corrosion prediction using long- and short-term polarization curves. *CORROSION 84*. Houston, TX: National Association of Corrosion Engineers: Paper No. 34.

Sedriks, A.J. 1979. *Corrosion of Stainless Steels*. New York, NY: John Wiley & Sons.

Seth, M.S., and P.C. Lichtner. 1996. *User's Manual for MULTIFLO: Part I—METRA 1.0β, Two-Phase Nonisothermal Flow Simulator*. CNWRA 96-005. San Antonio, TX: Center for Nuclear Waste Regulatory Analyses.

Shewmon, P. 1963. *Diffusion in Solids*. New York, NY: McGraw-Hill Book Co.

Shida, Y., and T. Moroishi. 1992. Effect of Aluminum and Titanium additions to Fe-21%Cr-32%Ni on the oxidation behavior in an impure Helium atmosphere at high temperatures. *Oxidation of Metals* 37: 327–348.

Smith, H.D., and D.L. Baldwin. 1993. An investigation of thermal release of carbon-14 from PWR Zircaloy spent fuel cladding. *Journal of Nuclear Materials* 200: 128–137.

Sridhar, N., G.A. Cragnolino, and D.S. Dunn. 1993a. *Experimental Investigations of Localized Corrosion of High-Level Waste Container Materials*. CNWRA 93-004. San Antonio, TX: Center for Nuclear Waste Regulatory Analyses.

Sridhar, N., J.C. Walton, G.A. Cragnolino, and P.K. Nair. 1993b. *Engineered Barrier Performance Assessment Codes (EBSPAC) Progress Report—October 1, 1992, through September 25, 1993.* CNWRA 93-021. San Antonio, TX: Center for Nuclear Waste Regulatory Analyses.

Sridhar, N. 1995. *Planning and Status Report on the Engineered Barrier System Performance Assessment Code (EBSPAC) and Supporting Detailed Analyses.* Letter Report (September 27, 1995). San Antonio, TX: Center for Nuclear Waste Regulatory Analyses.

Sridhar, N., G.A. Cragnolino, and D.S. Dunn. 1995. *Experimental Investigations of Failure Processes of High-Level Radioactive Waste Container Materials.* CNWRA 95-010. San Antonio, TX: Center for Nuclear Waste Regulatory Analyses.

Stacy, R.C., and J.H. Goode. 1978. Voloxidation and dissolution of irradiated LWR fuel. *American Nuclear Society* 19:X.11–X.13.

Stone, J.A., and D.R. Johnson. 1978. Measurement of radioactive gaseous effluents from voloxidation and dissolution of spent fuel. *Proceedings of the 15th DOE Nuclear Air Cleaning Conference.* M.F. First, ed. Boston, MA: U.S. Department of Energy and the Harvard Air Cleaning Laboratory: 570–583.

Stothoff, S.A. 1996. Sensitivity of Long-Term Bare-Soil Infiltration Simulations to Hydraulic Properties in an Arid Environment. *Water Resources Research.* Submitted for publication.

Stothoff, S.A., H. Castellaw, and A. Bagtzoglou. 1996. Simulating the Spatial Distribution of Infiltration at Yucca Mountain, Nevada. *Water Resources Research.* Submitted for publication.

Stratmann, M., H. Streckel, K.T. Kim, and S. Crockett. 1990. On the atmospheric corrosion of metals which are covered with thin electrolyte layers—III. The measurements of polarization curves on metal surfaces which are covered with thin electrolyte layers. *Corrosion Science* 30(6/7): 715–734.

Swaminathan, V.P., R. Viswanathan, and C.P. Clark. 1991. Material property studies of two high-pressure turbine rotors for remaining life assessment. *ASME Joint Power Generation Conference* New York, NY: The American Society of Mechanical Engineers: Paper No. 91-JPGC-Pwr-22.

Tasovac, A., R. Marković, and Ž. Štrbački. 1989. Comparative investigation of some austenitic chromium-nickel steels in hot air. *Materials Science and Engineering* A120: 229–234.

Thomas, L.E., and R.J. Guenther. 1989. Characterization of low-gas-release LWR fuels by transmission electron microscopy. *Materials Research Society Symposium Proceedings.* Pittsburgh, PA: Materials Research Society: 127: 293–300.

TRW Environmental Safety Systems Inc. 1995. *Total System Performance Assessment—1995: An Evaluation of the Potential Yucca Mountain Repository.* B00000000-01717-2200-00136, Rev. 01. Las Vegas, NV: TRW Environmental Safety Systems, Inc.

TRW Environmental Safety Systems, Inc. 1996. *Mined Geologic Disposal System Advanced conceptual Design Report. Engineered Barrier Segment/Waste Package.* B00000000-01717-5705-00027. Rev. 00. Las Vegas, NV: TRW Environmental Safety Systems, Inc. Vol. III.

Tsuru, T., A. Nishikata, and J. Wang. 1995. Electrochemical studies on corrosion under a water film. *Materials Science and Engineering* A198: 161–168.

U.S. Department of Energy. 1987. *Characteristics of Spent Fuel, High-Level Wastes Which May Require Long-Term Isolation.* DOE/RW-0184. Vol. 2, Appendix 1C. Washington, DC: U.S. Department of Energy.

U.S. Department of Energy. 1993. *Yucca Mountain Project Reference Information Base.* YMP/93-02. Rev. 3. Las Vegas, NV: U.S. Department of Energy.

Urquidi-Macdonald, M., D.D. Macdonald, and S. Lenhart. 1990. *Mathematical Models for the Redox and Corrosion Potentials for High Level Nuclear Waste Containers in Tuff Repositories.* Final Report SRI Project 8292. Menlo Park, CA: SRI International.

Vander Voort, G.F. 1990. Embrittlement of steels. *Metals Handbook, Vol. 1, 10th edition, Properties and Selection: Irons, Steels, and High-Performance Alloys.* Materials Park, OH: ASM International: 689–736.

Van Wylen, G.J., and R.E. Sonntag. 1978. *Fundamentals of Classical Thermodynamics.* New York, NY: John Wiley & Sons: p. 434.

Vatter, I.A., C.A. Hippsley, and S.G. Druce. 1993. Review of thermal ageing data and its application to operating reactor pressure vessels. *International Journal of Pressure Vessels and Piping* 54: 31–48.

Verma, L.S., R. Singh, and D.R. Chaudhary. 1994. Geometry dependent resistor model for predicting effective thermal conductivity of two phase systems. *International Journal of Heat and Mass Transfer* 37(4): 704–714.

Vetter, K.J. 1967. *Electrochemical Kinetics.* New York, NY: Academic Press.

Viswanathan, R. 1989. *Damage Mechanisms and Life Assessment of High-Temperature Components.* Metals Park, OH: ASM International.

Walton, J.C. 1993. Effects of evaporation and solute concentration on presence and composition of water in and around the waste package at Yucca Mountain. *Waste Management* 13: 293–301.

Whittle, D., Y. Shida, G. Wood, F. Stott, and B. Bastow. 1982. Enhanced diffusion of oxygen during internal oxidation of nickel-base alloys. *Philosophical Magazine* 46: 931–949.

Wilson, C.N. 1990. *Results from NNWSI Series 3 Spent Fuel Dissolution Tests.* PNL-7170. Richland, WA: Pacific Northwest Laboratory.

Wilson M.L., J.H. Gauthier, R.W. Barnard, G.E. Barr, H.A. Dockery, E. Dunn, R.R. Eaton, D.C. Guerin, N. Lu, M.J. Martinez, R. Nilson, C.A. Rautman, T.H. Robey, B. Ross, E.E. Ryder, A.R. Schenker, S.A. Shannon, L.H. Skinner, W.G. Haley, J.D. Gansemer, L.C. Lewis, A.D. Lamont, I.R. Triay, A. Meijer, and D.E. Morris. 1994. *Total-System Performance Assessment for Yucca Mountain—SNL Second Iteration (TSPA-93)*. Vol. 1 and 2. SAND93-2675. Albuquerque, NM: Sandia National Laboratory.

APPENDIX A

DATA FILE *temphumd.dat*—INPUT DATA FILE TO *ebspac_release.f* PROVIDING TEMPERATURE AND RELATIVE HUMIDITY

APPENDIX A

DATA FILE *temphumd.dat*—INPUT DATA FILE TO *ebspac_release.f* PROVIDING TEMPERATURE AND RELATIVE HUMIDITY

The simulation time is followed by the number of rows of temperature and relative humidity data. Each row contains the row number, time (yr), WP temperature (°C), drift wall temperature (°C), and relative humidity. WP failure time (yr), WP length (m), and WP diameter (m) are listed at the bottom of the file to pass on to the *ebspac_release.f* code.

```
 10000.0000
196
  1      0.0002     21.8700     21.0000      0.9480
  2     50.4200    161.9000    147.6000      0.1399
  3    100.5000    155.6000    146.4000      0.1645
  4    152.4000    150.7000    143.8000      0.1872
  5    206.0000    147.4000    141.6000      0.2046
  6    259.4000    145.8000    140.7000      0.2138
  7    312.8000    144.7000    140.0000      0.2203
  8    366.2000    143.9000    139.6000      0.2253
  9    419.7000    143.0000    139.1000      0.2310
 10    473.1000    142.3000    138.6000      0.2355
 11    533.8000    141.0000    137.6000      0.2443
 12    585.7000    139.9000    136.7000      0.2520
 13    637.5000    138.8000    135.8000      0.2600
 14    689.3000    137.7000    134.9000      0.2683
 15    741.1000    136.6000    133.9000      0.2770
 16    793.0000    135.6000    133.0000      0.2851
 17    844.8000    134.6000    132.2000      0.2935
 18    896.6000    133.7000    131.3000      0.3014
 19    948.4000    132.7000    130.5000      0.3104
 20   1000.0000    131.8000    129.6000      0.3187
 21   1065.0000    130.5000    128.5000      0.3313
 22   1129.0000    129.3000    127.3000      0.3434
 23   1194.0000    128.0000    126.2000      0.3572
 24   1258.0000    126.8000    125.0000      0.3705
 25   1323.0000    125.6000    123.9000      0.3843
 26   1388.0000    124.4000    122.8000      0.3988
 27   1452.0000    123.3000    121.7000      0.4126
 28   1517.0000    122.1000    120.6000      0.4284
 29   1581.0000    121.0000    119.5000      0.4435
 30   1646.0000    119.9000    118.5000      0.4592
 31   1710.0000    118.8000    117.4000      0.4755
 32   1775.0000    117.7000    116.4000      0.4926
 33   1839.0000    116.7000    115.4000      0.5087
 34   1904.0000    115.6000    114.4000      0.5272
 35   1986.0000    114.4000    113.1000      0.5483
 36   2036.0000    113.6000    112.4000      0.5629
 37   2086.0000    112.9000    111.7000      0.5760
 38   2136.0000    112.3000    111.1000      0.5876
 39   2186.0000    111.6000    110.4000      0.6014
 40   2236.0000    111.0000    109.8000      0.6136
 41   2286.0000    110.3000    109.2000      0.6282
 42   2336.0000    109.7000    108.6000      0.6410
 43   2386.0000    109.1000    108.0000      0.6541
 44   2436.0000    108.5000    107.4000      0.6675
 45   2486.0000    107.9000    106.8000      0.6813
```

46	2536.0000	107.3000	106.3000	0.6954
47	2586.0000	106.8000	105.7000	0.7074
48	2636.0000	106.2000	105.1000	0.7221
49	2686.0000	105.7000	104.6000	0.7347
50	2736.0000	105.1000	104.1000	0.7501
51	2786.0000	104.6000	103.5000	0.7632
52	2836.0000	104.0000	103.0000	0.7793
53	2886.0000	103.5000	102.5000	0.7930
54	2936.0000	103.0000	102.0000	0.8070
55	2986.0000	102.5000	101.5000	0.8213
56	3036.0000	102.0000	101.0000	0.8359
57	3086.0000	101.6000	100.6000	0.8478
58	3136.0000	101.1000	100.1000	0.8630
59	3186.0000	100.7000	99.6900	0.8753
60	3236.0000	100.3000	99.2700	0.8879
61	3286.0000	99.8400	98.8500	0.9026
62	3336.0000	99.4300	98.4500	0.9160
63	3386.0000	99.0300	98.0500	0.9292
64	3436.0000	98.6300	97.6600	0.9427
65	3486.0000	98.2500	97.2800	0.9557
66	3536.0000	97.8700	96.9000	0.9654
67	3586.0000	97.5000	96.5300	0.9653
68	3636.0000	97.1300	96.1700	0.9656
69	3686.0000	96.7700	95.8200	0.9659
70	3736.0000	96.4200	95.4700	0.9658
71	3786.0000	96.0800	95.1200	0.9654
72	3836.0000	95.7400	94.7900	0.9657
73	3886.0000	95.4000	94.4500	0.9656
74	3936.0000	95.0700	94.1300	0.9659
75	3986.0000	94.7500	93.8100	0.9658
76	4036.0000	94.4300	93.4900	0.9657
77	4086.0000	94.1100	93.1800	0.9660
78	4136.0000	93.8000	92.8700	0.9660
79	4186.0000	93.5000	92.5700	0.9659
80	4236.0000	93.2000	92.2700	0.9658
81	4286.0000	92.9000	91.9800	0.9661
82	4336.0000	92.6100	91.6900	0.9661
83	4386.0000	92.3300	91.4100	0.9660
84	4436.0000	92.0400	91.1300	0.9663
85	4486.0000	91.7600	90.8500	0.9663
86	4536.0000	91.4900	90.5800	0.9662
87	4586.0000	91.2200	90.3100	0.9662
88	4636.0000	90.9500	90.0500	0.9665
89	4686.0000	90.6900	89.7900	0.9664
90	4736.0000	90.4300	89.5300	0.9664
91	4786.0000	90.1700	89.2700	0.9663
92	4836.0000	89.9200	89.0200	0.9662
93	4886.0000	89.6700	88.7800	0.9666
94	4936.0000	89.4300	88.5300	0.9661
95	4986.0000	89.1800	88.2900	0.9665
96	5036.0000	88.9400	88.0500	0.9664
97	5086.0000	88.7000	87.8100	0.9664
98	5136.0000	88.4600	87.5700	0.9663
99	5186.0000	88.2200	87.3400	0.9666
100	5236.0000	87.9800	87.1100	0.9670
101	5286.0000	87.7500	86.8800	0.9669
102	5336.0000	87.5200	86.6500	0.9669
103	5386.0000	87.2900	86.4200	0.9668
104	5436.0000	87.0600	86.2000	0.9672
105	5486.0000	86.8400	85.9800	0.9671
106	5536.0000	86.6200	85.7600	0.9671
107	5586.0000	86.4000	85.5400	0.9670

108	5636.0000	86.1800	85.3200	0.9670
109	5686.0000	85.9600	85.1100	0.9673
110	5736.0000	85.7500	84.9000	0.9673
111	5786.0000	85.5400	84.6900	0.9672
112	5836.0000	85.3300	84.4800	0.9672
113	5886.0000	85.1200	84.2800	0.9675
114	5936.0000	84.9200	84.0700	0.9671
115	5986.0000	84.7100	83.8700	0.9674
116	6036.0000	84.5100	83.6700	0.9674
117	6086.0000	84.3100	83.4800	0.9677
118	6136.0000	84.1100	83.2800	0.9677
119	6186.0000	83.9200	83.0900	0.9676
120	6236.0000	83.7200	82.9000	0.9680
121	6286.0000	83.5300	82.7100	0.9680
122	6336.0000	83.3400	82.5200	0.9679
123	6386.0000	83.1500	82.3300	0.9679
124	6436.0000	82.9700	82.1500	0.9678
125	6486.0000	82.7800	81.9600	0.9678
126	6536.0000	82.6000	81.7800	0.9678
127	6586.0000	82.4200	81.6000	0.9677
128	6636.0000	82.2400	81.4300	0.9681
129	6686.0000	82.0600	81.2500	0.9680
130	6736.0000	81.8800	81.0700	0.9680
131	6786.0000	81.7100	80.9000	0.9680
132	6836.0000	81.5300	80.7300	0.9683
133	6886.0000	81.3600	80.5600	0.9683
134	6936.0000	81.1900	80.3900	0.9683
135	6986.0000	81.0200	80.2200	0.9682
136	7036.0000	80.8500	80.0600	0.9686
137	7086.0000	80.6900	79.8900	0.9682
138	7136.0000	80.5200	79.7300	0.9685
139	7186.0000	80.3600	79.5700	0.9685
140	7236.0000	80.1900	79.4100	0.9688
141	7286.0000	80.0300	79.2500	0.9688
142	7336.0000	79.8700	79.0900	0.9688
143	7386.0000	79.7200	78.9300	0.9684
144	7436.0000	79.5600	78.7800	0.9687
145	7486.0000	79.4000	78.6200	0.9687
146	7536.0000	79.2500	78.4700	0.9687
147	7586.0000	79.1000	78.3200	0.9686
148	7636.0000	78.9400	78.1700	0.9690
149	7686.0000	78.7900	78.0200	0.9690
150	7736.0000	78.6400	77.8700	0.9689
151	7786.0000	78.4900	77.7200	0.9689
152	7836.0000	78.3500	77.5800	0.9689
153	7886.0000	78.2000	77.4300	0.9688
154	7936.0000	78.0600	77.2900	0.9688
155	7986.0000	77.9100	77.1500	0.9692
156	8036.0000	77.7700	77.0100	0.9692
157	8086.0000	77.6300	76.8700	0.9691
158	8136.0000	77.4900	76.7300	0.9691
159	8186.0000	77.3500	76.5900	0.9691
160	8236.0000	77.2100	76.4500	0.9690
161	8286.0000	77.0700	76.3200	0.9694
162	8336.0000	76.9400	76.1800	0.9690
163	8386.0000	76.8000	76.0500	0.9694
164	8436.0000	76.6700	75.9100	0.9689
165	8486.0000	76.5300	75.7800	0.9693
166	8536.0000	76.4000	75.6500	0.9693
167	8586.0000	76.2700	75.5200	0.9693
168	8636.0000	76.1400	75.3900	0.9692
169	8686.0000	76.0100	75.2600	0.9692

170	8736.0000	75.8800	75.1400	0.9696
171	8786.0000	75.7500	75.0100	0.9696
172	8836.0000	75.6200	74.8800	0.9695
173	8886.0000	75.5000	74.7600	0.9695
174	8936.0000	75.3700	74.6400	0.9699
175	8986.0000	75.2500	74.5100	0.9695
176	9036.0000	75.1200	74.3900	0.9698
177	9086.0000	75.0000	74.2700	0.9698
178	9136.0000	74.8800	74.1500	0.9698
179	9186.0000	74.7600	74.0300	0.9698
180	9236.0000	74.6400	73.9100	0.9698
181	9286.0000	74.5200	73.7900	0.9697
182	9336.0000	74.4000	73.6700	0.9697
183	9386.0000	74.2800	73.5600	0.9701
184	9436.0000	74.1600	73.4400	0.9701
185	9486.0000	74.0500	73.3200	0.9696
186	9536.0000	73.9300	73.2100	0.9700
187	9586.0000	73.8200	73.1000	0.9700
188	9636.0000	73.7000	72.9800	0.9700
189	9686.0000	73.5900	72.8700	0.9700
190	9736.0000	73.4800	72.7600	0.9699
191	9786.0000	73.3600	72.6500	0.9703
192	9836.0000	73.2500	72.5400	0.9703
193	9886.0000	73.1400	72.4300	0.9703
194	9936.0000	73.0300	72.3200	0.9703
195	9986.0000	72.9200	72.2100	0.9702
196	10000.0000	72.8900	72.1800	0.9702

6536.0000
5.6820
1.8020

APPENDIX B

OUTPUT FILE *corrode.out*—DATA FILE PROVIDING REMAINING THICKNESS OF THE WASTE PACKAGE WITH TIME

APPENDIX B

OUTPUT FILE *corrode.out*—DATA FILE PROVIDING REMAINING THICKNESS OF THE WASTE PACKAGE WITH TIME

Each row contains layer number, time (yr), WP surface temperature (°C), critical potential (V_{SHE}), corrosion potential (V_{SHE}), and remaining WP thickness (m). WP wetting time (yr) and WP failure time (yr) are listed at the bottom of the file.

1	50.4200	161.9000	0.0000	0.0000	0.1100
1	100.5000	155.6000	0.0000	0.0000	0.1100
1	152.4000	150.7000	0.0000	0.0000	0.1100
1	206.0000	147.4000	0.0000	0.0000	0.1100
1	259.4000	145.8000	0.0000	0.0000	0.1100
1	312.8000	144.7000	0.0000	0.0000	0.1100
1	366.2000	143.9000	0.0000	0.0000	0.1100
1	419.7000	143.0000	0.0000	0.0000	0.1100
1	473.1000	142.3000	0.0000	0.0000	0.1100
1	533.8000	141.0000	0.0000	0.0000	0.1100
1	585.7000	139.9000	0.0000	0.0000	0.1100
1	637.5000	138.8000	0.0000	0.0000	0.1100
1	689.3000	137.7000	0.0000	0.0000	0.1100
1	741.1000	136.6000	0.0000	0.0000	0.1100
1	793.0000	135.6000	0.0000	0.0000	0.1100
1	844.8000	134.6000	0.0000	0.0000	0.1100
1	896.6000	133.7000	0.0000	0.0000	0.1100
1	948.4000	132.7000	0.0000	0.0000	0.1100
1	1000.0000	131.8000	0.0000	0.0000	0.1100
1	1065.0000	130.5000	0.0000	0.0000	0.1100
1	1129.0000	129.3000	0.0000	0.0000	0.1100
1	1194.0000	128.0000	0.0000	0.0000	0.1100
1	1258.0000	126.8000	0.0000	0.0000	0.1100
1	1323.0000	125.6000	0.0000	0.0000	0.1100
1	1388.0000	124.4000	0.0000	0.0000	0.1100
1	1452.0000	123.3000	0.0000	0.0000	0.1100
1	1517.0000	122.1000	0.0000	0.0000	0.1100
1	1581.0000	121.0000	0.0000	0.0000	0.1100
1	1646.0000	119.9000	0.0000	0.0000	0.1100
1	1710.0000	118.8000	0.0000	0.0000	0.1100
1	1775.0000	117.7000	0.0000	0.0000	0.1100
1	1839.0000	116.7000	0.0000	0.0000	0.1100
1	1904.0000	115.6000	0.0000	0.0000	0.1100
1	1986.0000	114.4000	0.0000	0.0000	0.1100
1	2036.0000	113.6000	0.0000	0.0000	0.1100
1	2086.0000	112.9000	0.0000	0.0000	0.1100
1	2136.0000	112.3000	0.0000	0.0000	0.1100
1	2186.0000	111.6000	0.0000	0.0000	0.1100
1	2236.0000	111.0000	0.0000	0.0000	0.1100
1	2286.0000	110.3000	0.0000	0.0000	0.1100
1	2336.0000	109.7000	0.0000	0.0000	0.1100
1	2386.0000	109.1000	-0.5694	0.1950	0.1073
1	2436.0000	108.5000	-0.5695	0.1945	0.1046
1	2486.0000	107.9000	-0.5695	0.1940	0.1019
1	2536.0000	107.3000	-0.5695	0.1935	0.0993
1	2586.0000	106.8000	-0.5695	0.1930	0.0967
1	2636.0000	106.2000	-0.5695	0.1925	0.0941
1	2686.0000	105.7000	-0.5695	0.1921	0.0916
1	2736.0000	105.1000	-0.5695	0.1916	0.0891

1	2786.0000	104.6000	-0.5695	0.1911	0.0866
1	2836.0000	104.0000	-0.5695	0.1906	0.0841
1	2886.0000	103.5000	-0.5695	0.1902	0.0817
1	2936.0000	103.0000	-0.5695	0.1898	0.0792
1	2986.0000	102.5000	-0.5695	0.1894	0.0768
1	3036.0000	102.0000	-0.5695	0.1889	0.0744
1	3086.0000	101.6000	-0.5695	0.1886	0.0721
1	3136.0000	101.1000	-0.5695	0.1882	0.0698
1	3186.0000	100.7000	-0.5695	0.1878	0.0674
1	3236.0000	100.3000	-0.5695	0.1875	0.0651
1	3286.0000	99.8400	-0.5695	0.1871	0.0629
1	3336.0000	99.4300	-0.5695	0.1867	0.0606
1	3386.0000	99.0300	-0.5695	0.1864	0.0584
1	3436.0000	98.6300	-0.5695	0.1861	0.0561
1	3486.0000	98.2500	-0.5696	0.1857	0.0539
1	3536.0000	97.8700	-0.5696	0.1854	0.0518
1	3586.0000	97.5000	-0.5696	0.1851	0.0496
1	3636.0000	97.1300	-0.5696	0.1848	0.0474
1	3686.0000	96.7700	-0.5696	0.1845	0.0453
1	3736.0000	96.4200	-0.5696	0.1842	0.0432
1	3786.0000	96.0800	-0.5696	0.1839	0.0411
1	3836.0000	95.7400	-0.5696	0.1836	0.0390
1	3886.0000	95.4000	-0.5696	0.1833	0.0369
1	3936.0000	95.0700	-0.5696	0.1830	0.0348
1	3986.0000	94.7500	-0.5696	0.1828	0.0328
1	4036.0000	94.4300	-0.5696	0.1825	0.0308
1	4086.0000	94.1100	-0.5696	0.1822	0.0287
1	4136.0000	93.8000	-0.5696	0.1820	0.0267
1	4186.0000	93.5000	-0.5696	0.1817	0.0248
1	4236.0000	93.2000	-0.5696	0.1815	0.0228
1	4286.0000	92.9000	-0.5696	0.1812	0.0208
1	4336.0000	92.6100	-0.5696	0.1810	0.0189
1	4386.0000	92.3300	-0.5696	0.1807	0.0169
1	4436.0000	92.0400	-0.5696	0.1805	0.0150
1	4486.0000	91.7600	-0.5696	0.1802	0.0131
1	4536.0000	91.4900	-0.5696	0.1800	0.0112
2	4586.0000	91.2200	-0.5696	0.1798	0.0093
2	4636.0000	90.9500	0.1214	0.1414	0.0090
2	4686.0000	90.6900	0.1224	0.1414	0.0086
2	4736.0000	90.4300	0.1233	0.1414	0.0083
2	4786.0000	90.1700	0.1243	0.1414	0.0080
2	4836.0000	89.9200	0.1252	0.1414	0.0077
2	4886.0000	89.6700	0.1261	0.1414	0.0074
2	4936.0000	89.4300	0.1270	0.1414	0.0071
2	4986.0000	89.1800	0.1279	0.1414	0.0068
2	5036.0000	88.9400	0.1288	0.1414	0.0064
2	5086.0000	88.7000	0.1297	0.1414	0.0061
2	5136.0000	88.4600	0.1306	0.1414	0.0058
2	5186.0000	88.2200	0.1315	0.1414	0.0055
2	5236.0000	87.9800	0.1323	0.1414	0.0052
2	5286.0000	87.7500	0.1332	0.1414	0.0049
2	5336.0000	87.5200	0.1340	0.1414	0.0045
2	5386.0000	87.2900	0.1349	0.1414	0.0042
2	5436.0000	87.0600	0.1357	0.1414	0.0039
2	5486.0000	86.8400	0.1365	0.1414	0.0036
2	5536.0000	86.6200	0.1374	0.1414	0.0033
2	5586.0000	86.4000	0.1382	0.1414	0.0030
2	5636.0000	86.1800	0.1390	0.1414	0.0027
2	5686.0000	85.9600	0.1398	0.1414	0.0023
2	5736.0000	85.7500	0.1406	0.1414	0.0020
2	5786.0000	85.5400	0.1413	0.1414	0.0017
2	5836.0000	85.3300	0.1421	0.1414	0.0016

2	5886.0000	85.1200	0.1429	0.1414	0.0015
2	5936.0000	84.9200	0.1436	0.1414	0.0014
2	5986.0000	84.7100	0.1444	0.1414	0.0012
2	6036.0000	84.5100	0.1451	0.1414	0.0011
2	6086.0000	84.3100	0.1459	0.1414	0.0010
2	6136.0000	84.1100	0.1466	0.1414	0.0009
2	6186.0000	83.9200	0.1473	0.1414	0.0008
2	6236.0000	83.7200	0.1480	0.1414	0.0007
2	6286.0000	83.5300	0.1487	0.1414	0.0006
2	6336.0000	83.3400	0.1494	0.1414	0.0005
2	6386.0000	83.1500	0.1501	0.1414	0.0003
2	6436.0000	82.9700	0.1508	0.1414	0.0002
2	6486.0000	82.7800	0.1515	0.1414	0.0001
2	6536.0000	82.6000	0.1522	0.1414	0.0000
2	6586.0000	82.4200	0.1528	0.1414	-0.0001

APPENDIX C

OUTPUT FILE *relcum.dat*—CUMULATIVE LIQUID RELEASE OF THE VARIOUS RADIONUCLIDES AT THE END OF SIMULATION TIME

APPENDIX C

OUTPUT FILE *relcum.dat*—CUMULATIVE LIQUID RELEASE OF THE VARIOUS RADIONUCLIDES AT THE END OF SIMULATION TIME

Each row shows the name of the radionuclide and the cumulative release in Ci.

```
 CM246    0.50776546480835
  PU242    0.43047050991026
   U238     4.6903005772887D-02
  CM245     4.7408651467356
  AM241     4.2075069159683
  NP237     24.663485246013
  AM243     5.7252103356747
  PU239     63.948505550593
  PU240     48.184917642068
   U236     5.0780599990757D-02
   U234    0.27056839224388
  TH230     6.4035263399283D-03
  RA226     4.3734648737807
  PB210     82.761633893716
  CS135     1220.7784794789
   I129     183.92564450236
  TC99      73639.786475113
  NI59      6469.9078366351
   C14      2693.8950252158
  SE79      7.9261995378647D-04
  NB94      2609.3431630179
```

APPENDIX D

OUTPUT FILE *release.out*—CUMULATIVE RELEASE OF THE VARIOUS RADIONUCLIDES WITH TIME

APPENDIX D

OUTPUT FILE *release.out*—CUMULATIVE RELEASE OF THE VARIOUS RADIONUCLIDES WITH TIME

Each row shows time (yr) and the cumulative release (Ci) for each radionuclide.

```
TIME   CM246   PU242   U238   CM245   AM241   NP237   AM243   PU239   PU240   U236   U234
TH230   RA226   PB210   CS135   I129   TC99   NI59   C14   SE79   NB94
 0.100E+03   0.000E+00   0.000E+00   0.000E+00   0.000E+00   0.000E+00   0.000E+00   0.000E+00
0.000E+00   0.000E+00   0.000E+00   0.000E+00   0.000E+00   0.000E+00   0.000E+00   0.000E+00
0.000E+00   0.000E+00   0.000E+00   0.000E+00   0.000E+00   0.000E+00   0.000E+00   0.000E+00
0.000E+00
 0.200E+03   0.000E+00   0.000E+00   0.000E+00   0.000E+00   0.000E+00   0.000E+00   0.000E+00
0.000E+00   0.000E+00   0.000E+00   0.000E+00   0.000E+00   0.000E+00   0.000E+00   0.000E+00
0.000E+00   0.000E+00   0.000E+00   0.000E+00   0.000E+00   0.000E+00   0.000E+00   0.000E+00
0.000E+00
 0.300E+03   0.000E+00   0.000E+00   0.000E+00   0.000E+00   0.000E+00   0.000E+00   0.000E+00
0.000E+00   0.000E+00   0.000E+00   0.000E+00   0.000E+00   0.000E+00   0.000E+00   0.000E+00
0.000E+00   0.000E+00   0.000E+00   0.000E+00   0.000E+00   0.000E+00   0.000E+00   0.000E+00
0.000E+00
 0.400E+03   0.000E+00   0.000E+00   0.000E+00   0.000E+00   0.000E+00   0.000E+00   0.000E+00
0.000E+00   0.000E+00   0.000E+00   0.000E+00   0.000E+00   0.000E+00   0.000E+00   0.000E+00
0.000E+00   0.000E+00   0.000E+00   0.000E+00   0.000E+00   0.000E+00   0.000E+00   0.000E+00
0.000E+00
 0.500E+03   0.000E+00   0.000E+00   0.000E+00   0.000E+00   0.000E+00   0.000E+00   0.000E+00
0.000E+00   0.000E+00   0.000E+00   0.000E+00   0.000E+00   0.000E+00   0.000E+00   0.000E+00
0.000E+00   0.000E+00   0.000E+00   0.000E+00   0.000E+00   0.000E+00   0.000E+00   0.000E+00
0.000E+00
 0.600E+03   0.000E+00   0.000E+00   0.000E+00   0.000E+00   0.000E+00   0.000E+00   0.000E+00
0.000E+00   0.000E+00   0.000E+00   0.000E+00   0.000E+00   0.000E+00   0.000E+00   0.000E+00
0.000E+00   0.000E+00   0.000E+00   0.000E+00   0.000E+00   0.000E+00   0.000E+00   0.000E+00
0.000E+00
 0.700E+03   0.000E+00   0.000E+00   0.000E+00   0.000E+00   0.000E+00   0.000E+00   0.000E+00
0.000E+00   0.000E+00   0.000E+00   0.000E+00   0.000E+00   0.000E+00   0.000E+00   0.000E+00
0.000E+00   0.000E+00   0.000E+00   0.000E+00   0.000E+00   0.000E+00   0.000E+00   0.000E+00
0.000E+00
 0.800E+03   0.000E+00   0.000E+00   0.000E+00   0.000E+00   0.000E+00   0.000E+00   0.000E+00
0.000E+00   0.000E+00   0.000E+00   0.000E+00   0.000E+00   0.000E+00   0.000E+00   0.000E+00
0.000E+00   0.000E+00   0.000E+00   0.000E+00   0.000E+00   0.000E+00   0.000E+00   0.000E+00
0.000E+00
 0.900E+03   0.000E+00   0.000E+00   0.000E+00   0.000E+00   0.000E+00   0.000E+00   0.000E+00
0.000E+00   0.000E+00   0.000E+00   0.000E+00   0.000E+00   0.000E+00   0.000E+00   0.000E+00
0.000E+00   0.000E+00   0.000E+00   0.000E+00   0.000E+00   0.000E+00   0.000E+00   0.000E+00
0.000E+00
 0.100E+04   0.000E+00   0.000E+00   0.000E+00   0.000E+00   0.000E+00   0.000E+00   0.000E+00
0.000E+00   0.000E+00   0.000E+00   0.000E+00   0.000E+00   0.000E+00   0.000E+00   0.000E+00
0.000E+00   0.000E+00   0.000E+00   0.000E+00   0.000E+00   0.000E+00   0.000E+00   0.000E+00
0.000E+00
 0.110E+04   0.000E+00   0.000E+00   0.000E+00   0.000E+00   0.000E+00   0.000E+00   0.000E+00
0.000E+00   0.000E+00   0.000E+00   0.000E+00   0.000E+00   0.000E+00   0.000E+00   0.000E+00
0.000E+00   0.000E+00   0.000E+00   0.000E+00   0.000E+00   0.000E+00   0.000E+00   0.000E+00
0.000E+00
 0.120E+04   0.000E+00   0.000E+00   0.000E+00   0.000E+00   0.000E+00   0.000E+00   0.000E+00
0.000E+00   0.000E+00   0.000E+00   0.000E+00   0.000E+00   0.000E+00   0.000E+00   0.000E+00
0.000E+00   0.000E+00   0.000E+00   0.000E+00   0.000E+00   0.000E+00   0.000E+00   0.000E+00
0.000E+00
```

```
 0.130E+04   0.000E+00   0.000E+00   0.000E+00   0.000E+00   0.000E+00   0.000E+00
0.000E+00   0.000E+00   0.000E+00   0.000E+00   0.000E+00   0.000E+00   0.000E+00
0.000E+00   0.000E+00   0.000E+00   0.000E+00   0.000E+00   0.000E+00   0.000E+00
0.000E+00
 0.140E+04   0.000E+00   0.000E+00   0.000E+00   0.000E+00   0.000E+00   0.000E+00
0.000E+00   0.000E+00   0.000E+00   0.000E+00   0.000E+00   0.000E+00   0.000E+00
0.000E+00   0.000E+00   0.000E+00   0.000E+00   0.000E+00   0.000E+00   0.000E+00
0.000E+00
 0.150E+04   0.000E+00   0.000E+00   0.000E+00   0.000E+00   0.000E+00   0.000E+00
0.000E+00   0.000E+00   0.000E+00   0.000E+00   0.000E+00   0.000E+00   0.000E+00
0.000E+00   0.000E+00   0.000E+00   0.000E+00   0.000E+00   0.000E+00   0.000E+00
0.000E+00
 0.160E+04   0.000E+00   0.000E+00   0.000E+00   0.000E+00   0.000E+00   0.000E+00
0.000E+00   0.000E+00   0.000E+00   0.000E+00   0.000E+00   0.000E+00   0.000E+00
0.000E+00   0.000E+00   0.000E+00   0.000E+00   0.000E+00   0.000E+00   0.000E+00
0.000E+00
 0.170E+04   0.000E+00   0.000E+00   0.000E+00   0.000E+00   0.000E+00   0.000E+00
0.000E+00   0.000E+00   0.000E+00   0.000E+00   0.000E+00   0.000E+00   0.000E+00
0.000E+00   0.000E+00   0.000E+00   0.000E+00   0.000E+00   0.000E+00   0.000E+00
0.000E+00
 0.180E+04   0.000E+00   0.000E+00   0.000E+00   0.000E+00   0.000E+00   0.000E+00
0.000E+00   0.000E+00   0.000E+00   0.000E+00   0.000E+00   0.000E+00   0.000E+00
0.000E+00   0.000E+00   0.000E+00   0.000E+00   0.000E+00   0.000E+00   0.000E+00
0.000E+00
 0.190E+04   0.000E+00   0.000E+00   0.000E+00   0.000E+00   0.000E+00   0.000E+00
0.000E+00   0.000E+00   0.000E+00   0.000E+00   0.000E+00   0.000E+00   0.000E+00
0.000E+00   0.000E+00   0.000E+00   0.000E+00   0.000E+00   0.000E+00   0.000E+00
0.000E+00
 0.200E+04   0.000E+00   0.000E+00   0.000E+00   0.000E+00   0.000E+00   0.000E+00
0.000E+00   0.000E+00   0.000E+00   0.000E+00   0.000E+00   0.000E+00   0.000E+00
0.000E+00   0.000E+00   0.000E+00   0.000E+00   0.000E+00   0.000E+00   0.000E+00
0.000E+00
 0.210E+04   0.000E+00   0.000E+00   0.000E+00   0.000E+00   0.000E+00   0.000E+00
0.000E+00   0.000E+00   0.000E+00   0.000E+00   0.000E+00   0.000E+00   0.000E+00
0.000E+00   0.000E+00   0.000E+00   0.000E+00   0.000E+00   0.000E+00   0.000E+00
0.000E+00
 0.220E+04   0.000E+00   0.000E+00   0.000E+00   0.000E+00   0.000E+00   0.000E+00
0.000E+00   0.000E+00   0.000E+00   0.000E+00   0.000E+00   0.000E+00   0.000E+00
0.000E+00   0.000E+00   0.000E+00   0.000E+00   0.000E+00   0.000E+00   0.000E+00
0.000E+00
 0.230E+04   0.000E+00   0.000E+00   0.000E+00   0.000E+00   0.000E+00   0.000E+00
0.000E+00   0.000E+00   0.000E+00   0.000E+00   0.000E+00   0.000E+00   0.000E+00
0.000E+00   0.000E+00   0.000E+00   0.000E+00   0.000E+00   0.000E+00   0.000E+00
0.000E+00
 0.240E+04   0.000E+00   0.000E+00   0.000E+00   0.000E+00   0.000E+00   0.000E+00
0.000E+00   0.000E+00   0.000E+00   0.000E+00   0.000E+00   0.000E+00   0.000E+00
0.000E+00   0.000E+00   0.000E+00   0.000E+00   0.000E+00   0.000E+00   0.000E+00
0.000E+00
 0.250E+04   0.000E+00   0.000E+00   0.000E+00   0.000E+00   0.000E+00   0.000E+00
0.000E+00   0.000E+00   0.000E+00   0.000E+00   0.000E+00   0.000E+00   0.000E+00
0.000E+00   0.000E+00   0.000E+00   0.000E+00   0.000E+00   0.000E+00   0.000E+00
0.000E+00
 0.260E+04   0.000E+00   0.000E+00   0.000E+00   0.000E+00   0.000E+00   0.000E+00
0.000E+00   0.000E+00   0.000E+00   0.000E+00   0.000E+00   0.000E+00   0.000E+00
0.000E+00   0.000E+00   0.000E+00   0.000E+00   0.000E+00   0.000E+00   0.000E+00
0.000E+00
 0.270E+04   0.000E+00   0.000E+00   0.000E+00   0.000E+00   0.000E+00   0.000E+00
0.000E+00   0.000E+00   0.000E+00   0.000E+00   0.000E+00   0.000E+00   0.000E+00
0.000E+00   0.000E+00   0.000E+00   0.000E+00   0.000E+00   0.000E+00   0.000E+00
0.000E+00
 0.280E+04   0.000E+00   0.000E+00   0.000E+00   0.000E+00   0.000E+00   0.000E+00
0.000E+00   0.000E+00   0.000E+00   0.000E+00   0.000E+00   0.000E+00   0.000E+00
```

0.000E+00 0.000E+00 0.000E+00 0.000E+00 0.000E+00 0.000E+00 0.000E+00
0.000E+00
0.290E+04 0.000E+00 0.000E+00 0.000E+00 0.000E+00 0.000E+00 0.000E+00
0.000E+00 0.000E+00 0.000E+00 0.000E+00 0.000E+00 0.000E+00 0.000E+00
0.000E+00 0.000E+00 0.000E+00 0.000E+00 0.000E+00 0.000E+00 0.000E+00
0.000E+00
0.300E+04 0.000E+00 0.000E+00 0.000E+00 0.000E+00 0.000E+00 0.000E+00
0.000E+00 0.000E+00 0.000E+00 0.000E+00 0.000E+00 0.000E+00 0.000E+00
0.000E+00 0.000E+00 0.000E+00 0.000E+00 0.000E+00 0.000E+00 0.000E+00
0.000E+00
0.310E+04 0.000E+00 0.000E+00 0.000E+00 0.000E+00 0.000E+00 0.000E+00
0.000E+00 0.000E+00 0.000E+00 0.000E+00 0.000E+00 0.000E+00 0.000E+00
0.000E+00 0.000E+00 0.000E+00 0.000E+00 0.000E+00 0.000E+00 0.000E+00
0.000E+00
0.320E+04 0.199E-15 0.252E-17 0.219E-21 0.112E-15 0.208E-14 0.496E-18
0.129E-15 0.406E-16 0.148E-15 0.425E-19 0.407E-17 0.132E-16 0.632E-15
0.111E-13 0.751E-18 0.115E-18 0.111E-16 0.494E-16 0.289E-14 0.454E-16
0.122E-15
0.330E+04 0.704E-15 0.907E-17 0.783E-21 0.396E-15 0.674E-14 0.192E-17
0.460E-15 0.146E-15 0.524E-15 0.153E-18 0.145E-16 0.470E-16 0.220E-14
0.850E-14 0.268E-17 0.411E-18 0.395E-16 0.176E-15 0.102E-13 0.162E-15
0.435E-15
0.340E+04 0.694E-15 0.919E-17 0.784E-21 0.393E-15 0.580E-14 0.212E-17
0.455E-15 0.147E-15 0.519E-15 0.154E-18 0.145E-16 0.470E-16 0.210E-14
0.257E-14 0.268E-17 0.411E-18 0.395E-16 0.176E-15 0.101E-13 0.162E-15
0.433E-15
0.350E+04 0.796E-03 0.318E-03 0.411E-04 0.488E-02 0.365E-02 0.216E-01
0.597E-02 0.560E-01 0.703E-01 0.367E-04 0.242E-03 0.663E-06 0.860E-02
0.239E+00 0.400E+01 0.434E+00 0.178E+03 0.578E+01 0.147E+02 0.712E-06
0.794E+01
0.360E+04 0.263E-02 0.106E-02 0.137E-03 0.162E-01 0.117E-01 0.720E-01
0.198E-01 0.186E+00 0.232E+00 0.123E-03 0.805E-03 0.254E-05 0.281E-01
0.454E+00 0.125E+02 0.143E+01 0.585E+03 0.193E+02 0.477E+02 0.237E-05
0.252E+02
0.370E+04 0.453E-02 0.185E-02 0.239E-03 0.281E-01 0.198E-01 0.125E+00
0.345E-01 0.324E+00 0.401E+00 0.215E-03 0.140E-02 0.503E-05 0.480E-01
0.620E+00 0.206E+02 0.246E+01 0.101E+04 0.335E+02 0.812E+02 0.413E-05
0.423E+02
0.380E+04 0.646E-02 0.267E-02 0.343E-03 0.403E-01 0.278E-01 0.181E+00
0.495E-01 0.467E+00 0.573E+00 0.310E-03 0.202E-02 0.812E-05 0.676E-01
0.791E+00 0.284E+02 0.352E+01 0.144E+04 0.482E+02 0.114E+03 0.593E-05
0.591E+02
0.390E+04 0.837E-02 0.350E-02 0.450E-03 0.526E-01 0.357E-01 0.236E+00
0.647E-01 0.611E+00 0.744E+00 0.408E-03 0.264E-02 0.118E-04 0.868E-01
0.967E+00 0.359E+02 0.457E+01 0.187E+04 0.631E+02 0.147E+03 0.777E-05
0.757E+02
0.400E+04 0.103E-01 0.435E-02 0.557E-03 0.649E-01 0.437E-01 0.293E+00
0.799E-01 0.756E+00 0.914E+00 0.508E-03 0.327E-02 0.161E-04 0.105E+00
0.115E+01 0.433E+02 0.563E+01 0.230E+04 0.782E+02 0.178E+03 0.962E-05
0.920E+02
0.410E+04 0.121E-01 0.520E-02 0.665E-03 0.771E-01 0.518E-01 0.349E+00
0.950E-01 0.902E+00 0.108E+01 0.609E-03 0.390E-02 0.209E-04 0.123E+00
0.134E+01 0.504E+02 0.667E+01 0.273E+04 0.932E+02 0.208E+03 0.115E-04
0.108E+03
0.420E+04 0.139E-01 0.606E-02 0.772E-03 0.893E-01 0.600E-01 0.406E+00
0.110E+00 0.105E+01 0.125E+01 0.711E-03 0.453E-02 0.263E-04 0.140E+00
0.154E+01 0.575E+02 0.771E+01 0.315E+04 0.108E+03 0.237E+03 0.133E-04
0.124E+03
0.430E+04 0.157E-01 0.692E-02 0.880E-03 0.101E+00 0.684E-01 0.463E+00
0.125E+00 0.119E+01 0.141E+01 0.814E-03 0.516E-02 0.323E-04 0.157E+00
0.174E+01 0.643E+02 0.874E+01 0.357E+04 0.123E+03 0.265E+03 0.152E-04
0.140E+03

0.440E+04 0.175E-01 0.779E-02 0.988E-03 0.113E+00 0.770E-01 0.520E+00
0.140E+00 0.134E+01 0.157E+01 0.917E-03 0.579E-02 0.389E-04 0.172E+00
0.195E+01 0.711E+02 0.976E+01 0.398E+04 0.138E+03 0.292E+03 0.170E-04
0.155E+03
0.450E+04 0.192E-01 0.866E-02 0.110E-02 0.125E+00 0.858E-01 0.577E+00
0.155E+00 0.149E+01 0.173E+01 0.102E-02 0.642E-02 0.460E-04 0.187E+00
0.217E+01 0.778E+02 0.108E+02 0.439E+04 0.154E+03 0.318E+03 0.189E-04
0.171E+03
0.460E+04 0.209E-01 0.954E-02 0.120E-02 0.137E+00 0.948E-01 0.633E+00
0.169E+00 0.163E+01 0.188E+01 0.113E-02 0.706E-02 0.537E-04 0.202E+00
0.239E+01 0.843E+02 0.117E+02 0.479E+04 0.169E+03 0.342E+03 0.207E-04
0.186E+03
0.470E+04 0.225E-01 0.104E-01 0.131E-02 0.149E+00 0.104E+00 0.690E+00
0.184E+00 0.178E+01 0.203E+01 0.123E-02 0.769E-02 0.620E-04 0.216E+00
0.262E+01 0.908E+02 0.127E+02 0.519E+04 0.184E+03 0.366E+03 0.226E-04
0.201E+03
0.480E+04 0.247E-01 0.116E-01 0.145E-02 0.165E+00 0.114E+00 0.765E+00
0.203E+00 0.197E+01 0.223E+01 0.137E-02 0.852E-02 0.714E-04 0.236E+00
0.317E+01 0.998E+02 0.140E+02 0.570E+04 0.204E+03 0.397E+03 0.250E-04
0.221E+03
0.490E+04 0.324E-01 0.153E-01 0.191E-02 0.217E+00 0.131E+00 0.100E+01
0.269E+00 0.259E+01 0.292E+01 0.180E-02 0.112E-01 0.868E-04 0.320E+00
0.509E+01 0.131E+03 0.178E+02 0.724E+04 0.267E+03 0.499E+03 0.328E-04
0.283E+03
0.500E+04 0.414E-01 0.197E-01 0.244E-02 0.279E+00 0.154E+00 0.128E+01
0.346E+00 0.333E+01 0.372E+01 0.231E-02 0.143E-01 0.106E-03 0.417E+00
0.612E+01 0.163E+03 0.220E+02 0.895E+04 0.342E+03 0.611E+03 0.420E-04
0.349E+03
0.510E+04 0.505E-01 0.242E-01 0.299E-02 0.343E+00 0.183E+00 0.157E+01
0.425E+00 0.409E+01 0.454E+01 0.284E-02 0.175E-01 0.129E-03 0.514E+00
0.707E+01 0.193E+03 0.261E+02 0.106E+05 0.419E+03 0.716E+03 0.515E-04
0.410E+03
0.520E+04 0.596E-01 0.289E-01 0.355E-02 0.407E+00 0.217E+00 0.187E+01
0.505E+00 0.487E+01 0.535E+01 0.338E-02 0.208E-01 0.154E-03 0.608E+00
0.805E+01 0.220E+03 0.301E+02 0.123E+05 0.498E+03 0.817E+03 0.612E-04
0.469E+03
0.530E+04 0.685E-01 0.336E-01 0.412E-02 0.471E+00 0.255E+00 0.217E+01
0.585E+00 0.565E+01 0.616E+01 0.394E-02 0.241E-01 0.183E-03 0.700E+00
0.904E+01 0.246E+03 0.340E+02 0.139E+05 0.577E+03 0.911E+03 0.709E-04
0.526E+03
0.540E+04 0.774E-01 0.384E-01 0.469E-02 0.536E+00 0.297E+00 0.247E+01
0.665E+00 0.643E+01 0.696E+01 0.449E-02 0.274E-01 0.215E-03 0.788E+00
0.100E+02 0.271E+03 0.379E+02 0.154E+05 0.657E+03 0.100E+04 0.807E-04
0.582E+03
0.550E+04 0.860E-01 0.432E-01 0.526E-02 0.600E+00 0.342E+00 0.277E+01
0.744E+00 0.721E+01 0.775E+01 0.506E-02 0.307E-01 0.249E-03 0.873E+00
0.111E+02 0.296E+03 0.417E+02 0.170E+05 0.736E+03 0.109E+04 0.905E-04
0.637E+03
0.560E+04 0.945E-01 0.480E-01 0.583E-02 0.663E+00 0.389E+00 0.307E+01
0.823E+00 0.800E+01 0.852E+01 0.563E-02 0.341E-01 0.287E-03 0.954E+00
0.121E+02 0.320E+03 0.454E+02 0.185E+05 0.816E+03 0.117E+04 0.100E-03
0.691E+03
0.570E+04 0.103E+00 0.528E-01 0.640E-02 0.726E+00 0.439E+00 0.337E+01
0.900E+00 0.878E+01 0.928E+01 0.620E-02 0.374E-01 0.328E-03 0.103E+01
0.132E+02 0.344E+03 0.491E+02 0.199E+05 0.896E+03 0.125E+04 0.110E-03
0.745E+03
0.580E+04 0.111E+00 0.577E-01 0.697E-02 0.789E+00 0.490E+00 0.367E+01
0.978E+00 0.956E+01 0.100E+02 0.677E-02 0.407E-01 0.372E-03 0.111E+01
0.143E+02 0.368E+03 0.527E+02 0.214E+05 0.975E+03 0.132E+04 0.120E-03
0.799E+03
0.590E+04 0.119E+00 0.626E-01 0.755E-02 0.851E+00 0.543E+00 0.397E+01
0.105E+01 0.103E+02 0.108E+02 0.735E-02 0.440E-01 0.419E-03 0.118E+01

0.155E+02 0.391E+03 0.562E+02 0.228E+05 0.105E+04 0.139E+04 0.130E-03
0.851E+03
0.600E+04 0.127E+00 0.675E-01 0.812E-02 0.912E+00 0.598E+00 0.427E+01
0.113E+01 0.111E+02 0.115E+02 0.794E-02 0.474E-01 0.468E-03 0.125E+01
0.166E+02 0.415E+03 0.598E+02 0.243E+05 0.113E+04 0.146E+04 0.139E-03
0.904E+03
0.610E+04 0.134E+00 0.724E-01 0.869E-02 0.974E+00 0.653E+00 0.457E+01
0.120E+01 0.119E+02 0.122E+02 0.853E-02 0.507E-01 0.521E-03 0.131E+01
0.178E+02 0.437E+03 0.632E+02 0.257E+05 0.121E+04 0.153E+04 0.149E-03
0.956E+03
0.620E+04 0.142E+00 0.773E-01 0.926E-02 0.103E+01 0.709E+00 0.487E+01
0.128E+01 0.127E+02 0.129E+02 0.912E-02 0.540E-01 0.577E-03 0.138E+01
0.190E+02 0.460E+03 0.667E+02 0.270E+05 0.129E+04 0.159E+04 0.159E-03
0.101E+04
0.630E+04 0.149E+00 0.823E-01 0.983E-02 0.109E+01 0.766E+00 0.517E+01
0.135E+01 0.135E+02 0.136E+02 0.971E-02 0.573E-01 0.636E-03 0.144E+01
0.202E+02 0.482E+03 0.701E+02 0.284E+05 0.137E+04 0.165E+04 0.169E-03
0.106E+04
0.640E+04 0.156E+00 0.873E-01 0.104E-01 0.115E+01 0.823E+00 0.547E+01
0.143E+01 0.142E+02 0.143E+02 0.103E-01 0.606E-01 0.698E-03 0.149E+01
0.215E+02 0.505E+03 0.734E+02 0.298E+05 0.145E+04 0.170E+04 0.178E-03
0.111E+04
0.650E+04 0.163E+00 0.923E-01 0.110E-01 0.121E+01 0.881E+00 0.577E+01
0.150E+01 0.150E+02 0.149E+02 0.109E-01 0.640E-01 0.762E-03 0.155E+01
0.227E+02 0.527E+03 0.767E+02 0.311E+05 0.153E+04 0.176E+04 0.188E-03
0.116E+04
0.660E+04 0.170E+00 0.973E-01 0.115E-01 0.127E+01 0.939E+00 0.607E+01
0.157E+01 0.158E+02 0.156E+02 0.115E-01 0.673E-01 0.830E-03 0.160E+01
0.240E+02 0.548E+03 0.800E+02 0.324E+05 0.161E+04 0.181E+04 0.198E-03
0.121E+04
0.670E+04 0.177E+00 0.102E+00 0.121E-01 0.133E+01 0.997E+00 0.637E+01
0.164E+01 0.166E+02 0.162E+02 0.121E-01 0.706E-01 0.901E-03 0.165E+01
0.254E+02 0.570E+03 0.832E+02 0.337E+05 0.169E+04 0.186E+04 0.207E-03
0.125E+04
0.680E+04 0.183E+00 0.107E+00 0.127E-01 0.139E+01 0.106E+01 0.668E+01
0.171E+01 0.173E+02 0.168E+02 0.127E-01 0.739E-01 0.975E-03 0.170E+01
0.264E+02 0.589E+03 0.862E+02 0.349E+05 0.177E+04 0.190E+04 0.217E-03
0.130E+04
0.690E+04 0.193E+00 0.114E+00 0.135E-01 0.147E+01 0.112E+01 0.708E+01
0.181E+01 0.184E+02 0.177E+02 0.135E-01 0.783E-01 0.105E-02 0.179E+01
0.288E+02 0.612E+03 0.898E+02 0.363E+05 0.187E+04 0.195E+04 0.230E-03
0.135E+04
0.700E+04 0.206E+00 0.123E+00 0.145E-01 0.158E+01 0.118E+01 0.762E+01
0.195E+01 0.198E+02 0.189E+02 0.146E-01 0.843E-01 0.114E-02 0.192E+01
0.309E+02 0.643E+03 0.944E+02 0.382E+05 0.202E+04 0.203E+04 0.248E-03
0.141E+04
0.710E+04 0.219E+00 0.133E+00 0.155E-01 0.170E+01 0.126E+01 0.817E+01
0.209E+01 0.213E+02 0.201E+02 0.157E-01 0.904E-01 0.124E-02 0.206E+01
0.326E+02 0.670E+03 0.988E+02 0.400E+05 0.216E+04 0.210E+04 0.266E-03
0.147E+04
0.720E+04 0.233E+00 0.142E+00 0.166E-01 0.181E+01 0.134E+01 0.873E+01
0.223E+01 0.228E+02 0.214E+02 0.168E-01 0.965E-01 0.134E-02 0.219E+01
0.343E+02 0.696E+03 0.103E+03 0.416E+05 0.231E+04 0.216E+04 0.284E-03
0.152E+04
0.730E+04 0.246E+00 0.152E+00 0.177E-01 0.193E+01 0.142E+01 0.930E+01
0.237E+01 0.242E+02 0.226E+02 0.180E-01 0.103E+00 0.144E-02 0.232E+01
0.359E+02 0.720E+03 0.107E+03 0.432E+05 0.246E+04 0.221E+04 0.302E-03
0.158E+04
0.740E+04 0.259E+00 0.162E+00 0.188E-01 0.204E+01 0.151E+01 0.986E+01
0.251E+01 0.257E+02 0.238E+02 0.191E-01 0.109E+00 0.155E-02 0.245E+01
0.376E+02 0.743E+03 0.111E+03 0.447E+05 0.261E+04 0.226E+04 0.320E-03
0.163E+04

0.750E+04 0.271E+00 0.172E+00 0.198E-01 0.215E+01 0.160E+01 0.104E+02
0.265E+01 0.272E+02 0.250E+02 0.203E-01 0.115E+00 0.167E-02 0.257E+01
0.393E+02 0.766E+03 0.114E+03 0.462E+05 0.276E+04 0.231E+04 0.339E-03
0.168E+04
0.760E+04 0.284E+00 0.182E+00 0.209E-01 0.227E+01 0.170E+01 0.110E+02
0.278E+01 0.287E+02 0.261E+02 0.214E-01 0.121E+00 0.179E-02 0.268E+01
0.411E+02 0.788E+03 0.118E+03 0.476E+05 0.291E+04 0.235E+04 0.357E-03
0.173E+04
0.770E+04 0.296E+00 0.192E+00 0.220E-01 0.238E+01 0.180E+01 0.116E+02
0.292E+01 0.302E+02 0.273E+02 0.226E-01 0.128E+00 0.192E-02 0.280E+01
0.428E+02 0.810E+03 0.121E+03 0.490E+05 0.306E+04 0.239E+04 0.376E-03
0.177E+04
0.780E+04 0.308E+00 0.201E+00 0.231E-01 0.249E+01 0.190E+01 0.121E+02
0.305E+01 0.317E+02 0.284E+02 0.237E-01 0.134E+00 0.206E-02 0.290E+01
0.446E+02 0.832E+03 0.125E+03 0.504E+05 0.321E+04 0.242E+04 0.394E-03
0.182E+04
0.790E+04 0.319E+00 0.211E+00 0.242E-01 0.260E+01 0.201E+01 0.127E+02
0.319E+01 0.332E+02 0.295E+02 0.249E-01 0.140E+00 0.220E-02 0.300E+01
0.464E+02 0.854E+03 0.128E+03 0.517E+05 0.336E+04 0.245E+04 0.412E-03
0.187E+04
0.800E+04 0.331E+00 0.222E+00 0.252E-01 0.271E+01 0.211E+01 0.133E+02
0.332E+01 0.347E+02 0.306E+02 0.261E-01 0.146E+00 0.234E-02 0.310E+01
0.481E+02 0.876E+03 0.131E+03 0.530E+05 0.351E+04 0.248E+04 0.431E-03
0.192E+04
0.810E+04 0.342E+00 0.232E+00 0.263E-01 0.282E+01 0.222E+01 0.138E+02
0.345E+01 0.362E+02 0.316E+02 0.273E-01 0.153E+00 0.249E-02 0.319E+01
0.500E+02 0.897E+03 0.135E+03 0.543E+05 0.366E+04 0.251E+04 0.449E-03
0.196E+04
0.820E+04 0.353E+00 0.242E+00 0.274E-01 0.293E+01 0.232E+01 0.144E+02
0.358E+01 0.376E+02 0.327E+02 0.285E-01 0.159E+00 0.265E-02 0.328E+01
0.518E+02 0.918E+03 0.138E+03 0.555E+05 0.381E+04 0.254E+04 0.467E-03
0.201E+04
0.830E+04 0.363E+00 0.252E+00 0.285E-01 0.304E+01 0.243E+01 0.150E+02
0.371E+01 0.391E+02 0.337E+02 0.297E-01 0.165E+00 0.281E-02 0.337E+01
0.537E+02 0.939E+03 0.141E+03 0.568E+05 0.396E+04 0.256E+04 0.485E-03
0.205E+04
0.840E+04 0.373E+00 0.262E+00 0.296E-01 0.314E+01 0.254E+01 0.156E+02
0.384E+01 0.406E+02 0.347E+02 0.309E-01 0.171E+00 0.298E-02 0.345E+01
0.555E+02 0.960E+03 0.144E+03 0.580E+05 0.410E+04 0.259E+04 0.504E-03
0.210E+04
0.850E+04 0.384E+00 0.272E+00 0.307E-01 0.325E+01 0.264E+01 0.161E+02
0.396E+01 0.421E+02 0.357E+02 0.321E-01 0.178E+00 0.315E-02 0.353E+01
0.574E+02 0.981E+03 0.147E+03 0.592E+05 0.425E+04 0.261E+04 0.522E-03
0.214E+04
0.860E+04 0.393E+00 0.283E+00 0.317E-01 0.335E+01 0.275E+01 0.167E+02
0.409E+01 0.435E+02 0.366E+02 0.333E-01 0.184E+00 0.333E-02 0.360E+01
0.593E+02 0.100E+04 0.150E+03 0.604E+05 0.440E+04 0.263E+04 0.540E-03
0.218E+04
0.870E+04 0.403E+00 0.293E+00 0.328E-01 0.346E+01 0.286E+01 0.173E+02
0.421E+01 0.450E+02 0.376E+02 0.345E-01 0.190E+00 0.351E-02 0.367E+01
0.613E+02 0.102E+04 0.153E+03 0.616E+05 0.455E+04 0.265E+04 0.558E-03
0.222E+04
0.880E+04 0.412E+00 0.303E+00 0.339E-01 0.356E+01 0.296E+01 0.178E+02
0.434E+01 0.465E+02 0.385E+02 0.358E-01 0.196E+00 0.370E-02 0.374E+01
0.632E+02 0.104E+04 0.156E+03 0.628E+05 0.470E+04 0.267E+04 0.576E-03
0.226E+04
0.890E+04 0.421E+00 0.314E+00 0.350E-01 0.366E+01 0.307E+01 0.184E+02
0.446E+01 0.480E+02 0.394E+02 0.370E-01 0.202E+00 0.390E-02 0.381E+01
0.652E+02 0.106E+04 0.159E+03 0.640E+05 0.485E+04 0.268E+04 0.594E-03
0.230E+04
0.900E+04 0.430E+00 0.324E+00 0.361E-01 0.376E+01 0.318E+01 0.190E+02
0.458E+01 0.494E+02 0.403E+02 0.382E-01 0.209E+00 0.410E-02 0.387E+01

```
 0.672E+02   0.108E+04   0.162E+03   0.651E+05   0.500E+04   0.270E+04   0.613E-03
0.234E+04
  0.910E+04   0.439E+00   0.335E+00   0.372E-01   0.387E+01   0.328E+01   0.195E+02
0.470E+01   0.509E+02   0.412E+02   0.394E-01   0.215E+00   0.430E-02   0.393E+01
0.692E+02   0.110E+04   0.165E+03   0.663E+05   0.514E+04   0.271E+04   0.631E-03
0.238E+04
  0.920E+04   0.447E+00   0.345E+00   0.382E-01   0.397E+01   0.339E+01   0.201E+02
0.482E+01   0.523E+02   0.420E+02   0.407E-01   0.221E+00   0.451E-02   0.399E+01
0.712E+02   0.112E+04   0.168E+03   0.674E+05   0.529E+04   0.272E+04   0.649E-03
0.242E+04
  0.930E+04   0.456E+00   0.356E+00   0.393E-01   0.407E+01   0.349E+01   0.207E+02
0.493E+01   0.538E+02   0.428E+02   0.419E-01   0.227E+00   0.473E-02   0.405E+01
0.733E+02   0.114E+04   0.171E+03   0.685E+05   0.544E+04   0.274E+04   0.667E-03
0.246E+04
  0.940E+04   0.464E+00   0.366E+00   0.404E-01   0.416E+01   0.360E+01   0.212E+02
0.505E+01   0.553E+02   0.436E+02   0.432E-01   0.233E+00   0.495E-02   0.410E+01
0.753E+02   0.116E+04   0.174E+03   0.696E+05   0.559E+04   0.275E+04   0.685E-03
0.250E+04
  0.950E+04   0.472E+00   0.377E+00   0.415E-01   0.426E+01   0.370E+01   0.218E+02
0.517E+01   0.567E+02   0.444E+02   0.444E-01   0.240E+00   0.518E-02   0.415E+01
0.773E+02   0.118E+04   0.176E+03   0.707E+05   0.573E+04   0.276E+04   0.703E-03
0.253E+04
  0.960E+04   0.479E+00   0.387E+00   0.426E-01   0.436E+01   0.380E+01   0.224E+02
0.528E+01   0.582E+02   0.452E+02   0.457E-01   0.246E+00   0.542E-02   0.420E+01
0.786E+02   0.120E+04   0.179E+03   0.716E+05   0.588E+04   0.276E+04   0.721E-03
0.256E+04
  0.970E+04   0.487E+00   0.398E+00   0.437E-01   0.446E+01   0.391E+01   0.230E+02
0.539E+01   0.596E+02   0.460E+02   0.470E-01   0.252E+00   0.565E-02   0.424E+01
0.796E+02   0.121E+04   0.180E+03   0.723E+05   0.603E+04   0.275E+04   0.739E-03
0.258E+04
  0.980E+04   0.494E+00   0.409E+00   0.447E-01   0.455E+01   0.401E+01   0.235E+02
0.550E+01   0.611E+02   0.467E+02   0.482E-01   0.258E+00   0.590E-02   0.429E+01
0.807E+02   0.121E+04   0.182E+03   0.729E+05   0.618E+04   0.273E+04   0.757E-03
0.259E+04
  0.990E+04   0.501E+00   0.420E+00   0.458E-01   0.465E+01   0.411E+01   0.241E+02
0.562E+01   0.625E+02   0.475E+02   0.495E-01   0.264E+00   0.615E-02   0.433E+01
0.817E+02   0.122E+04   0.183E+03   0.733E+05   0.632E+04   0.272E+04   0.775E-03
0.260E+04
  0.100E+05   0.508E+00   0.430E+00   0.469E-01   0.474E+01   0.421E+01   0.247E+02
0.573E+01   0.639E+02   0.482E+02   0.508E-01   0.271E+00   0.640E-02   0.437E+01
0.828E+02   0.122E+04   0.184E+03   0.736E+05   0.647E+04   0.269E+04   0.793E-03
0.261E+04
```

APPENDIX E

DATA FILE *ebsnef.dat*—DATA FILE TO BE USED AS INPUT TO NEFTRAN MODULE IN THE TPA CODE

APPENDIX E

DATA FILE *ebsnef.dat*—DATA FILE TO BE USED AS INPUT TO NEFTRAN MODULE IN THE TPA CODE

Radionuclide release rate (Ci/yr) are given as a function of time for all radionuclides. At the top of the file is the title line, followed by the number of radionuclides, and the number of data rows for each radionuclide. Each data set is preceded by the radionuclide name.

```
release rates from ebspac
         21          196  num nucs, ntemp
CM246
     100.0000000    0.0000000E+00
     200.0000000    0.0000000E+00
     300.0000000    0.0000000E+00
     400.0000000    0.0000000E+00
     500.0000000    0.0000000E+00
     600.0000000    0.0000000E+00
     700.0000000    0.0000000E+00
     800.0000000    0.0000000E+00
     900.0000000    0.0000000E+00
    1000.0000000    0.0000000E+00
    1100.0000000    0.0000000E+00
    1200.0000000    0.0000000E+00
    1300.0000000    0.0000000E+00
    1400.0000000    0.0000000E+00
    1500.0000000    0.0000000E+00
    1600.0000000    0.0000000E+00
    1700.0000000    0.0000000E+00
    1800.0000000    0.0000000E+00
    1900.0000000    0.0000000E+00
    2000.0000000    0.0000000E+00
    2100.0000000    0.0000000E+00
    2200.0000000    0.0000000E+00
    2300.0000000    0.0000000E+00
    2400.0000000    0.0000000E+00
    2500.0000000    0.0000000E+00
    2600.0000000    0.0000000E+00
    2700.0000000    0.0000000E+00
    2800.0000000    0.0000000E+00
    2900.0000000    0.0000000E+00
    3000.0000000    0.0000000E+00
    3100.0000000    0.0000000E+00
    3200.0000000    0.9125188E-06
    3300.0000000    0.6641986E-05
    3400.0000000    0.1305211E-04
    3500.0000000    0.3507196E-04
    3600.0000000    0.3701918E-04
    3700.0000000    0.3793778E-04
    3800.0000000    0.3824779E-04
    3900.0000000    0.3823943E-04
    4000.0000000    0.3807052E-04
    4100.0000000    0.3782398E-04
    4200.0000000    0.3754249E-04
    4300.0000000    0.3724769E-04
    4400.0000000    0.3695044E-04
    4500.0000000    0.3665620E-04
    4600.0000000    0.5198899E-04
```

4700.0000000	0.7513983E-04
4800.0000000	0.1179955E-03
4900.0000000	0.1787388E-03
5000.0000000	0.1840261E-03
5100.0000000	0.1860162E-03
5200.0000000	0.1862566E-03
5300.0000000	0.1856005E-03
5400.0000000	0.1845030E-03
5500.0000000	0.1832004E-03
5600.0000000	0.1818132E-03
5700.0000000	0.1804018E-03
5800.0000000	0.1789960E-03
5900.0000000	0.1776099E-03
6000.0000000	0.1762503E-03
6100.0000000	0.1749192E-03
6200.0000000	0.1736165E-03
6300.0000000	0.1723410E-03
6400.0000000	0.1710914E-03
6500.0000000	0.1698663E-03
6600.0000000	0.1721619E-03
6700.0000000	0.1930636E-03
6800.0000000	0.2166323E-03
6900.0000000	0.3002088E-03
7000.0000000	0.3067654E-03
7100.0000000	0.3091995E-03
7200.0000000	0.3092976E-03
7300.0000000	0.3081797E-03
7400.0000000	0.3064548E-03
7500.0000000	0.3044428E-03
7600.0000000	0.3023081E-03
7700.0000000	0.3001337E-03
7800.0000000	0.2979607E-03
7900.0000000	0.2958088E-03
8000.0000000	0.2936867E-03
8100.0000000	0.2915980E-03
8200.0000000	0.2895436E-03
8300.0000000	0.2875233E-03
8400.0000000	0.2855355E-03
8500.0000000	0.2835786E-03
8600.0000000	0.2816509E-03
8700.0000000	0.2797509E-03
8800.0000000	0.2778770E-03
8900.0000000	0.2760279E-03
9000.0000000	0.2742021E-03
9100.0000000	0.2723986E-03
9200.0000000	0.2706163E-03
9300.0000000	0.2688540E-03
9400.0000000	0.2671109E-03
9500.0000000	0.2653140E-03
9600.0000000	0.2636730E-03
9700.0000000	0.2619838E-03
9800.0000000	0.2603100E-03
9900.0000000	0.2586512E-03
10000.0000000	0.2569169E-03
PU242	
100.0000000	0.0000000E+00
200.0000000	0.0000000E+00
300.0000000	0.0000000E+00
400.0000000	0.0000000E+00
500.0000000	0.0000000E+00
600.0000000	0.0000000E+00
700.0000000	0.0000000E+00

800.0000000	0.0000000E+00
900.0000000	0.0000000E+00
1000.0000000	0.0000000E+00
1100.0000000	0.0000000E+00
1200.0000000	0.0000000E+00
1300.0000000	0.0000000E+00
1400.0000000	0.0000000E+00
1500.0000000	0.0000000E+00
1600.0000000	0.0000000E+00
1700.0000000	0.0000000E+00
1800.0000000	0.0000000E+00
1900.0000000	0.0000000E+00
2000.0000000	0.0000000E+00
2100.0000000	0.0000000E+00
2200.0000000	0.0000000E+00
2300.0000000	0.0000000E+00
2400.0000000	0.0000000E+00
2500.0000000	0.0000000E+00
2600.0000000	0.0000000E+00
2700.0000000	0.0000000E+00
2800.0000000	0.0000000E+00
2900.0000000	0.0000000E+00
3000.0000000	0.0000000E+00
3100.0000000	0.0000000E+00
3200.0000000	0.3533081E-06
3300.0000000	0.2586480E-05
3400.0000000	0.5132391E-05
3500.0000000	0.1392630E-04
3600.0000000	0.1483680E-04
3700.0000000	0.1534728E-04
3800.0000000	0.1561398E-04
3900.0000000	0.1574968E-04
4000.0000000	0.1581655E-04
4100.0000000	0.1584778E-04
4200.0000000	0.1586076E-04
4300.0000000	0.1586455E-04
4400.0000000	0.1586391E-04
4500.0000000	0.1586154E-04
4600.0000000	0.2281180E-04
4700.0000000	0.3339532E-04
4800.0000000	0.5315196E-04
4900.0000000	0.8138929E-04
5000.0000000	0.8455982E-04
5100.0000000	0.8623961E-04
5200.0000000	0.8710376E-04
5300.0000000	0.8753538E-04
5400.0000000	0.8774186E-04
5500.0000000	0.8783271E-04
5600.0000000	0.8786509E-04
5700.0000000	0.8786862E-04
5800.0000000	0.8785857E-04
5900.0000000	0.8784292E-04
6000.0000000	0.8782699E-04
6100.0000000	0.8781307E-04
6200.0000000	0.8780208E-04
6300.0000000	0.8779449E-04
6400.0000000	0.8779049E-04
6500.0000000	0.8779014E-04
6600.0000000	0.8970440E-04
6700.0000000	0.1018504E-03
6800.0000000	0.1156493E-03
6900.0000000	0.1633791E-03

7000.0000000	0.1684566E-03
7100.0000000	0.1712541E-03
7200.0000000	0.1727265E-03
7300.0000000	0.1734878E-03
7400.0000000	0.1738770E-03
7500.0000000	0.1740749E-03
7600.0000000	0.1741762E-03
7700.0000000	0.1742302E-03
7800.0000000	0.1742623E-03
7900.0000000	0.1742856E-03
8000.0000000	0.1743069E-03
8100.0000000	0.1743295E-03
8200.0000000	0.1743561E-03
8300.0000000	0.1743885E-03
8400.0000000	0.1744269E-03
8500.0000000	0.1744715E-03
8600.0000000	0.1745223E-03
8700.0000000	0.1745793E-03
8800.0000000	0.1746423E-03
8900.0000000	0.1747113E-03
9000.0000000	0.1747863E-03
9100.0000000	0.1748672E-03
9200.0000000	0.1749539E-03
9300.0000000	0.1750463E-03
9400.0000000	0.1751445E-03
9500.0000000	0.1751536E-03
9600.0000000	0.1752855E-03
9700.0000000	0.1754334E-03
9800.0000000	0.1755872E-03
9900.0000000	0.1757459E-03
10000.0000000	0.1759093E-03
U238	
100.0000000	0.0000000E+00
200.0000000	0.0000000E+00
300.0000000	0.0000000E+00
400.0000000	0.0000000E+00
500.0000000	0.0000000E+00
600.0000000	0.0000000E+00
700.0000000	0.0000000E+00
800.0000000	0.0000000E+00
900.0000000	0.0000000E+00
1000.0000000	0.0000000E+00
1100.0000000	0.0000000E+00
1200.0000000	0.0000000E+00
1300.0000000	0.0000000E+00
1400.0000000	0.0000000E+00
1500.0000000	0.0000000E+00
1600.0000000	0.0000000E+00
1700.0000000	0.0000000E+00
1800.0000000	0.0000000E+00
1900.0000000	0.0000000E+00
2000.0000000	0.0000000E+00
2100.0000000	0.0000000E+00
2200.0000000	0.0000000E+00
2300.0000000	0.0000000E+00
2400.0000000	0.0000000E+00
2500.0000000	0.0000000E+00
2600.0000000	0.0000000E+00
2700.0000000	0.0000000E+00
2800.0000000	0.0000000E+00
2900.0000000	0.0000000E+00
3000.0000000	0.0000000E+00

3100.0000000	0.0000000E+00
3200.0000000	0.4047655E-07
3300.0000000	0.2662433E-06
3400.0000000	0.4398978E-06
3500.0000000	0.1261238E-05
3600.0000000	0.1271774E-05
3700.0000000	0.1262379E-05
3800.0000000	0.1247828E-05
3900.0000000	0.1233675E-05
4000.0000000	0.1221632E-05
4100.0000000	0.1211839E-05
4200.0000000	0.1203919E-05
4300.0000000	0.1197420E-05
4400.0000000	0.1191971E-05
4500.0000000	0.1187306E-05
4600.0000000	0.1914717E-05
4700.0000000	0.2733205E-05
4800.0000000	0.4195403E-05
4900.0000000	0.6622512E-05
5000.0000000	0.6611626E-05
5100.0000000	0.6553761E-05
5200.0000000	0.6488631E-05
5300.0000000	0.6430171E-05
5400.0000000	0.6381603E-05
5500.0000000	0.6342076E-05
5600.0000000	0.6309688E-05
5700.0000000	0.6282621E-05
5800.0000000	0.6259460E-05
5900.0000000	0.6239198E-05
6000.0000000	0.6221195E-05
6100.0000000	0.6204969E-05
6200.0000000	0.6190175E-05
6300.0000000	0.6176571E-05
6400.0000000	0.6163982E-05
6500.0000000	0.6152271E-05
6600.0000000	0.6331841E-05
6700.0000000	0.7389219E-05
6800.0000000	0.8198117E-05
6900.0000000	0.1208369E-04
7000.0000000	0.1212211E-04
7100.0000000	0.1206723E-04
7200.0000000	0.1198995E-04
7300.0000000	0.1191543E-04
7400.0000000	0.1185150E-04
7500.0000000	0.1179864E-04
7600.0000000	0.1175498E-04
7700.0000000	0.1171832E-04
7800.0000000	0.1168684E-04
7900.0000000	0.1165918E-04
8000.0000000	0.1163439E-04
8100.0000000	0.1161183E-04
8200.0000000	0.1159109E-04
8300.0000000	0.1157189E-04
8400.0000000	0.1155399E-04
8500.0000000	0.1153721E-04
8600.0000000	0.1152141E-04
8700.0000000	0.1150649E-04
8800.0000000	0.1149234E-04
8900.0000000	0.1147890E-04
9000.0000000	0.1146609E-04
9100.0000000	0.1145385E-04
9200.0000000	0.1144212E-04

9300.0000000	0.1143087E-04
9400.0000000	0.1142006E-04
9500.0000000	0.1140742E-04
9600.0000000	0.1139831E-04
9700.0000000	0.1138917E-04
9800.0000000	0.1138032E-04
9900.0000000	0.1137172E-04
10000.0000000	0.1136276E-04

CM245

100.0000000	0.0000000E+00
200.0000000	0.0000000E+00
300.0000000	0.0000000E+00
400.0000000	0.0000000E+00
500.0000000	0.0000000E+00
600.0000000	0.0000000E+00
700.0000000	0.0000000E+00
800.0000000	0.0000000E+00
900.0000000	0.0000000E+00
1000.0000000	0.0000000E+00
1100.0000000	0.0000000E+00
1200.0000000	0.0000000E+00
1300.0000000	0.0000000E+00
1400.0000000	0.0000000E+00
1500.0000000	0.0000000E+00
1600.0000000	0.0000000E+00
1700.0000000	0.0000000E+00
1800.0000000	0.0000000E+00
1900.0000000	0.0000000E+00
2000.0000000	0.0000000E+00
2100.0000000	0.0000000E+00
2200.0000000	0.0000000E+00
2300.0000000	0.0000000E+00
2400.0000000	0.0000000E+00
2500.0000000	0.0000000E+00
2600.0000000	0.0000000E+00
2700.0000000	0.0000000E+00
2800.0000000	0.0000000E+00
2900.0000000	0.0000000E+00
3000.0000000	0.0000000E+00
3100.0000000	0.0000000E+00
3200.0000000	0.5488101E-05
3300.0000000	0.4009305E-04
3400.0000000	0.7927884E-04
3500.0000000	0.2143751E-03
3600.0000000	0.2276528E-03
3700.0000000	0.2347392E-03
3800.0000000	0.2380976E-03
3900.0000000	0.2394774E-03
4000.0000000	0.2398385E-03
4100.0000000	0.2396901E-03
4200.0000000	0.2392974E-03
4300.0000000	0.2387969E-03
4400.0000000	0.2382590E-03
4500.0000000	0.2377211E-03
4600.0000000	0.3398709E-03
4700.0000000	0.4948717E-03
4800.0000000	0.7832345E-03
4900.0000000	0.1194238E-02
5000.0000000	0.1237063E-02
5100.0000000	0.1258067E-02
5200.0000000	0.1267282E-02
5300.0000000	0.1270348E-02

5400.0000000	0.1270300E-02
5500.0000000	0.1268733E-02
5600.0000000	0.1266470E-02
5700.0000000	0.1263933E-02
5800.0000000	0.1261334E-02
5900.0000000	0.1258782E-02
6000.0000000	0.1256335E-02
6100.0000000	0.1254018E-02
6200.0000000	0.1251837E-02
6300.0000000	0.1249790E-02
6400.0000000	0.1247874E-02
6500.0000000	0.1246083E-02
6600.0000000	0.1270649E-02
6700.0000000	0.1435538E-02
6800.0000000	0.1622277E-02
6900.0000000	0.2269256E-02
7000.0000000	0.2333369E-02
7100.0000000	0.2366386E-02
7200.0000000	0.2381514E-02
7300.0000000	0.2387175E-02
7400.0000000	0.2387992E-02
7500.0000000	0.2386417E-02
7600.0000000	0.2383724E-02
7700.0000000	0.2380569E-02
7800.0000000	0.2377283E-02
7900.0000000	0.2374031E-02
8000.0000000	0.2370896E-02
8100.0000000	0.2367912E-02
8200.0000000	0.2365100E-02
8300.0000000	0.2362469E-02
8400.0000000	0.2360014E-02
8500.0000000	0.2357727E-02
8600.0000000	0.2355602E-02
8700.0000000	0.2353630E-02
8800.0000000	0.2351802E-02
8900.0000000	0.2350112E-02
9000.0000000	0.2348551E-02
9100.0000000	0.2347113E-02
9200.0000000	0.2345791E-02
9300.0000000	0.2344580E-02
9400.0000000	0.2343472E-02
9500.0000000	0.2342014E-02
9600.0000000	0.2341270E-02
9700.0000000	0.2340573E-02
9800.0000000	0.2339949E-02
9900.0000000	0.2339393E-02
10000.0000000	0.2338851E-02
AM241	
100.0000000	0.0000000E+00
200.0000000	0.0000000E+00
300.0000000	0.0000000E+00
400.0000000	0.0000000E+00
500.0000000	0.0000000E+00
600.0000000	0.0000000E+00
700.0000000	0.0000000E+00
800.0000000	0.0000000E+00
900.0000000	0.0000000E+00
1000.0000000	0.0000000E+00
1100.0000000	0.0000000E+00
1200.0000000	0.0000000E+00
1300.0000000	0.0000000E+00
1400.0000000	0.0000000E+00

1500.0000000	0.0000000E+00
1600.0000000	0.0000000E+00
1700.0000000	0.0000000E+00
1800.0000000	0.0000000E+00
1900.0000000	0.0000000E+00
2000.0000000	0.0000000E+00
2100.0000000	0.0000000E+00
2200.0000000	0.0000000E+00
2300.0000000	0.0000000E+00
2400.0000000	0.0000000E+00
2500.0000000	0.0000000E+00
2600.0000000	0.0000000E+00
2700.0000000	0.0000000E+00
2800.0000000	0.0000000E+00
2900.0000000	0.0000000E+00
3000.0000000	0.0000000E+00
3100.0000000	0.0000000E+00
3200.0000000	0.5764057E-05
3300.0000000	0.3889782E-04
3400.0000000	0.6707391E-04
3500.0000000	0.1572295E-03
3600.0000000	0.1455652E-03
3700.0000000	0.1303529E-03
3800.0000000	0.1148193E-03
3900.0000000	0.1002914E-03
4000.0000000	0.8724021E-04
4100.0000000	0.7574588E-04
4200.0000000	0.6572500E-04
4300.0000000	0.5703551E-04
4400.0000000	0.4952265E-04
4500.0000000	0.4303798E-04
4600.0000000	0.5267707E-04
4700.0000000	0.6655174E-04
4800.0000000	0.9073602E-04
4900.0000000	0.1216092E-03
5000.0000000	0.1109217E-03
5100.0000000	0.9939615E-04
5200.0000000	0.8848249E-04
5300.0000000	0.7863402E-04
5400.0000000	0.6995344E-04
5500.0000000	0.6239296E-04
5600.0000000	0.5584861E-04
5700.0000000	0.5020228E-04
5800.0000000	0.4533934E-04
5900.0000000	0.4115524E-04
6000.0000000	0.3755733E-04
6100.0000000	0.3446468E-04
6200.0000000	0.3180713E-04
6300.0000000	0.2952402E-04
6400.0000000	0.2756305E-04
6500.0000000	0.2587919E-04
6600.0000000	0.2490381E-04
6700.0000000	0.2653079E-04
6800.0000000	0.2850565E-04
6900.0000000	0.3776089E-04
7000.0000000	0.3744287E-04
7100.0000000	0.3678411E-04
7200.0000000	0.3600755E-04
7300.0000000	0.3523341E-04
7400.0000000	0.3451579E-04
7500.0000000	0.3387453E-04
7600.0000000	0.3331288E-04

7700.0000000	0.3282669E-04
7800.0000000	0.3240889E-04
7900.0000000	0.3205163E-04
8000.0000000	0.3174732E-04
8100.0000000	0.3148896E-04
8200.0000000	0.3127035E-04
8300.0000000	0.3108600E-04
8400.0000000	0.3093118E-04
8500.0000000	0.3080176E-04
8600.0000000	0.3069419E-04
8700.0000000	0.3060541E-04
8800.0000000	0.3053277E-04
8900.0000000	0.3047401E-04
9000.0000000	0.3042718E-04
9100.0000000	0.3039059E-04
9200.0000000	0.3036279E-04
9300.0000000	0.3034256E-04
9400.0000000	0.3032880E-04
9500.0000000	0.3032072E-04
9600.0000000	0.3031740E-04
9700.0000000	0.3031726E-04
9800.0000000	0.3031974E-04
9900.0000000	0.3032444E-04
10000.0000000	0.3033140E-04
NP237	
100.0000000	0.0000000E+00
200.0000000	0.0000000E+00
300.0000000	0.0000000E+00
400.0000000	0.0000000E+00
500.0000000	0.0000000E+00
600.0000000	0.0000000E+00
700.0000000	0.0000000E+00
800.0000000	0.0000000E+00
900.0000000	0.0000000E+00
1000.0000000	0.0000000E+00
1100.0000000	0.0000000E+00
1200.0000000	0.0000000E+00
1300.0000000	0.0000000E+00
1400.0000000	0.0000000E+00
1500.0000000	0.0000000E+00
1600.0000000	0.0000000E+00
1700.0000000	0.0000000E+00
1800.0000000	0.0000000E+00
1900.0000000	0.0000000E+00
2000.0000000	0.0000000E+00
2100.0000000	0.0000000E+00
2200.0000000	0.0000000E+00
2300.0000000	0.0000000E+00
2400.0000000	0.0000000E+00
2500.0000000	0.0000000E+00
2600.0000000	0.0000000E+00
2700.0000000	0.0000000E+00
2800.0000000	0.0000000E+00
2900.0000000	0.0000000E+00
3000.0000000	0.0000000E+00
3100.0000000	0.0000000E+00
3200.0000000	0.2425072E-04
3300.0000000	0.1766540E-03
3400.0000000	0.3474549E-03
3500.0000000	0.9370779E-03
3600.0000000	0.9903275E-03
3700.0000000	0.1015711E-02

3800.0000000	0.1024490E-02
3900.0000000	0.1024470E-02
4000.0000000	0.1019931E-02
4100.0000000	0.1013143E-02
4200.0000000	0.1005288E-02
4300.0000000	0.9969787E-03
4400.0000000	0.9885374E-03
4500.0000000	0.9801549E-03
4600.0000000	0.1422017E-02
4700.0000000	0.2090345E-02
4800.0000000	0.3331810E-02
4900.0000000	0.5097156E-02
5000.0000000	0.5255388E-02
5100.0000000	0.5316763E-02
5200.0000000	0.5326125E-02
5300.0000000	0.5308429E-02
5400.0000000	0.5277108E-02
5500.0000000	0.5239218E-02
5600.0000000	0.5198418E-02
5700.0000000	0.5156585E-02
5800.0000000	0.5114676E-02
5900.0000000	0.5073183E-02
6000.0000000	0.5032478E-02
6100.0000000	0.4992690E-02
6200.0000000	0.4953850E-02
6300.0000000	0.4915960E-02
6400.0000000	0.4879010E-02
6500.0000000	0.4842979E-02
6600.0000000	0.4921840E-02
6700.0000000	0.5606066E-02
6800.0000000	0.6376367E-02
6900.0000000	0.9129161E-02
7000.0000000	0.9357726E-02
7100.0000000	0.9449532E-02
7200.0000000	0.9463368E-02
7300.0000000	0.9436145E-02
7400.0000000	0.9388121E-02
7500.0000000	0.9330043E-02
7600.0000000	0.9267509E-02
7700.0000000	0.9203400E-02
7800.0000000	0.9139184E-02
7900.0000000	0.9075604E-02
8000.0000000	0.9013022E-02
8100.0000000	0.8951613E-02
8200.0000000	0.8891533E-02
8300.0000000	0.8832883E-02
8400.0000000	0.8775647E-02
8500.0000000	0.8719801E-02
8600.0000000	0.8665311E-02
8700.0000000	0.8612146E-02
8800.0000000	0.8560271E-02
8900.0000000	0.8509654E-02
9000.0000000	0.8460264E-02
9100.0000000	0.8412071E-02
9200.0000000	0.8365043E-02
9300.0000000	0.8319153E-02
9400.0000000	0.8274372E-02
9500.0000000	0.8221492E-02
9600.0000000	0.8182664E-02
9700.0000000	0.8143528E-02
9800.0000000	0.8105363E-02
9900.0000000	0.8068077E-02

10000.0000000	0.8029077E-02
AM243	
100.0000000	0.0000000E+00
200.0000000	0.0000000E+00
300.0000000	0.0000000E+00
400.0000000	0.0000000E+00
500.0000000	0.0000000E+00
600.0000000	0.0000000E+00
700.0000000	0.0000000E+00
800.0000000	0.0000000E+00
900.0000000	0.0000000E+00
1000.0000000	0.0000000E+00
1100.0000000	0.0000000E+00
1200.0000000	0.0000000E+00
1300.0000000	0.0000000E+00
1400.0000000	0.0000000E+00
1500.0000000	0.0000000E+00
1600.0000000	0.0000000E+00
1700.0000000	0.0000000E+00
1800.0000000	0.0000000E+00
1900.0000000	0.0000000E+00
2000.0000000	0.0000000E+00
2100.0000000	0.0000000E+00
2200.0000000	0.0000000E+00
2300.0000000	0.0000000E+00
2400.0000000	0.0000000E+00
2500.0000000	0.0000000E+00
2600.0000000	0.0000000E+00
2700.0000000	0.0000000E+00
2800.0000000	0.0000000E+00
2900.0000000	0.0000000E+00
3000.0000000	0.0000000E+00
3100.0000000	0.0000000E+00
3200.0000000	0.6640317E-05
3300.0000000	0.4874465E-04
3400.0000000	0.9713426E-04
3500.0000000	0.2641366E-03
3600.0000000	0.2821202E-03
3700.0000000	0.2924730E-03
3800.0000000	0.2980982E-03
3900.0000000	0.3011324E-03
4000.0000000	0.3027637E-03
4100.0000000	0.3036327E-03
4200.0000000	0.3040806E-03
4300.0000000	0.3042896E-03
4400.0000000	0.3043584E-03
4500.0000000	0.3043425E-03
4600.0000000	0.4329736E-03
4700.0000000	0.6285520E-03
4800.0000000	0.9927704E-03
4900.0000000	0.1512149E-02
5000.0000000	0.1568924E-02
5100.0000000	0.1598212E-02
5200.0000000	0.1612520E-02
5300.0000000	0.1618915E-02
5400.0000000	0.1621208E-02
5500.0000000	0.1621407E-02
5600.0000000	0.1620558E-02
5700.0000000	0.1619203E-02
5800.0000000	0.1617620E-02
5900.0000000	0.1615955E-02
6000.0000000	0.1614286E-02

```
     6100.0000000   0.1612653E-02
     6200.0000000   0.1611072E-02
     6300.0000000   0.1609552E-02
     6400.0000000   0.1608096E-02
     6500.0000000   0.1606703E-02
     6600.0000000   0.1638131E-02
     6700.0000000   0.1845011E-02
     6800.0000000   0.2080040E-02
     6900.0000000   0.2890886E-02
     7000.0000000   0.2973496E-02
     7100.0000000   0.3017345E-02
     7200.0000000   0.3038769E-02
     7300.0000000   0.3048248E-02
     7400.0000000   0.3051536E-02
     7500.0000000   0.3051686E-02
     7600.0000000   0.3050291E-02
     7700.0000000   0.3048171E-02
     7800.0000000   0.3045747E-02
     7900.0000000   0.3043231E-02
     8000.0000000   0.3040730E-02
     8100.0000000   0.3038296E-02
     8200.0000000   0.3035956E-02
     8300.0000000   0.3033724E-02
     8400.0000000   0.3031600E-02
     8500.0000000   0.3029583E-02
     8600.0000000   0.3027669E-02
     8700.0000000   0.3025853E-02
     8800.0000000   0.3024131E-02
     8900.0000000   0.3022498E-02
     9000.0000000   0.3020949E-02
     9100.0000000   0.3019481E-02
     9200.0000000   0.3018088E-02
     9300.0000000   0.3016768E-02
     9400.0000000   0.3015517E-02
     9500.0000000   0.3014036E-02
     9600.0000000   0.3013038E-02
     9700.0000000   0.3012050E-02
     9800.0000000   0.3011114E-02
     9900.0000000   0.3010222E-02
    10000.0000000   0.3009315E-02
PU239
      100.0000000   0.0000000E+00
      200.0000000   0.0000000E+00
      300.0000000   0.0000000E+00
      400.0000000   0.0000000E+00
      500.0000000   0.0000000E+00
      600.0000000   0.0000000E+00
      700.0000000   0.0000000E+00
      800.0000000   0.0000000E+00
      900.0000000   0.0000000E+00
     1000.0000000   0.0000000E+00
     1100.0000000   0.0000000E+00
     1200.0000000   0.0000000E+00
     1300.0000000   0.0000000E+00
     1400.0000000   0.0000000E+00
     1500.0000000   0.0000000E+00
     1600.0000000   0.0000000E+00
     1700.0000000   0.0000000E+00
     1800.0000000   0.0000000E+00
     1900.0000000   0.0000000E+00
     2000.0000000   0.0000000E+00
     2100.0000000   0.0000000E+00
```

2200.0000000	0.0000000E+00
2300.0000000	0.0000000E+00
2400.0000000	0.0000000E+00
2500.0000000	0.0000000E+00
2600.0000000	0.0000000E+00
2700.0000000	0.0000000E+00
2800.0000000	0.0000000E+00
2900.0000000	0.0000000E+00
3000.0000000	0.0000000E+00
3100.0000000	0.0000000E+00
3200.0000000	0.6268886E-04
3300.0000000	0.4582626E-03
3400.0000000	0.9070954E-03
3500.0000000	0.2455209E-02
3600.0000000	0.2609499E-02
3700.0000000	0.2692800E-02
3800.0000000	0.2733143E-02
3900.0000000	0.2750533E-02
4000.0000000	0.2755965E-02
4100.0000000	0.2755291E-02
4200.0000000	0.2751567E-02
4300.0000000	0.2746376E-02
4400.0000000	0.2740548E-02
4500.0000000	0.2734540E-02
4600.0000000	0.3919482E-02
4700.0000000	0.5719944E-02
4800.0000000	0.9073569E-02
4900.0000000	0.1385633E-01
5000.0000000	0.1436224E-01
5100.0000000	0.1461349E-01
5200.0000000	0.1472638E-01
5300.0000000	0.1476643E-01
5400.0000000	0.1476901E-01
5500.0000000	0.1475273E-01
5600.0000000	0.1472726E-01
5700.0000000	0.1469760E-01
5800.0000000	0.1466630E-01
5900.0000000	0.1463468E-01
6000.0000000	0.1460358E-01
6100.0000000	0.1457334E-01
6200.0000000	0.1454410E-01
6300.0000000	0.1451590E-01
6400.0000000	0.1448875E-01
6500.0000000	0.1446265E-01
6600.0000000	0.1474802E-01
6700.0000000	0.1669306E-01
6800.0000000	0.1889834E-01
6900.0000000	0.2656614E-01
7000.0000000	0.2732868E-01
7100.0000000	0.2772156E-01
7200.0000000	0.2790089E-01
7300.0000000	0.2796640E-01
7400.0000000	0.2797297E-01
7500.0000000	0.2794977E-01
7600.0000000	0.2791203E-01
7700.0000000	0.2786761E-01
7800.0000000	0.2782058E-01
7900.0000000	0.2777299E-01
8000.0000000	0.2772587E-01
8100.0000000	0.2767975E-01
8200.0000000	0.2763498E-01
8300.0000000	0.2759177E-01

```
     8400.0000000   0.2755013E-01
     8500.0000000   0.2751006E-01
     8600.0000000   0.2747153E-01
     8700.0000000   0.2743448E-01
     8800.0000000   0.2739887E-01
     8900.0000000   0.2736468E-01
     9000.0000000   0.2733185E-01
     9100.0000000   0.2730034E-01
     9200.0000000   0.2727011E-01
     9300.0000000   0.2724113E-01
     9400.0000000   0.2721336E-01
     9500.0000000   0.2717551E-01
     9600.0000000   0.2715405E-01
     9700.0000000   0.2713305E-01
     9800.0000000   0.2711307E-01
     9900.0000000   0.2709399E-01
    10000.0000000   0.2707399E-01
PU240
      100.0000000   0.0000000E+00
      200.0000000   0.0000000E+00
      300.0000000   0.0000000E+00
      400.0000000   0.0000000E+00
      500.0000000   0.0000000E+00
      600.0000000   0.0000000E+00
      700.0000000   0.0000000E+00
      800.0000000   0.0000000E+00
      900.0000000   0.0000000E+00
     1000.0000000   0.0000000E+00
     1100.0000000   0.0000000E+00
     1200.0000000   0.0000000E+00
     1300.0000000   0.0000000E+00
     1400.0000000   0.0000000E+00
     1500.0000000   0.0000000E+00
     1600.0000000   0.0000000E+00
     1700.0000000   0.0000000E+00
     1800.0000000   0.0000000E+00
     1900.0000000   0.0000000E+00
     2000.0000000   0.0000000E+00
     2100.0000000   0.0000000E+00
     2200.0000000   0.0000000E+00
     2300.0000000   0.0000000E+00
     2400.0000000   0.0000000E+00
     2500.0000000   0.0000000E+00
     2600.0000000   0.0000000E+00
     2700.0000000   0.0000000E+00
     2800.0000000   0.0000000E+00
     2900.0000000   0.0000000E+00
     3000.0000000   0.0000000E+00
     3100.0000000   0.0000000E+00
     3200.0000000   0.8050335E-04
     3300.0000000   0.5858936E-03
     3400.0000000   0.1151051E-02
     3500.0000000   0.3091955E-02
     3600.0000000   0.3262391E-02
     3700.0000000   0.3341802E-02
     3800.0000000   0.3367326E-02
     3900.0000000   0.3364597E-02
     4000.0000000   0.3347563E-02
     4100.0000000   0.3323563E-02
     4200.0000000   0.3296384E-02
     4300.0000000   0.3267954E-02
     4400.0000000   0.3239251E-02
```

4500.0000000	0.3210779E-02
4600.0000000	0.4556966E-02
4700.0000000	0.6589844E-02
4800.0000000	0.1035289E-01
4900.0000000	0.1568392E-01
5000.0000000	0.1613918E-01
5100.0000000	0.1630345E-01
5200.0000000	0.1631319E-01
5300.0000000	0.1624354E-01
5400.0000000	0.1613465E-01
5500.0000000	0.1600736E-01
5600.0000000	0.1587236E-01
5700.0000000	0.1573505E-01
5800.0000000	0.1559810E-01
5900.0000000	0.1546281E-01
6000.0000000	0.1532988E-01
6100.0000000	0.1519952E-01
6200.0000000	0.1507175E-01
6300.0000000	0.1494652E-01
6400.0000000	0.1482373E-01
6500.0000000	0.1470328E-01
6600.0000000	0.1489057E-01
6700.0000000	0.1670200E-01
6800.0000000	0.1874455E-01
6900.0000000	0.2602032E-01
7000.0000000	0.2657231E-01
7100.0000000	0.2676349E-01
7200.0000000	0.2675024E-01
7300.0000000	0.2663050E-01
7400.0000000	0.2645756E-01
7500.0000000	0.2625943E-01
7600.0000000	0.2605052E-01
7700.0000000	0.2583815E-01
7800.0000000	0.2562597E-01
7900.0000000	0.2541576E-01
8000.0000000	0.2520833E-01
8100.0000000	0.2500401E-01
8200.0000000	0.2480296E-01
8300.0000000	0.2460519E-01
8400.0000000	0.2441059E-01
8500.0000000	0.2421904E-01
8600.0000000	0.2403041E-01
8700.0000000	0.2384458E-01
8800.0000000	0.2366140E-01
8900.0000000	0.2348078E-01
9000.0000000	0.2330259E-01
9100.0000000	0.2312674E-01
9200.0000000	0.2295312E-01
9300.0000000	0.2278164E-01
9400.0000000	0.2261222E-01
9500.0000000	0.2243678E-01
9600.0000000	0.2227807E-01
9700.0000000	0.2211484E-01
9800.0000000	0.2195329E-01
9900.0000000	0.2179336E-01
10000.0000000	0.2162631E-01
U236	
100.0000000	0.0000000E+00
200.0000000	0.0000000E+00
300.0000000	0.0000000E+00
400.0000000	0.0000000E+00
500.0000000	0.0000000E+00

600.0000000	0.0000000E+00
700.0000000	0.0000000E+00
800.0000000	0.0000000E+00
900.0000000	0.0000000E+00
1000.0000000	0.0000000E+00
1100.0000000	0.0000000E+00
1200.0000000	0.0000000E+00
1300.0000000	0.0000000E+00
1400.0000000	0.0000000E+00
1500.0000000	0.0000000E+00
1600.0000000	0.0000000E+00
1700.0000000	0.0000000E+00
1800.0000000	0.0000000E+00
1900.0000000	0.0000000E+00
2000.0000000	0.0000000E+00
2100.0000000	0.0000000E+00
2200.0000000	0.0000000E+00
2300.0000000	0.0000000E+00
2400.0000000	0.0000000E+00
2500.0000000	0.0000000E+00
2600.0000000	0.0000000E+00
2700.0000000	0.0000000E+00
2800.0000000	0.0000000E+00
2900.0000000	0.0000000E+00
3000.0000000	0.0000000E+00
3100.0000000	0.0000000E+00
3200.0000000	0.3571650E-07
3300.0000000	0.2355042E-06
3400.0000000	0.3908659E-06
3500.0000000	0.1124635E-05
3600.0000000	0.1139182E-05
3700.0000000	0.1135718E-05
3800.0000000	0.1127285E-05
3900.0000000	0.1118909E-05
4000.0000000	0.1112195E-05
4100.0000000	0.1107330E-05
4200.0000000	0.1104018E-05
4300.0000000	0.1101884E-05
4400.0000000	0.1100615E-05
4500.0000000	0.1099991E-05
4600.0000000	0.1776686E-05
4700.0000000	0.2542334E-05
4800.0000000	0.3913939E-05
4900.0000000	0.6193678E-05
5000.0000000	0.6206055E-05
5100.0000000	0.6173276E-05
5200.0000000	0.6132304E-05
5300.0000000	0.6096484E-05
5400.0000000	0.6069114E-05
5500.0000000	0.6049609E-05
5600.0000000	0.6036330E-05
5700.0000000	0.6027665E-05
5800.0000000	0.6022344E-05
5900.0000000	0.6019464E-05
6000.0000000	0.6018475E-05
6100.0000000	0.6018933E-05
6200.0000000	0.6020515E-05
6300.0000000	0.6023000E-05
6400.0000000	0.6026226E-05
6500.0000000	0.6030072E-05
6600.0000000	0.6220884E-05
6700.0000000	0.7272180E-05

6800.0000000	0.8084354E-05
6900.0000000	0.1193235E-04
7000.0000000	0.1200251E-04
7100.0000000	0.1197926E-04
7200.0000000	0.1193237E-04
7300.0000000	0.1188692E-04
7400.0000000	0.1185093E-04
7500.0000000	0.1182512E-04
7600.0000000	0.1180780E-04
7700.0000000	0.1179690E-04
7800.0000000	0.1179068E-04
7900.0000000	0.1178784E-04
8000.0000000	0.1178748E-04
8100.0000000	0.1178898E-04
8200.0000000	0.1179196E-04
8300.0000000	0.1179617E-04
8400.0000000	0.1180137E-04
8500.0000000	0.1180738E-04
8600.0000000	0.1181407E-04
8700.0000000	0.1182135E-04
8800.0000000	0.1182911E-04
8900.0000000	0.1183729E-04
9000.0000000	0.1184582E-04
9100.0000000	0.1185466E-04
9200.0000000	0.1186376E-04
9300.0000000	0.1187307E-04
9400.0000000	0.1188255E-04
9500.0000000	0.1188897E-04
9600.0000000	0.1190011E-04
9700.0000000	0.1191147E-04
9800.0000000	0.1192256E-04
9900.0000000	0.1193346E-04
10000.0000000	0.1194448E-04
U234	
100.0000000	0.0000000E+00
200.0000000	0.0000000E+00
300.0000000	0.0000000E+00
400.0000000	0.0000000E+00
500.0000000	0.0000000E+00
600.0000000	0.0000000E+00
700.0000000	0.0000000E+00
800.0000000	0.0000000E+00
900.0000000	0.0000000E+00
1000.0000000	0.0000000E+00
1100.0000000	0.0000000E+00
1200.0000000	0.0000000E+00
1300.0000000	0.0000000E+00
1400.0000000	0.0000000E+00
1500.0000000	0.0000000E+00
1600.0000000	0.0000000E+00
1700.0000000	0.0000000E+00
1800.0000000	0.0000000E+00
1900.0000000	0.0000000E+00
2000.0000000	0.0000000E+00
2100.0000000	0.0000000E+00
2200.0000000	0.0000000E+00
2300.0000000	0.0000000E+00
2400.0000000	0.0000000E+00
2500.0000000	0.0000000E+00
2600.0000000	0.0000000E+00
2700.0000000	0.0000000E+00
2800.0000000	0.0000000E+00

2900.0000000	0.0000000E+00
3000.0000000	0.0000000E+00
3100.0000000	0.0000000E+00
3200.0000000	0.2380163E-06
3300.0000000	0.1565467E-05
3400.0000000	0.2586361E-05
3500.0000000	0.7414658E-05
3600.0000000	0.7475866E-05
3700.0000000	0.7419866E-05
3800.0000000	0.7333403E-05
3900.0000000	0.7249109E-05
4000.0000000	0.7177081E-05
4100.0000000	0.7118164E-05
4200.0000000	0.7070177E-05
4300.0000000	0.7030494E-05
4400.0000000	0.6996944E-05
4500.0000000	0.6967977E-05
4600.0000000	0.1122734E-04
4700.0000000	0.1601924E-04
4800.0000000	0.2458085E-04
4900.0000000	0.3879115E-04
5000.0000000	0.3872256E-04
5100.0000000	0.3837828E-04
5200.0000000	0.3799079E-04
5300.0000000	0.3764174E-04
5400.0000000	0.3735008E-04
5500.0000000	0.3711097E-04
5600.0000000	0.3691340E-04
5700.0000000	0.3674682E-04
5800.0000000	0.3660301E-04
5900.0000000	0.3647611E-04
6000.0000000	0.3636238E-04
6100.0000000	0.3625902E-04
6200.0000000	0.3616403E-04
6300.0000000	0.3607600E-04
6400.0000000	0.3599389E-04
6500.0000000	0.3591693E-04
6600.0000000	0.3695402E-04
6700.0000000	0.4310319E-04
6800.0000000	0.4780540E-04
6900.0000000	0.7041839E-04
7000.0000000	0.7062935E-04
7100.0000000	0.7029718E-04
7200.0000000	0.6983397E-04
7300.0000000	0.6938611E-04
7400.0000000	0.6899923E-04
7500.0000000	0.6867636E-04
7600.0000000	0.6840670E-04
7700.0000000	0.6817758E-04
7800.0000000	0.6797843E-04
7900.0000000	0.6780145E-04
8000.0000000	0.6764117E-04
8100.0000000	0.6749388E-04
8200.0000000	0.6735717E-04
8300.0000000	0.6722938E-04
8400.0000000	0.6710916E-04
8500.0000000	0.6699546E-04
8600.0000000	0.6688750E-04
8700.0000000	0.6678463E-04
8800.0000000	0.6668629E-04
8900.0000000	0.6659204E-04
9000.0000000	0.6650147E-04

9100.0000000	0.6641424E-04
9200.0000000	0.6633004E-04
9300.0000000	0.6624860E-04
9400.0000000	0.6616969E-04
9500.0000000	0.6608164E-04
9600.0000000	0.6601214E-04
9700.0000000	0.6594217E-04
9800.0000000	0.6587413E-04
9900.0000000	0.6580773E-04
10000.0000000	0.6573873E-04
TH230	
100.0000000	0.0000000E+00
200.0000000	0.0000000E+00
300.0000000	0.0000000E+00
400.0000000	0.0000000E+00
500.0000000	0.0000000E+00
600.0000000	0.0000000E+00
700.0000000	0.0000000E+00
800.0000000	0.0000000E+00
900.0000000	0.0000000E+00
1000.0000000	0.0000000E+00
1100.0000000	0.0000000E+00
1200.0000000	0.0000000E+00
1300.0000000	0.0000000E+00
1400.0000000	0.0000000E+00
1500.0000000	0.0000000E+00
1600.0000000	0.0000000E+00
1700.0000000	0.0000000E+00
1800.0000000	0.0000000E+00
1900.0000000	0.0000000E+00
2000.0000000	0.0000000E+00
2100.0000000	0.0000000E+00
2200.0000000	0.0000000E+00
2300.0000000	0.0000000E+00
2400.0000000	0.0000000E+00
2500.0000000	0.0000000E+00
2600.0000000	0.0000000E+00
2700.0000000	0.0000000E+00
2800.0000000	0.0000000E+00
2900.0000000	0.0000000E+00
3000.0000000	0.0000000E+00
3100.0000000	0.0000000E+00
3200.0000000	0.6758934E-09
3300.0000000	0.4935891E-08
3400.0000000	0.9753253E-08
3500.0000000	0.2635105E-07
3600.0000000	0.2795695E-07
3700.0000000	0.2879532E-07
3800.0000000	0.2917082E-07
3900.0000000	0.2929912E-07
4000.0000000	0.2929856E-07
4100.0000000	0.2923201E-07
4200.0000000	0.2913228E-07
4300.0000000	0.2901634E-07
4400.0000000	0.2889308E-07
4500.0000000	0.2876749E-07
4600.0000000	0.4119495E-07
4700.0000000	0.6006447E-07
4800.0000000	0.9518240E-07
4900.0000000	0.1451888E-06
5000.0000000	0.1502314E-06
5100.0000000	0.1525842E-06

```
     5200.0000000   0.1534791E-06
     5300.0000000   0.1536065E-06
     5400.0000000   0.1533380E-06
     5500.0000000   0.1528695E-06
     5600.0000000   0.1523024E-06
     5700.0000000   0.1516890E-06
     5800.0000000   0.1510564E-06
     5900.0000000   0.1504184E-06
     6000.0000000   0.1497840E-06
     6100.0000000   0.1491573E-06
     6200.0000000   0.1485396E-06
     6300.0000000   0.1479317E-06
     6400.0000000   0.1473337E-06
     6500.0000000   0.1467458E-06
     6600.0000000   0.1493448E-06
     6700.0000000   0.1688945E-06
     6800.0000000   0.1910519E-06
     6900.0000000   0.2688613E-06
     7000.0000000   0.2761340E-06
     7100.0000000   0.2796186E-06
     7200.0000000   0.2809182E-06
     7300.0000000   0.2810538E-06
     7400.0000000   0.2805861E-06
     7500.0000000   0.2798128E-06
     7600.0000000   0.2788895E-06
     7700.0000000   0.2778964E-06
     7800.0000000   0.2768749E-06
     7900.0000000   0.2758461E-06
     8000.0000000   0.2748208E-06
     8100.0000000   0.2738043E-06
     8200.0000000   0.2728007E-06
     8300.0000000   0.2718125E-06
     8400.0000000   0.2708400E-06
     8500.0000000   0.2698834E-06
     8600.0000000   0.2689424E-06
     8700.0000000   0.2680170E-06
     8800.0000000   0.2671068E-06
     8900.0000000   0.2662115E-06
     9000.0000000   0.2653311E-06
     9100.0000000   0.2644652E-06
     9200.0000000   0.2636135E-06
     9300.0000000   0.2627759E-06
     9400.0000000   0.2619521E-06
     9500.0000000   0.2609814E-06
     9600.0000000   0.2602506E-06
     9700.0000000   0.2595103E-06
     9800.0000000   0.2587830E-06
     9900.0000000   0.2580673E-06
    10000.0000000   0.2573133E-06
RA226
      100.0000000   0.0000000E+00
      200.0000000   0.0000000E+00
      300.0000000   0.0000000E+00
      400.0000000   0.0000000E+00
      500.0000000   0.0000000E+00
      600.0000000   0.0000000E+00
      700.0000000   0.0000000E+00
      800.0000000   0.0000000E+00
      900.0000000   0.0000000E+00
     1000.0000000   0.0000000E+00
     1100.0000000   0.0000000E+00
     1200.0000000   0.0000000E+00
```

1300.0000000	0.0000000E+00
1400.0000000	0.0000000E+00
1500.0000000	0.0000000E+00
1600.0000000	0.0000000E+00
1700.0000000	0.0000000E+00
1800.0000000	0.0000000E+00
1900.0000000	0.0000000E+00
2000.0000000	0.0000000E+00
2100.0000000	0.0000000E+00
2200.0000000	0.0000000E+00
2300.0000000	0.0000000E+00
2400.0000000	0.0000000E+00
2500.0000000	0.0000000E+00
2600.0000000	0.0000000E+00
2700.0000000	0.0000000E+00
2800.0000000	0.0000000E+00
2900.0000000	0.0000000E+00
3000.0000000	0.0000000E+00
3100.0000000	0.0000000E+00
3200.0000000	0.9726079E-05
3300.0000000	0.7068513E-04
3400.0000000	0.1385882E-03
3500.0000000	0.3747307E-03
3600.0000000	0.3964712E-03
3700.0000000	0.4076516E-03
3800.0000000	0.4127055E-03
3900.0000000	0.4146640E-03
4000.0000000	0.4151483E-03
4100.0000000	0.4149866E-03
4200.0000000	0.4145847E-03
4300.0000000	0.4141319E-03
4400.0000000	0.4137099E-03
4500.0000000	0.4133486E-03
4600.0000000	0.5934598E-03
4700.0000000	0.8627796E-03
4800.0000000	0.1360980E-02
4900.0000000	0.2073221E-02
5000.0000000	0.2142190E-02
5100.0000000	0.2174896E-02
5200.0000000	0.2188759E-02
5300.0000000	0.2193369E-02
5400.0000000	0.2193733E-02
5500.0000000	0.2192355E-02
5600.0000000	0.2190436E-02
5700.0000000	0.2188514E-02
5800.0000000	0.2186806E-02
5900.0000000	0.2185373E-02
6000.0000000	0.2184215E-02
6100.0000000	0.2183295E-02
6200.0000000	0.2182574E-02
6300.0000000	0.2182011E-02
6400.0000000	0.2181575E-02
6500.0000000	0.2181238E-02
6600.0000000	0.2226698E-02
6700.0000000	0.2515082E-02
6800.0000000	0.2836042E-02
6900.0000000	0.3950503E-02
7000.0000000	0.4055565E-02
7100.0000000	0.4108442E-02
7200.0000000	0.4132327E-02
7300.0000000	0.4141557E-02
7400.0000000	0.4143811E-02

7500.0000000	0.4143012E-02
7600.0000000	0.4141081E-02
7700.0000000	0.4138914E-02
7800.0000000	0.4136895E-02
7900.0000000	0.4135159E-02
8000.0000000	0.4133729E-02
8100.0000000	0.4132581E-02
8200.0000000	0.4131675E-02
8300.0000000	0.4130969E-02
8400.0000000	0.4130421E-02
8500.0000000	0.4129997E-02
8600.0000000	0.4129671E-02
8700.0000000	0.4129419E-02
8800.0000000	0.4129225E-02
8900.0000000	0.4129077E-02
9000.0000000	0.4128962E-02
9100.0000000	0.4128874E-02
9200.0000000	0.4128807E-02
9300.0000000	0.4128755E-02
9400.0000000	0.4128715E-02
9500.0000000	0.4128675E-02
9600.0000000	0.4128657E-02
9700.0000000	0.4128641E-02
9800.0000000	0.4128628E-02
9900.0000000	0.4128619E-02
10000.0000000	0.4128611E-02
PB210	
100.0000000	0.0000000E+00
200.0000000	0.0000000E+00
300.0000000	0.0000000E+00
400.0000000	0.0000000E+00
500.0000000	0.0000000E+00
600.0000000	0.0000000E+00
700.0000000	0.0000000E+00
800.0000000	0.0000000E+00
900.0000000	0.0000000E+00
1000.0000000	0.0000000E+00
1100.0000000	0.0000000E+00
1200.0000000	0.0000000E+00
1300.0000000	0.0000000E+00
1400.0000000	0.0000000E+00
1500.0000000	0.0000000E+00
1600.0000000	0.0000000E+00
1700.0000000	0.0000000E+00
1800.0000000	0.0000000E+00
1900.0000000	0.0000000E+00
2000.0000000	0.0000000E+00
2100.0000000	0.0000000E+00
2200.0000000	0.0000000E+00
2300.0000000	0.0000000E+00
2400.0000000	0.0000000E+00
2500.0000000	0.0000000E+00
2600.0000000	0.0000000E+00
2700.0000000	0.0000000E+00
2800.0000000	0.0000000E+00
2900.0000000	0.0000000E+00
3000.0000000	0.0000000E+00
3100.0000000	0.0000000E+00
3200.0000000	0.4641716E-03
3300.0000000	0.3454060E-02
3400.0000000	0.7081124E-02
3500.0000000	0.2083192E-01

3600.0000000	0.2815370E-01
3700.0000000	0.3654217E-01
3800.0000000	0.4538578E-01
3900.0000000	0.5468087E-01
4000.0000000	0.6443774E-01
4100.0000000	0.7466274E-01
4200.0000000	0.8535976E-01
4300.0000000	0.9653028E-01
4400.0000000	0.1081740E+00
4500.0000000	0.1202880E+00
4600.0000000	0.1443513E+00
4700.0000000	0.1753685E+00
4800.0000000	0.2241077E+00
4900.0000000	0.3063382E+00
5000.0000000	0.3538797E+00
5100.0000000	0.4038869E+00
5200.0000000	0.4554516E+00
5300.0000000	0.5086157E+00
5400.0000000	0.5634188E+00
5500.0000000	0.6198985E+00
5600.0000000	0.6780648E+00
5700.0000000	0.7379167E+00
5800.0000000	0.7994532E+00
5900.0000000	0.8626590E+00
6000.0000000	0.9275152E+00
6100.0000000	0.9940120E+00
6200.0000000	0.1062130E+01
6300.0000000	0.1131850E+01
6400.0000000	0.1203145E+01
6500.0000000	0.1275999E+01
6600.0000000	0.1354133E+01
6700.0000000	0.1456109E+01
6800.0000000	0.1533661E+01
6900.0000000	0.1668035E+01
7000.0000000	0.1751704E+01
7100.0000000	0.1840736E+01
7200.0000000	0.1931024E+01
7300.0000000	0.2022550E+01
7400.0000000	0.2115392E+01
7500.0000000	0.2209623E+01
7600.0000000	0.2305285E+01
7700.0000000	0.2402398E+01
7800.0000000	0.2500962E+01
7900.0000000	0.2600977E+01
8000.0000000	0.2702439E+01
8100.0000000	0.2805332E+01
8200.0000000	0.2909635E+01
8300.0000000	0.3015333E+01
8400.0000000	0.3122410E+01
8500.0000000	0.3230844E+01
8600.0000000	0.3340626E+01
8700.0000000	0.3451737E+01
8800.0000000	0.3564166E+01
8900.0000000	0.3677889E+01
9000.0000000	0.3792896E+01
9100.0000000	0.3909168E+01
9200.0000000	0.4026692E+01
9300.0000000	0.4145446E+01
9400.0000000	0.4265421E+01
9500.0000000	0.4386543E+01
9600.0000000	0.4443121E+01
9700.0000000	0.4502635E+01

9800.0000000	0.4562176E+01
9900.0000000	0.4621689E+01
10000.0000000	0.4684441E+01
CS135	
100.0000000	0.0000000E+00
200.0000000	0.0000000E+00
300.0000000	0.0000000E+00
400.0000000	0.0000000E+00
500.0000000	0.0000000E+00
600.0000000	0.0000000E+00
700.0000000	0.0000000E+00
800.0000000	0.0000000E+00
900.0000000	0.0000000E+00
1000.0000000	0.0000000E+00
1100.0000000	0.0000000E+00
1200.0000000	0.0000000E+00
1300.0000000	0.0000000E+00
1400.0000000	0.0000000E+00
1500.0000000	0.0000000E+00
1600.0000000	0.0000000E+00
1700.0000000	0.0000000E+00
1800.0000000	0.0000000E+00
1900.0000000	0.0000000E+00
2000.0000000	0.0000000E+00
2100.0000000	0.0000000E+00
2200.0000000	0.0000000E+00
2300.0000000	0.0000000E+00
2400.0000000	0.0000000E+00
2500.0000000	0.0000000E+00
2600.0000000	0.0000000E+00
2700.0000000	0.0000000E+00
2800.0000000	0.0000000E+00
2900.0000000	0.0000000E+00
3000.0000000	0.0000000E+00
3100.0000000	0.0000000E+00
3200.0000000	0.9589851E-02
3300.0000000	0.5162699E-01
3400.0000000	0.7779236E-01
3500.0000000	0.1741978E+00
3600.0000000	0.1628238E+00
3700.0000000	0.1536158E+00
3800.0000000	0.1466385E+00
3900.0000000	0.1412945E+00
4000.0000000	0.1370610E+00
4100.0000000	0.1335479E+00
4200.0000000	0.1305098E+00
4300.0000000	0.1277960E+00
4400.0000000	0.1253155E+00
4500.0000000	0.1230040E+00
4600.0000000	0.2566855E+00
4700.0000000	0.3437768E+00
4800.0000000	0.4892754E+00
4900.0000000	0.6728097E+00
5000.0000000	0.5901048E+00
5100.0000000	0.5360940E+00
5200.0000000	0.5027250E+00
5300.0000000	0.4812028E+00
5400.0000000	0.4663657E+00
5500.0000000	0.4553669E+00
5600.0000000	0.4465475E+00
5700.0000000	0.4390005E+00
5800.0000000	0.4322580E+00

```
     5900.0000000    0.4260224E+00
     6000.0000000    0.4201265E+00
     6100.0000000    0.4145282E+00
     6200.0000000    0.4091520E+00
     6300.0000000    0.4039683E+00
     6400.0000000    0.3989218E+00
     6500.0000000    0.3940200E+00
     6600.0000000    0.4219921E+00
     6700.0000000    0.5454918E+00
     6800.0000000    0.5042735E+00
     6900.0000000    0.6451890E+00
     7000.0000000    0.5397111E+00
     7100.0000000    0.4773355E+00
     7200.0000000    0.4404518E+00
     7300.0000000    0.4181149E+00
     7400.0000000    0.4039520E+00
     7500.0000000    0.3943869E+00
     7600.0000000    0.3874070E+00
     7700.0000000    0.3818819E+00
     7800.0000000    0.3771714E+00
     7900.0000000    0.3729650E+00
     8000.0000000    0.3690819E+00
     8100.0000000    0.3654099E+00
     8200.0000000    0.3618648E+00
     8300.0000000    0.3584343E+00
     8400.0000000    0.3551003E+00
     8500.0000000    0.3518358E+00
     8600.0000000    0.3486642E+00
     8700.0000000    0.3455626E+00
     8800.0000000    0.3425457E+00
     8900.0000000    0.3395811E+00
     9000.0000000    0.3366854E+00
     9100.0000000    0.3338473E+00
     9200.0000000    0.3310709E+00
     9300.0000000    0.3283357E+00
     9400.0000000    0.3256613E+00
     9500.0000000    0.3033956E+00
     9600.0000000    0.1692399E+00
     9700.0000000    0.8890841E-01
     9800.0000000    0.4678036E-01
     9900.0000000    0.2468669E-01
    10000.0000000    0.1253402E-01
I129
      100.0000000    0.0000000E+00
      200.0000000    0.0000000E+00
      300.0000000    0.0000000E+00
      400.0000000    0.0000000E+00
      500.0000000    0.0000000E+00
      600.0000000    0.0000000E+00
      700.0000000    0.0000000E+00
      800.0000000    0.0000000E+00
      900.0000000    0.0000000E+00
     1000.0000000    0.0000000E+00
     1100.0000000    0.0000000E+00
     1200.0000000    0.0000000E+00
     1300.0000000    0.0000000E+00
     1400.0000000    0.0000000E+00
     1500.0000000    0.0000000E+00
     1600.0000000    0.0000000E+00
     1700.0000000    0.0000000E+00
     1800.0000000    0.0000000E+00
     1900.0000000    0.0000000E+00
```

2000.0000000	0.0000000E+00
2100.0000000	0.0000000E+00
2200.0000000	0.0000000E+00
2300.0000000	0.0000000E+00
2400.0000000	0.0000000E+00
2500.0000000	0.0000000E+00
2600.0000000	0.0000000E+00
2700.0000000	0.0000000E+00
2800.0000000	0.0000000E+00
2900.0000000	0.0000000E+00
3000.0000000	0.0000000E+00
3100.0000000	0.0000000E+00
3200.0000000	0.5908720E-03
3300.0000000	0.2700659E-02
3400.0000000	0.3297447E-02
3500.0000000	0.1154294E-01
3600.0000000	0.1169635E-01
3700.0000000	0.1174354E-01
3800.0000000	0.1168886E-01
3900.0000000	0.1157077E-01
4000.0000000	0.1141944E-01
4100.0000000	0.1125148E-01
4200.0000000	0.1107679E-01
4300.0000000	0.1090081E-01
4400.0000000	0.1072649E-01
4500.0000000	0.1055478E-01
4600.0000000	0.1833368E-01
4700.0000000	0.2052424E-01
4800.0000000	0.2917707E-01
4900.0000000	0.4852653E-01
5000.0000000	0.4544489E-01
5100.0000000	0.4366532E-01
5200.0000000	0.4238254E-01
5300.0000000	0.4130644E-01
5400.0000000	0.4036374E-01
5500.0000000	0.3953039E-01
5600.0000000	0.3878283E-01
5700.0000000	0.3810429E-01
5800.0000000	0.3748265E-01
5900.0000000	0.3690528E-01
6000.0000000	0.3636226E-01
6100.0000000	0.3585097E-01
6200.0000000	0.3536435E-01
6300.0000000	0.3489910E-01
6400.0000000	0.3444998E-01
6500.0000000	0.3401656E-01
6600.0000000	0.3557309E-01
6700.0000000	0.4132162E-01
6800.0000000	0.3431084E-01
6900.0000000	0.4971323E-01
7000.0000000	0.4525173E-01
7100.0000000	0.4237598E-01
7200.0000000	0.4019527E-01
7300.0000000	0.3845761E-01
7400.0000000	0.3705396E-01
7500.0000000	0.3591234E-01
7600.0000000	0.3497389E-01
7700.0000000	0.3419044E-01
7800.0000000	0.3352390E-01
7900.0000000	0.3294837E-01
8000.0000000	0.3244302E-01
8100.0000000	0.3199107E-01

8200.0000000	0.3157886E-01
8300.0000000	0.3119936E-01
8400.0000000	0.3084578E-01
8500.0000000	0.3051221E-01
8600.0000000	0.3019719E-01
8700.0000000	0.2989643E-01
8800.0000000	0.2960916E-01
8900.0000000	0.2933174E-01
9000.0000000	0.2906406E-01
9100.0000000	0.2880475E-01
9200.0000000	0.2855316E-01
9300.0000000	0.2830736E-01
9400.0000000	0.2806857E-01
9500.0000000	0.2632672E-01
9600.0000000	0.1667547E-01
9700.0000000	0.1154531E-01
9800.0000000	0.8487271E-02
9900.0000000	0.6392602E-02
10000.0000000	0.4825757E-02

TC99

100.0000000	0.0000000E+00
200.0000000	0.0000000E+00
300.0000000	0.0000000E+00
400.0000000	0.0000000E+00
500.0000000	0.0000000E+00
600.0000000	0.0000000E+00
700.0000000	0.0000000E+00
800.0000000	0.0000000E+00
900.0000000	0.0000000E+00
1000.0000000	0.0000000E+00
1100.0000000	0.0000000E+00
1200.0000000	0.0000000E+00
1300.0000000	0.0000000E+00
1400.0000000	0.0000000E+00
1500.0000000	0.0000000E+00
1600.0000000	0.0000000E+00
1700.0000000	0.0000000E+00
1800.0000000	0.0000000E+00
1900.0000000	0.0000000E+00
2000.0000000	0.0000000E+00
2100.0000000	0.0000000E+00
2200.0000000	0.0000000E+00
2300.0000000	0.0000000E+00
2400.0000000	0.0000000E+00
2500.0000000	0.0000000E+00
2600.0000000	0.0000000E+00
2700.0000000	0.0000000E+00
2800.0000000	0.0000000E+00
2900.0000000	0.0000000E+00
3000.0000000	0.0000000E+00
3100.0000000	0.0000000E+00
3200.0000000	0.2423012E+00
3300.0000000	0.1107414E+01
3400.0000000	0.1352226E+01
3500.0000000	0.4730728E+01
3600.0000000	0.4791743E+01
3700.0000000	0.4809344E+01
3800.0000000	0.4785262E+01
3900.0000000	0.4735275E+01
4000.0000000	0.4671743E+01
4100.0000000	0.4601474E+01
4200.0000000	0.4528513E+01

```
     4300.0000000   0.4455081E+01
     4400.0000000   0.4382389E+01
     4500.0000000   0.4310808E+01
     4600.0000000   0.7485537E+01
     4700.0000000   0.8378552E+01
     4800.0000000   0.1190824E+02
     4900.0000000   0.1979730E+02
     5000.0000000   0.1853352E+02
     5100.0000000   0.1780135E+02
     5200.0000000   0.1727224E+02
     5300.0000000   0.1682782E+02
     5400.0000000   0.1643817E+02
     5500.0000000   0.1609339E+02
     5600.0000000   0.1578382E+02
     5700.0000000   0.1550257E+02
     5800.0000000   0.1524468E+02
     5900.0000000   0.1500497E+02
     6000.0000000   0.1477939E+02
     6100.0000000   0.1456685E+02
     6200.0000000   0.1436448E+02
     6300.0000000   0.1417092E+02
     6400.0000000   0.1398404E+02
     6500.0000000   0.1380366E+02
     6600.0000000   0.1443060E+02
     6700.0000000   0.1675810E+02
     6800.0000000   0.1391277E+02
     6900.0000000   0.2015102E+02
     7000.0000000   0.1833536E+02
     7100.0000000   0.1716371E+02
     7200.0000000   0.1627457E+02
     7300.0000000   0.1556559E+02
     7400.0000000   0.1499242E+02
     7500.0000000   0.1452572E+02
     7600.0000000   0.1414155E+02
     7700.0000000   0.1382033E+02
     7800.0000000   0.1354658E+02
     7900.0000000   0.1330978E+02
     8000.0000000   0.1310148E+02
     8100.0000000   0.1291486E+02
     8200.0000000   0.1274440E+02
     8300.0000000   0.1258724E+02
     8400.0000000   0.1244062E+02
     8500.0000000   0.1230217E+02
     8600.0000000   0.1217127E+02
     8700.0000000   0.1204620E+02
     8800.0000000   0.1192665E+02
     8900.0000000   0.1181113E+02
     9000.0000000   0.1169960E+02
     9100.0000000   0.1159150E+02
     9200.0000000   0.1148658E+02
     9300.0000000   0.1138405E+02
     9400.0000000   0.1128440E+02
     9500.0000000   0.1058125E+02
     9600.0000000   0.6699944E+01
     9700.0000000   0.4636577E+01
     9800.0000000   0.3406661E+01
     9900.0000000   0.2564450E+01
    10000.0000000   0.1934724E+01
NI59
      100.0000000   0.0000000E+00
      200.0000000   0.0000000E+00
      300.0000000   0.0000000E+00
```

400.0000000	0.0000000E+00
500.0000000	0.0000000E+00
600.0000000	0.0000000E+00
700.0000000	0.0000000E+00
800.0000000	0.0000000E+00
900.0000000	0.0000000E+00
1000.0000000	0.0000000E+00
1100.0000000	0.0000000E+00
1200.0000000	0.0000000E+00
1300.0000000	0.0000000E+00
1400.0000000	0.0000000E+00
1500.0000000	0.0000000E+00
1600.0000000	0.0000000E+00
1700.0000000	0.0000000E+00
1800.0000000	0.0000000E+00
1900.0000000	0.0000000E+00
2000.0000000	0.0000000E+00
2100.0000000	0.0000000E+00
2200.0000000	0.0000000E+00
2300.0000000	0.0000000E+00
2400.0000000	0.0000000E+00
2500.0000000	0.0000000E+00
2600.0000000	0.0000000E+00
2700.0000000	0.0000000E+00
2800.0000000	0.0000000E+00
2900.0000000	0.0000000E+00
3000.0000000	0.0000000E+00
3100.0000000	0.0000000E+00
3200.0000000	0.5694328E-02
3300.0000000	0.3746658E-01
3400.0000000	0.6195644E-01
3500.0000000	0.1777307E+00
3600.0000000	0.1793556E+00
3700.0000000	0.1781624E+00
3800.0000000	0.1762196E+00
3900.0000000	0.1743110E+00
4000.0000000	0.1726827E+00
4100.0000000	0.1713587E+00
4200.0000000	0.1702898E+00
4300.0000000	0.1694154E+00
4400.0000000	0.1686850E+00
4500.0000000	0.1680624E+00
4600.0000000	0.2704574E+00
4700.0000000	0.3857963E+00
4800.0000000	0.5920892E+00
4900.0000000	0.9345670E+00
5000.0000000	0.9336580E+00
5100.0000000	0.9260391E+00
5200.0000000	0.9172969E+00
5300.0000000	0.9094102E+00
5400.0000000	0.9028534E+00
5500.0000000	0.8975252E+00
5600.0000000	0.8931719E+00
5700.0000000	0.8895479E+00
5800.0000000	0.8864607E+00
5900.0000000	0.8837730E+00
6000.0000000	0.8813972E+00
6100.0000000	0.8792667E+00
6200.0000000	0.8773341E+00
6300.0000000	0.8755660E+00
6400.0000000	0.8739380E+00
6500.0000000	0.8724312E+00

```
      6600.0000000   0.8978452E+00
      6700.0000000   0.1046872E+01
      6800.0000000   0.1161156E+01
      6900.0000000   0.1709218E+01
      7000.0000000   0.1715429E+01
      7100.0000000   0.1708432E+01
      7200.0000000   0.1698164E+01
      7300.0000000   0.1688181E+01
      7400.0000000   0.1679607E+01
      7500.0000000   0.1672533E+01
      7600.0000000   0.1666714E+01
      7700.0000000   0.1661853E+01
      7800.0000000   0.1657702E+01
      7900.0000000   0.1654077E+01
      8000.0000000   0.1650848E+01
      8100.0000000   0.1647928E+01
      8200.0000000   0.1645260E+01
      8300.0000000   0.1642804E+01
      8400.0000000   0.1640528E+01
      8500.0000000   0.1638407E+01
      8600.0000000   0.1636421E+01
      8700.0000000   0.1634556E+01
      8800.0000000   0.1632798E+01
      8900.0000000   0.1631136E+01
      9000.0000000   0.1629560E+01
      9100.0000000   0.1628064E+01
      9200.0000000   0.1626638E+01
      9300.0000000   0.1625277E+01
      9400.0000000   0.1623975E+01
      9500.0000000   0.1622452E+01
      9600.0000000   0.1621372E+01
      9700.0000000   0.1620294E+01
      9800.0000000   0.1619254E+01
      9900.0000000   0.1618247E+01
     10000.0000000   0.1617204E+01
C14
       100.0000000   0.0000000E+00
       200.0000000   0.0000000E+00
       300.0000000   0.0000000E+00
       400.0000000   0.0000000E+00
       500.0000000   0.0000000E+00
       600.0000000   0.0000000E+00
       700.0000000   0.0000000E+00
       800.0000000   0.0000000E+00
       900.0000000   0.0000000E+00
      1000.0000000   0.0000000E+00
      1100.0000000   0.0000000E+00
      1200.0000000   0.0000000E+00
      1300.0000000   0.0000000E+00
      1400.0000000   0.0000000E+00
      1500.0000000   0.0000000E+00
      1600.0000000   0.0000000E+00
      1700.0000000   0.0000000E+00
      1800.0000000   0.0000000E+00
      1900.0000000   0.0000000E+00
      2000.0000000   0.0000000E+00
      2100.0000000   0.0000000E+00
      2200.0000000   0.0000000E+00
      2300.0000000   0.0000000E+00
      2400.0000000   0.0000000E+00
      2500.0000000   0.0000000E+00
      2600.0000000   0.0000000E+00
```

2700.0000000	0.0000000E+00
2800.0000000	0.0000000E+00
2900.0000000	0.0000000E+00
3000.0000000	0.0000000E+00
3100.0000000	0.0000000E+00
3200.0000000	0.2055124E-01
3300.0000000	0.9489969E-01
3400.0000000	0.1168274E+00
3500.0000000	0.4006716E+00
3600.0000000	0.4000379E+00
3700.0000000	0.3961798E+00
3800.0000000	0.3890737E+00
3900.0000000	0.3800880E+00
4000.0000000	0.3702652E+00
4100.0000000	0.3601585E+00
4200.0000000	0.3500809E+00
4300.0000000	0.3401935E+00
4400.0000000	0.3305733E+00
4500.0000000	0.3212323E+00
4600.0000000	0.5469830E+00
4700.0000000	0.6124885E+00
4800.0000000	0.8651460E+00
4900.0000000	0.1417532E+01
5000.0000000	0.1309725E+01
5100.0000000	0.1241300E+01
5200.0000000	0.1188604E+01
5300.0000000	0.1143170E+01
5400.0000000	0.1102688E+01
5500.0000000	0.1066245E+01
5600.0000000	0.1032999E+01
5700.0000000	0.1002345E+01
5800.0000000	0.9738479E+00
5900.0000000	0.9470875E+00
6000.0000000	0.9217245E+00
6100.0000000	0.8976597E+00
6200.0000000	0.8746798E+00
6300.0000000	0.8526693E+00
6400.0000000	0.8314706E+00
6500.0000000	0.8110488E+00
6600.0000000	0.8365895E+00
6700.0000000	0.9614436E+00
6800.0000000	0.7946222E+00
6900.0000000	0.1138005E+01
7000.0000000	0.1020424E+01
7100.0000000	0.9419871E+00
7200.0000000	0.8812623E+00
7300.0000000	0.8320403E+00
7400.0000000	0.7914304E+00
7500.0000000	0.7574797E+00
7600.0000000	0.7286357E+00
7700.0000000	0.7036687E+00
7800.0000000	0.6816330E+00
7900.0000000	0.6618865E+00
8000.0000000	0.6439260E+00
8100.0000000	0.6273565E+00
8200.0000000	0.6118559E+00
8300.0000000	0.5972558E+00
8400.0000000	0.5834063E+00
8500.0000000	0.5701756E+00
8600.0000000	0.5575189E+00
8700.0000000	0.5453420E+00
8800.0000000	0.5336179E+00

```
     8900.0000000   0.5222693E+00
     9000.0000000   0.5112853E+00
     9100.0000000   0.5006324E+00
     9200.0000000   0.4902920E+00
     9300.0000000   0.4802236E+00
     9400.0000000   0.4704415E+00
     9500.0000000   0.4364017E+00
     9600.0000000   0.2724359E+00
     9700.0000000   0.1849767E+00
     9800.0000000   0.1329642E+00
     9900.0000000   0.9776054E-01
    10000.0000000   0.7183673E-01
SE79
      100.0000000   0.0000000E+00
      200.0000000   0.0000000E+00
      300.0000000   0.0000000E+00
      400.0000000   0.0000000E+00
      500.0000000   0.0000000E+00
      600.0000000   0.0000000E+00
      700.0000000   0.0000000E+00
      800.0000000   0.0000000E+00
      900.0000000   0.0000000E+00
     1000.0000000   0.0000000E+00
     1100.0000000   0.0000000E+00
     1200.0000000   0.0000000E+00
     1300.0000000   0.0000000E+00
     1400.0000000   0.0000000E+00
     1500.0000000   0.0000000E+00
     1600.0000000   0.0000000E+00
     1700.0000000   0.0000000E+00
     1800.0000000   0.0000000E+00
     1900.0000000   0.0000000E+00
     2000.0000000   0.0000000E+00
     2100.0000000   0.0000000E+00
     2200.0000000   0.0000000E+00
     2300.0000000   0.0000000E+00
     2400.0000000   0.0000000E+00
     2500.0000000   0.0000000E+00
     2600.0000000   0.0000000E+00
     2700.0000000   0.0000000E+00
     2800.0000000   0.0000000E+00
     2900.0000000   0.0000000E+00
     3000.0000000   0.0000000E+00
     3100.0000000   0.0000000E+00
     3200.0000000   0.6185804E-09
     3300.0000000   0.3780016E-08
     3400.0000000   0.5637454E-08
     3500.0000000   0.1933033E-07
     3600.0000000   0.2005437E-07
     3700.0000000   0.2038483E-07
     3800.0000000   0.2049715E-07
     3900.0000000   0.2049985E-07
     4000.0000000   0.2045298E-07
     4100.0000000   0.2038718E-07
     4200.0000000   0.2031715E-07
     4300.0000000   0.2024941E-07
     4400.0000000   0.2018658E-07
     4500.0000000   0.2012946E-07
     4600.0000000   0.3104648E-07
     4700.0000000   0.4086589E-07
     4800.0000000   0.6188799E-07
     4900.0000000   0.1046728E-06
```

```
      5000.0000000   0.1068284E-06
      5100.0000000   0.1076821E-06
      5200.0000000   0.1078610E-06
      5300.0000000   0.1077183E-06
      5400.0000000   0.1074407E-06
      5500.0000000   0.1071204E-06
      5600.0000000   0.1067998E-06
      5700.0000000   0.1064970E-06
      5800.0000000   0.1062178E-06
      5900.0000000   0.1059627E-06
      6000.0000000   0.1057306E-06
      6100.0000000   0.1055190E-06
      6200.0000000   0.1053248E-06
      6300.0000000   0.1051456E-06
      6400.0000000   0.1049791E-06
      6500.0000000   0.1048237E-06
      6600.0000000   0.1075954E-06
      6700.0000000   0.1224153E-06
      6800.0000000   0.1310271E-06
      6900.0000000   0.1958052E-06
      7000.0000000   0.1990665E-06
      7100.0000000   0.2004905E-06
      7200.0000000   0.2009141E-06
      7300.0000000   0.2008283E-06
      7400.0000000   0.2005129E-06
      7500.0000000   0.2001118E-06
      7600.0000000   0.1996940E-06
      7700.0000000   0.1992902E-06
      7800.0000000   0.1989121E-06
      7900.0000000   0.1985626E-06
      8000.0000000   0.1982405E-06
      8100.0000000   0.1979432E-06
      8200.0000000   0.1976681E-06
      8300.0000000   0.1974126E-06
      8400.0000000   0.1971741E-06
      8500.0000000   0.1969502E-06
      8600.0000000   0.1967391E-06
      8700.0000000   0.1965392E-06
      8800.0000000   0.1963493E-06
      8900.0000000   0.1961683E-06
      9000.0000000   0.1959953E-06
      9100.0000000   0.1958297E-06
      9200.0000000   0.1956709E-06
      9300.0000000   0.1955183E-06
      9400.0000000   0.1953716E-06
      9500.0000000   0.1951986E-06
      9600.0000000   0.1950760E-06
      9700.0000000   0.1949534E-06
      9800.0000000   0.1948352E-06
      9900.0000000   0.1947209E-06
     10000.0000000   0.1946025E-06
NB94
       100.0000000   0.0000000E+00
       200.0000000   0.0000000E+00
       300.0000000   0.0000000E+00
       400.0000000   0.0000000E+00
       500.0000000   0.0000000E+00
       600.0000000   0.0000000E+00
       700.0000000   0.0000000E+00
       800.0000000   0.0000000E+00
       900.0000000   0.0000000E+00
      1000.0000000   0.0000000E+00
```

1100.0000000	0.0000000E+00
1200.0000000	0.0000000E+00
1300.0000000	0.0000000E+00
1400.0000000	0.0000000E+00
1500.0000000	0.0000000E+00
1600.0000000	0.0000000E+00
1700.0000000	0.0000000E+00
1800.0000000	0.0000000E+00
1900.0000000	0.0000000E+00
2000.0000000	0.0000000E+00
2100.0000000	0.0000000E+00
2200.0000000	0.0000000E+00
2300.0000000	0.0000000E+00
2400.0000000	0.0000000E+00
2500.0000000	0.0000000E+00
2600.0000000	0.0000000E+00
2700.0000000	0.0000000E+00
2800.0000000	0.0000000E+00
2900.0000000	0.0000000E+00
3000.0000000	0.0000000E+00
3100.0000000	0.0000000E+00
3200.0000000	0.1272161E-01
3300.0000000	0.8387841E-01
3400.0000000	0.1398093E+00
3500.0000000	0.3283082E+00
3600.0000000	0.3133449E+00
3700.0000000	0.2994203E+00
3800.0000000	0.2878423E+00
3900.0000000	0.2783017E+00
4000.0000000	0.2702872E+00
4100.0000000	0.2633267E+00
4200.0000000	0.2571035E+00
4300.0000000	0.2514129E+00
4400.0000000	0.2461285E+00
4500.0000000	0.2411552E+00
4600.0000000	0.4035779E+00
4700.0000000	0.5913670E+00
4800.0000000	0.8710279E+00
4900.0000000	0.1225111E+01
5000.0000000	0.1090944E+01
5100.0000000	0.1001899E+01
5200.0000000	0.9460009E+00
5300.0000000	0.9087892E+00
5400.0000000	0.8819782E+00
5500.0000000	0.8611155E+00
5600.0000000	0.8436209E+00
5700.0000000	0.8281092E+00
5800.0000000	0.8138867E+00
5900.0000000	0.8005017E+00
6000.0000000	0.7877179E+00
6100.0000000	0.7754784E+00
6200.0000000	0.7636498E+00
6300.0000000	0.7521832E+00
6400.0000000	0.7409809E+00
6500.0000000	0.7300606E+00
6600.0000000	0.7499230E+00
6700.0000000	0.9116745E+00
6800.0000000	0.8493965E+00
6900.0000000	0.1077631E+01
7000.0000000	0.9253557E+00
7100.0000000	0.8356134E+00
7200.0000000	0.7816690E+00

7300.0000000	0.7477561E+00
7400.0000000	0.7249574E+00
7500.0000000	0.7083814E+00
7600.0000000	0.6953069E+00
7700.0000000	0.6842160E+00
7800.0000000	0.6742505E+00
7900.0000000	0.6650155E+00
8000.0000000	0.6562770E+00
8100.0000000	0.6478835E+00
8200.0000000	0.6397215E+00
8300.0000000	0.6317842E+00
8400.0000000	0.6240383E+00
8500.0000000	0.6164373E+00
8600.0000000	0.6090218E+00
8700.0000000	0.6017524E+00
8800.0000000	0.5946541E+00
8900.0000000	0.5876718E+00
9000.0000000	0.5808336E+00
9100.0000000	0.5741206E+00
9200.0000000	0.5675395E+00
9300.0000000	0.5610557E+00
9400.0000000	0.5547024E+00
9500.0000000	0.5153963E+00
9600.0000000	0.2909740E+00
9700.0000000	0.1593780E+00
9800.0000000	0.9166359E-01
9900.0000000	0.5659837E-01
10000.0000000	0.3752762E-01

ENGINEERED BARRIER SYSTEM PERFORMANCE ASSESSMENT CODE: EBSPAC VERSION 1.0 β

TECHNICAL DESCRIPTION AND USER'S MANUAL